WIND EFFECTS ON EMERGENCY VEHICLES

Final Report submitted to:

Daniel H. Rocque, Fire Chief

SATELLITE BEACH FIRE DEPARTMENT

&

David Halstead, Senior Management Analyst I

DIVISION OF EMERGENCY MANAGEMENT

FLORIDA DEPARTMENT OF COMMUNITY AFFAIRS

Principal Investigator:
Jean-Paul Pinelli, Ph.D., P.E.
Associate Professor
Civil Engineering Program
Ph: (321) 674-8085
Fax: (321) 674-7565
Email: pinelli@fit.edu

Co- Principal Investigator:
Chelakara Subramanian, Ph.D., P.E. (UK)
Associate Professor
Aerospace Engineering Program
Ph: (321) 674-7614
Fax: (321) 674-8813
Email: subraman@fit.edu

Research Assistant: Morgan M. Plamondon
Aerospace Engineering Graduate Student

Research Assistant: Vidya Chakravarthi
Mechanical Engineering Graduate Student

Florida Institute of Technology
150 W. University Blvd.
Melbourne, Florida 32901-6988
(321) 674-8085

Wind Effects on Emergency Vehicles

Final Report

August 31, 2003

Note: Figure adapted from Manufactures website see [1]

ABSTRACT:

The report presents the results of a study to define the wind speed limits and conditions beyond which fire and rescue vehicles should not be operated during a hurricane. For that purpose, reduced scale models of a typical fire truck, ambulance, and sports utility vehicle (SUV) were tested in a wind tunnel. For the fire truck the wind tunnel tests are compared with full-scale measurements on a real truck and to computer simulations using the Fluent software. The report presents and compares the results of the different tests: experimental, field, and numerical. The resulting wind pressure distributions on the vehicles are used to obtain drag, lift, and side forces, in addition to overturning, yawing, and pitching moments. Based on the results of the tests and the analyses, safe wind speeds are found for the operation of these fire and rescue vehicles.

KEYWORDS: Emergency Vehicles; Hurricanes; Wind Tunnel; Simulations, Coefficient of Static Friction; Critical Wind Speed; Vehicle Aerodynamics

Table of Contents

ABSTRACT: 3
1 INTRODUCTION 10
2 FIRE TRUCK 2-1
2.1 WIND TUNNEL EXPERIMENTATION 2-1
2.1.1 Experimental Setup 2-1
2.1.2 Experimental Procedure 2-2
2.2 WIND TUNNEL RESULTS 2-3
2.2.1 Scatter in Measurements 2-3
2.2.2 Wind Tunnel Test Results 2-6
2.3 FULL SCALE FIRE TRUCK – FIELD TEST 2-11
2.3.1 Introduction 2-11
2.3.2 Preliminary Testing 2-11
2.3.3 Experimental Setup 2-12
2.3.4 Field Test Results 2-13
2.4 COMPUTER SIMULATION 2-18
2.4.1 Introduction 2-18
2.4.2 Theory of the CFD model: k-ε model 2-18
2.4.3 Preliminary Testing 2-19
2.4.4 Modeling 2-20
2.5 COMPARISON BETWEEN THE DIFFERENT TESTS AND VALIDATION OF THE RESULTS 2-24
2.5.1 Comparison of Results from the Different Tests 2-24
2.5.2 Determination of Forces Acting on the Vehicle 2-27
2.6 CRITICAL WIND SPEEDS 2-34
2.6.1 Introduction 2-34
2.6.2 Determination of Critical Wind Speeds Due to Course Deviation 2-34
2.6.3 Course Deviation For the Typhoon Pumper 2-41
2.6.4 Extrapolating the Typhoon data to the Cyclone II X-113 2-43
2.6.5 Determination of Critical Wind Speeds Due to Overturning 2-44
3 AMBULANCE TESTING 3-1
3.1 WIND TUNNEL EXPERIMENTATION 3-1
3.1.1 Wind Tunnel Experimentation 3-1
3.1.2 Experimental Procedure 3-2
3.2 WIND TUNNEL RESULTS 3-3
3.2.1 Scatter in Measurements 3-3
3.2.2 Wind Tunnel Testing Results 3-3
3.3 COMPARISON BETWEEN THE FORCE BALANCE AND PRESSURE DISTRIBUTION - VALIDATION OF THE RESULTS 3-10
3.3.1 Determination of Forces Acting on the Vehicle 3-10
3.3.2 Comparison between force balance results and measured pressure results3-13
3.3.3 Influence of Reynolds Number 3-15
3.4 CRITICAL WIND SPEEDS 3-16
3.4.1 Introduction 3-16
3.4.2 Determination of Critical Wind Speeds Due to Course Deviation 3-16

3.4.3 Course Deviation 3-20
3.4.4 Determination of Critical Wind Speeds Due to Overturning..... 3-22
4 SPORTS UTILITY VEHICLE SECTION 4-1
4.1 WIND TUNNEL EXPERIMENTATION 4-1
4.1.1 Experimental Setup 4-1
4.1.2 Experimental Procedure 4-2
4.2 WIND TUNNEL RESULTS 4-2
4.2.1 Scatter in Measurements 4-2
4.2.2 Wind Tunnel Testing Results 4-3
4.3 COMPARISON BETWEEN THE FORCE BALANCE AND PRESSURE DISTRIBUTION - VALIDATION OF THE RESULTS 4-8
4.3.1 Determination of Forces Acting on the Vehicle 4-8
4.4 CRITICAL WIND SPEEDS 4-14
4.4.1 Introduction 4-14
4.4.2 Determination of Critical Wind Speeds Due to Course Deviation 4-14
4.4.3 Course Deviation 4-18
4.4.4 Determination of Critical Wind Speeds Due to Overturning..... 4-20
5 CONCLUSIONS AND RECOMMENDATIONS 5-1
5.1 TYPES OF VEHICLE ACCIDENTS 5-1
5.2 FIRE TRUCK CONCLUSIONS 5-1
5.3 AMBULANCE CONCLUSIONS 5-1
5.4 SUV CONCLUSIONS 5-2
5.5 RECOMMENDATIONS 5-2
5.6 RECOMMENDATIONS FOR FURTHER STUDIES 5-5
6 AKCKNOWLEDGMENTS 6-1
7 REFERENCES 7-1

List of Figures

Figure 2-1: Experimental setup with the fire truck at 0 degrees orientation 2-1
Figure 2-2: Convention used to define the angle with respect to incoming wind 2-2
Figure 2-3: Scatter in the freestream total pressure pap vs. time at different speeds 2-4
Figure 2-4: Scatter in tap #10 pressures vs. time at different speeds..... 2-4
Figure 2-5: Scatter in tap #10 pressures vs. time after corrective steps were taken 2-5
Figure 2-6: Typical Cp vs. velocity distributions at windward tap locations for 90 degrees angle of attack..... 2-7
Figure 2-7: 0 degree coefficient of pressure test results 2-8
Figure 2-8: 45 degree coefficient of pressure test results 2-8
Figure 2-9: 90 degree coefficient of pressure test results 2-9
Figure 2-10: 135 degree coefficient of pressure test results 2-9
Figure 2-11: 180 degree coefficient of pressure test results 2-10
Figure 2-12: Schematic drawing of the E-One Cyclone II X113 Pumper [1] 2-11
Figure 2-13: Schematic of the E-One Typhoon Pumper [1]..... 2-11
Figure 2-14: Instrumented Minivan for preliminary testing. 2-12
Figure 2-15: Surface pressure brass tube and Tygon tubing mounted to the fire truck 2-13
Figure 2-16: Instrumented Fire Truck..... 2-13
Figure 2-17: Time history plot of velocity measured from Pitot-static tube. 2-14
Figure 2-18: Time history plot of velocity measured from Anemometer..... 2-15
Figure 2-19: Comparison of the average speeds measured from all the 3 instruments 2-15
Figure 2-20: Vector representation of the measured speeds..... 2-16
Figure 2-21: Time history of pressure for tap FC on the front face of the fire truck.... 2-16
Figure 2-22: 0 Degree Coefficient of Pressure Field Test Results 2-17
Figure 2-23: 2D-model of truck..... 2-19
Figure 2-24: Test on a Cube model..... 2-20
Figure 2-25: Grid display..... 2-21
Figure 2-26: Contours of Pressure Coefficient 2-22
Figure 2-27: After using the Grid adaptation function 2-22
Figure 2-28: The pressure coefficient contours after the grid adaptation..... 2-23
Figure 2-29: Front of Truck Comparisons Between the Field Test, Wind Tunnel testing, and Computer Simulation 2-24
Figure 2-30: Left Side Comparisons between the Field Test, Wind tunnel testing, and Computer Simulation..... 2-25
Figure 2-31: Top Side Comparisons between the Field Test, Wind tunnel testing, and Computer Simulation..... 2-25
Figure 2-32: Rear of Truck Comparisons between the Field Test, Wind tunnel testing, and Computer Simulation 2-26
Figure 2-33: Protrusion visible on the top of the Protector Cab 2-26
Figure 2-34: Virtually no protrusions windward of the pressure taps on the Wind Tunnel Model in a 0 Degree test..... 2-27
Figure 2-35: Panel division on the top of the fire truck..... 2-28
Figure 2-36: Panel division on the sides of the fire truck 2-29
Figure 2-37: Panel division on the rear of the fire truck..... 2-29
Figure 2-38: Panel Division on the front of the fire truck 2-30
Figure 2-39: Force Balance and Pressure Distribution comparison at 0 Degrees 2-31

Figure 2-40: Force Balance and Pressure Distribution Comparison at 45 Degrees 2-31
Figure 2-41: Force Balance and Pressure Distribution comparison at 90 Degrees 2-32
Figure 2-42: Definition of forces and moments acting on a vehicle [7]. 2-34
Figure 2-43: Center of Gravity of a Truck 2-36
Figure 2-44: The Forces acting in the X-Y plane which create a yawing moment and resultant force. 2-37
Figure 2-45: Reduction of forces in the X-Y plane to a single yawing moment and side force about the center of gravity 2-38
Figure 2-46: Balancing yawing moment and side force against the resistive force per axle. 2-39
Figure 2-47: Lift and Pitching Moment affect weight 2-40
Figure 2-48: The Difference between Relative Wind and Resultant wind 2-43
Figure 2-49: Generation of rolling moments pitched against the weight stabilizing moment. 2-45
Figure 3-1: Experimental setup with the ambulance at a 25 degrees orientation 3-1
Figure 3-2: Convention used to define the Yaw angle with respect to incoming wind.. 3-3
Figure 3-3: Ambulance Cp vs. Velocity distributions for 90 degrees angle of attack..... 3-5
Figure 3-4: Ambulance Cp vs. Velocity distributions for 90 degrees angle of attack including retests (Note: lines were drawn through the experimental data to help differentiate between the different test runs.) 3-6
Figure 3-5: 0 Degree Coefficient of Pressure Test results 3-6
Figure 3-6: 25 Degree Coefficient of Pressure Test results 3-7
Figure 3-7: 45 Degree Coefficient of Pressure test results 3-7
Figure 3-8: 65 Degree Coefficient of Pressure Test results 3-8
Figure 3-9: 90 Degree Coefficient of Pressure Test results 3-8
Figure 3-10: 135 Degree Coefficient of Pressure Test results 3-9
Figure 3-11: 180 Degree coefficient of pressure test results 3-9
Figure 3-12: Panel division on the top of the ambulance 3-11
Figure 3-13: Panel division on the sides of the ambulance 3-11
Figure 3-14: Panel division on the rear of the ambulance 3-12
Figure 3-15: Panel Division on the front of the ambulance 3-12
Figure 3-16: Force Balance and Pressure Distribution comparison at 0 Degrees 3-13
Figure 3-17: Force Balance and Pressure Distribution Comparison at 45 Degrees 3-14
Figure 3-18: Force Balance and Pressure Distribution comparison at 90 Degrees 3-14
Figure 3-19: Definition of forces and moments acting on a vehicle [7]. 3-16
Figure 3-20: Balancing yawing moment and side force against the resistive force per axle. 3-18
Figure 4-1: Experimental setup with the SUV at a 25 degrees orientation 4-1
Figure 4-2: 0 Degree Coefficient of Pressure Test results 4-4
Figure 4-3: 25 Degree Coefficient of Pressure Test results 4-5
Figure 4-4: 45 Degree Coefficient of Pressure test results 4-5
Figure 4-5: 65 Degree Coefficient of Pressure Test results 4-6
Figure 4-6: 90 Degree Coefficient of Pressure Test results 4-6
Figure 4-7: 135 Degree Coefficient of Pressure Test results 4-7
Figure 4-8: 180 Degree Coefficient of Pressure Test results 4-7
Figure 4-9: Panel division on the top of the Suburban 4-9

Figure 4-10: Panel division on the sides of the suburban 4-9
Figure 4-11: Panel division on the rear of the Suburban 4-10
Figure 4-12: Panel Division on the front of the Suburban..... 4-10
Figure 4-13: Force balance and pressure distribution comparison at 0 Degrees 4-11
Figure 4-14: Force balance and pressure distribution comparison at 45 degrees 4-12
Figure 4-15: Force balance and pressure distribution comparison at 90 degrees 4-12
Figure 4-16: Definition of forces and moments acting on a vehicle [7]. 4-14
Figure 4-17: Balancing Yawing Moment & Side Force against the resistive force per axle..... 4-16
Figure 5-1: Wind speed- vehicle speed recommendations for the Typhoon fire truck .. 5-4
Figure 5-2: Wind speed – vehicle speed recommendations for a F-450 Type I ambulance 5-4
Figure 5-3: Wind speed – vehicle speed recommendations for a 4x4 ¾ ton Suburban (full of equipment)..... 5-5

List of Tables

Table 2-1: Center of gravity of the Typhoon truck 2-36
Table 2-2: Wind speed to cause a static course deviation-Typhoon -The fire truck is not moving. 2-42
Table 2-3: Typhoon vehicle speed and necessary crosswind speed to cause a resultant wind speed of 40m/s at 45degrees. 2-43
Table 2-4: Center of Gravity of the Cyclone II X113 2-44
Table 2-5: Wind Speed to Cause a Static Course Deviation-Cyclone. 2-44
Table 2-6: Cyclone Vehicle speed and necessary crosswind speed to cause a resultant wind speed of 40m/s at 45degrees. 2-44
Table 2-7: Wind speeds to cause static overturning at different yaw angles 2-45
Table 2-8: Vehicle speed and necessary crosswind speed to cause a resultant wind speed of 87m/s at 45degrees. 2-46
Table 3-1: Wind Speed to Cause a Static Course Deviation-Ambulance-The vehicle is not moving. *Denotes instability in the rear axle. 3-20
Table 3-2: Ambulance vehicle speed and necessary crosswind speed to cause a resultant wind speed of 34m/s at 25degrees. 3-21
Table 3-3: Ambulance vehicle speed and necessary crosswind speed to cause a resultant wind speed of 28.m/s at 45degrees. 3-21
Table 3-4: Ambulance vehicle speed and necessary crosswind speed to cause a resultant wind speed of 28.4m/s at 65degrees. 3-22
Table 3-5: Ambulance wind speeds to cause static Overturning at different Yaw Angles 3-22
Table 3-6: Vehicle speed and necessary crosswind speed to cause a resultant wind speed of 68m/s at 25degrees. 3-23
Table 3-7: Vehicle speed and necessary crosswind speed to cause a resultant wind speed of 54m/s at 45degrees. 3-23
Table 3-8: Vehicle speed and necessary crosswind speed to cause a resultant wind speed of 50m/s at 65degrees. 3-23
Table 4-1: Wind Speed to Cause a Static Course Deviation-Ambulance-The vehicle is not moving. *Denotes instability in the rear axle. 4-18
Table 4-2: Suburban vehicle speed and necessary crosswind speed to cause a resultant wind speed of 65m/s at 25degrees. 4-19
Table 4-3: Suburban vehicle speed and necessary crosswind speed to cause a resultant wind speed of 67m/s at 45degrees. 4-19
Table 4-4: Suburban vehicle speed and necessary crosswind speed to cause a resultant wind speed of 38m/s at 65degrees. 4-20
Table 4-5: Suburban wind speeds to cause static Overturning at different Yaw Angles . 4-20
Table 4-6: Vehicle speed and necessary crosswind speed to cause a resultant wind speed of 68m/s at 65degrees. 4-21
Table 5.1: Classification of wind speed driving conditions for each vehicle 5-3

1 INTRODUCTION

When a hurricane hits a municipality, the fire and rescue department plays a very active role in helping with the preparation, evacuation, and recovery tasks. Consequently, fire department, as well as law enforcement, personnel and vehicles might have to be on the road even when the wind speeds are so high that the safety of the vehicles might be compromised. It is therefore important to define the threshold wind speed beyond which vehicles should not be allowed to operate. Likewise, in the event of an evacuation it is important to define when the fire vehicle can safely evacuate.

Some fire and rescue departments do not allow vehicles on the road with sustained winds of 35 mph while others may use a wind speed of 45 or 55 mph, or 60 mph. These wind speeds limits vary from department to department because there are no undisputed scientific criteria on which to base the decision. So, each department must rely on its experience and subjective evaluation of the risk involved when defining the wind speed limits.

For this reason the Florida Department of Community Affairs asked a group of researchers to develop a set of criteria to define unequivocally the upper limit wind speeds at which different fire and rescue vehicles can operate safely. This report describes the results of this project for a fire truck, ambulance, and a sports utility vehicle.

The strategy adopted for this research was to investigate the effect of the wind on the vehicles following on the steps of previous researchers [1-6; 15-34], though a series of wind tunnel tests. The method of computing force based upon pressure distribution around each model was validated through a comparison with force balance measurements. For the fire truck the results were compared to a full-scale field tests and computer simulations. The wind forces and moments acting on the vehicles for different wind speeds were estimated from the tests. The critical wind speed occurs when the wind induced forces and moments exceed the resisting effects.

2 FIRE TRUCK

2.1 WIND TUNNEL EXPERIMENTATION

2.1.1 Experimental Setup

Testing was conducted at Florida Tech's Low Speed Wind Tunnel facility with a test chamber section 54 cm x 54 cm. A fire truck model 31 cm long, 11 cm wide, and 9 cm tall was tested for pressure distributions on its surfaces at various incoming wind angles. The model tested was a generic toy fire truck manufactured by Tonka™, which closely resembles the Typhoon Pumper constructed by the manufacturer E-One (Emergency One).

Figure 2-1: Experimental setup with the fire truck at 0 degrees orientation

Figure 2-1 above is a picture of the fire truck supported in the center of the test chamber. The platform serves the purposes of dampening vibrations and mimicking the ground effect a vehicle experiences. A Pitot-static tube above the model gives the reference dynamic pressure by measuring the free stream total and static pressures. The Pitot-static tube is 61cm long (24 inches) constructed from stainless steel. Located on the front, sides, top, and rear of the fire truck are fifteen pressure taps, which are used to measure surface pressure at their respective locations. These pressure taps are constructed from holes drilled into the model at certain locations. The holes have a 1.6mm diameter 5cm length brass tube mounted flush with the outer surface and held in place with a strong epoxy. Inside the model these brass tubes are attached to flexible 1.6mm diameter Tygon

tubing that runs out of a hole cut in the bottom of the model, through a PVC piping underneath the platform and attaches to a *Multiple Port Pneumatic Intelligent Pressure Scanner* (Model 9010). The PVC piping underneath the platform protects the tubing from flapping at higher wind speeds. The location of the pressure taps and numbering convention can be seen in the pictures displayed in Appendix 1A.

The Model 9010 Pneumatic Intelligent Pressure Scanner is manufactured by Pressure Systems and is a completely self–contained pressure acquisition module for multiple measurements of dry, non-corrosive gases. The scanner can be easily interfaced with an RS-232 serial port on any personal computer. The start up software runs through MS-DOS and allows for the collection of data at a specified interval of time. There are 16 pressure input channels, in addition to a run-reference channel and a calibration-reference channel. Dynamic pressures up to 5 psi can be read between the run-reference channel and any of the 16 input channels. Compressed air is used at 85 psi during startup of the equipment to calibrate and re-zero the system. During testing dynamic pressures from 15 locations on the model and one from the Pitot tube are recorded through the 16 channels on the scanner.

2.1.2 Experimental Procedure

For varying velocities up to 20 m/s, surface pressures at the 15 tap locations were recorded. The pressure data was recorded every 3 seconds for a total time of 8 minutes. Prior to data acquisition at least two minutes were allowed for the wind tunnel to settle at each velocity. Another parameter tested was pressure distribution as a function of incoming wind angle. This was done by repeating the test for all velocities at yaw angles of 0, ± 45, ± 90, ± 135, and ±180 degrees. 0 degrees is defined as the condition where the front of the fire truck faces the oncoming wind. Viewed from above: positive angles were defined in the clockwise direction and negative angles were defined as counter clockwise. This is shown in Figure 2-2 below.

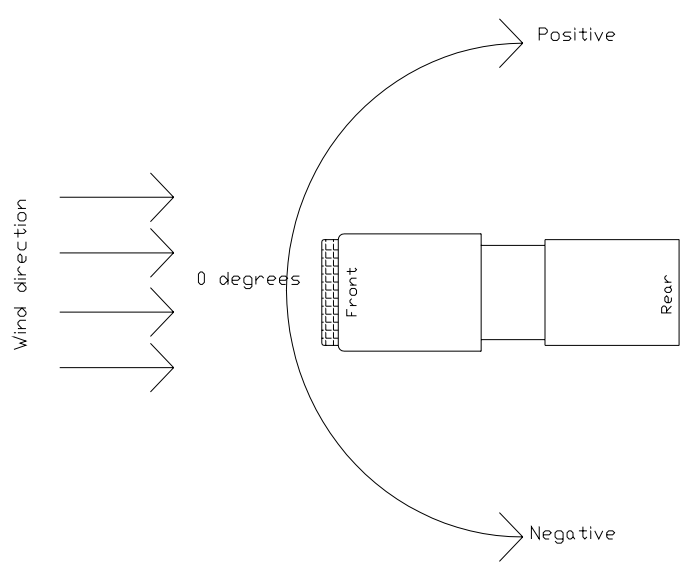

Figure 2-2: Convention used to define the angle with respect to incoming wind

2.2 WIND TUNNEL RESULTS

2.2.1 Scatter in Measurements

The initial problem encountered during testing was an apparent wide range of scatter in the results. For pressure measured through the Pitot-static tube there was an increase in deviation from the mean with increasing velocity, but it was much less than the deviation observed for the pressure taps on the model. Initially the source of this scatter was unknown and a cause for concern. Figure 2-3 below displays the reference pressure measured through the Pitot-static tube for a 0 degree test. Figure 2-4 below displays the pressure measured through tap #10 on the fire truck model for the same test. Tap #10 faces the oncoming flow and is located roughly in the middle of the model so it should display the same results as the total pressure (measured with the pitot static tube; note that the static reading from the Pitot-static tube is used for all the freestream static reference). The graphs show pressure with respect to time. The graphs also illustrate the pressure changes corresponding to a change in velocity, since each rise in pressure corresponds to a change in the wind speed. For a Pitot-static tube, the velocity can be computed with the use of Bernoulli's equation [2]:

$$V = \sqrt{\frac{2(p_{total} - p_{static})}{\rho_{air}}} \tag{2-1}$$

In this equation

ρ is the density of air

V is the velocity

p_{static} is the static pressure measured with the Pitot-static tube

p_{total} is the total pressure measured with the Pitot-static tube

The step increases in pressure caused by an increase in wind velocity are very distinct for the freestream total pressure tap displayed in Figure 2-3, but less distinct for tap #10 on the fire truck as seen in Figure 2-4.

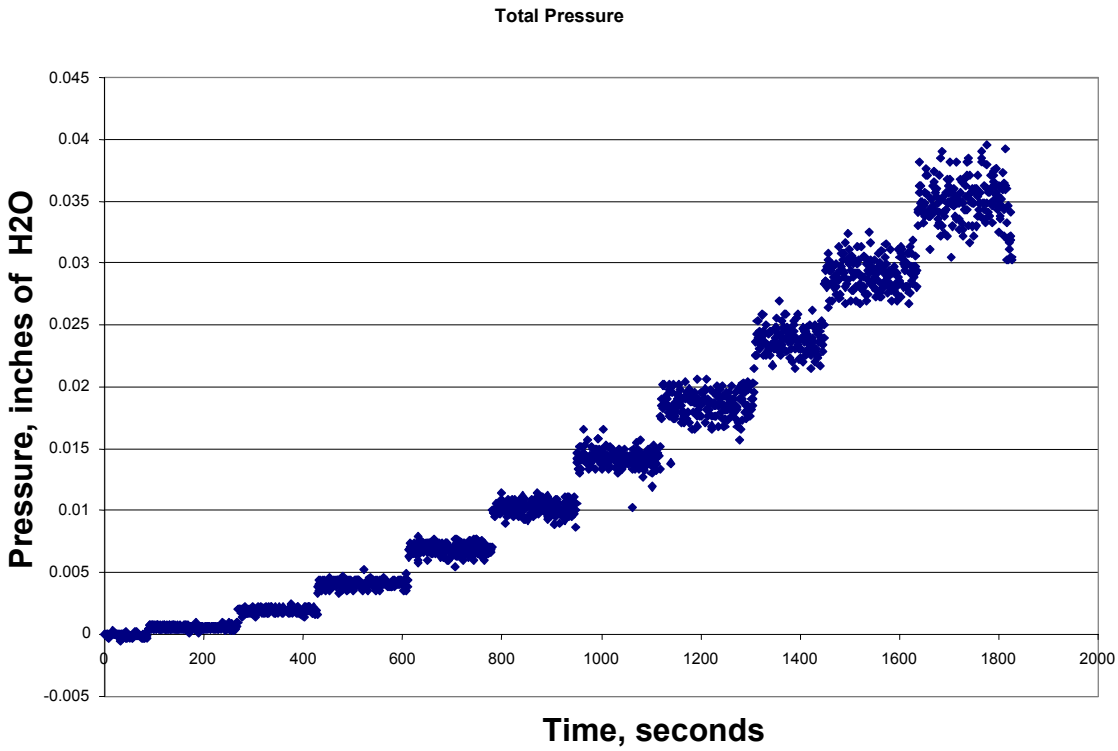

Figure 2-3: Scatter in the freestream total pressure pap vs. time at different speeds

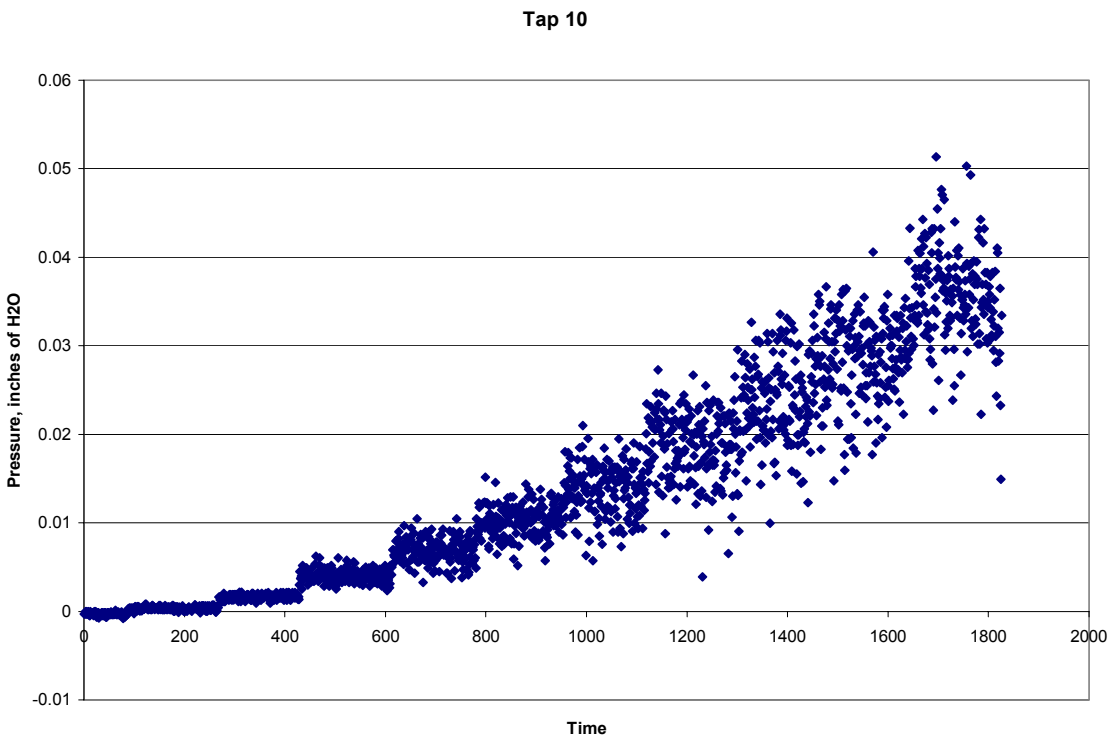

Figure 2-4: Scatter in tap #10 pressures vs. time at different speeds

It was felt that this scatter might be caused by the surface roughness of the model resulting in transition to turbulence in the boundary layer. This is a desired quality for matching Reynolds number between the model and a full-scale fire truck, as will be discussed in detail later in this report. Nevertheless, it was felt that steps should be taken to ensure that this scatter was not a product of the experimental setup itself. Thus the following steps were taken:

1) The electronics were shielded to ensure that electro-magnetic field created by wind tunnel's 15 kW electric motor were not causing interference.

2) The connections for the pressure taps were individually checked to ensure that there were no leaks.

3) A platform was constructed for the model to ensure that all possible vibrations would be dampened. The platform served the dual purpose of mimicking a ground effect.

4) A PVC piping system was constructed to protect the thin Tygon tubing from vibrations at higher wind tunnel velocities.

Figure 2-5 below shows the results of these efforts for a test similar to the ones presented above. As can be seen the scatter was somewhat reduced, but was not eliminated.

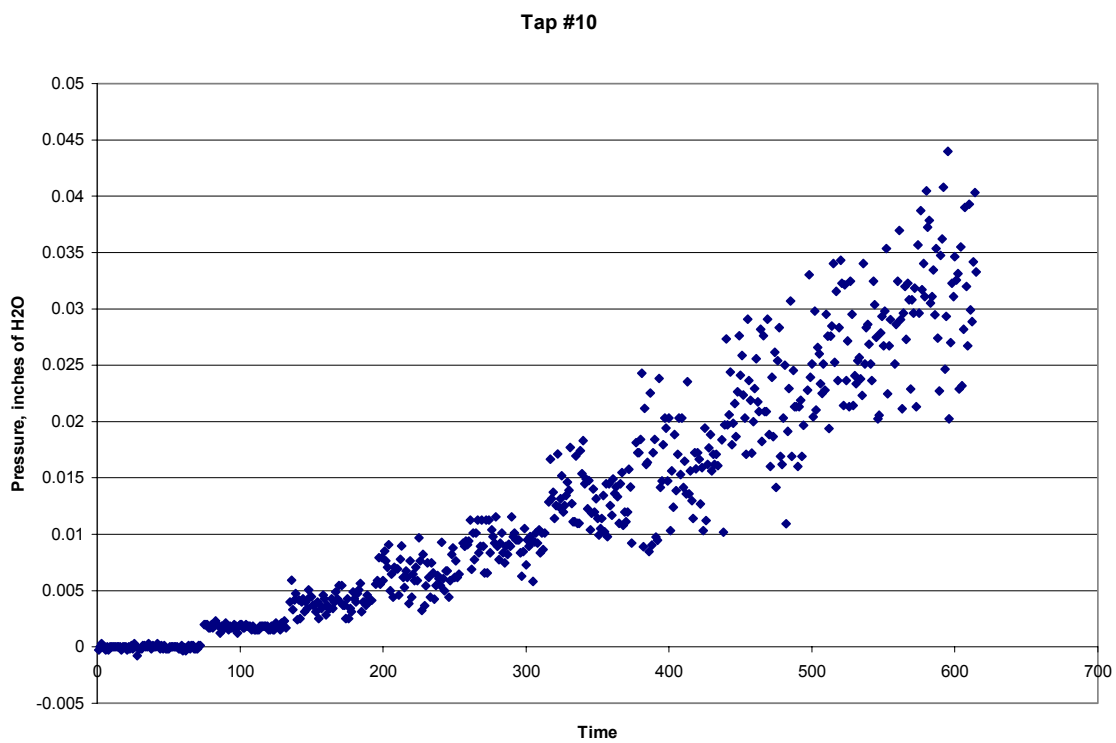

Figure 2-5: Scatter in tap #10 pressures vs. time after corrective steps were taken

2.2.2 Wind Tunnel Test Results

The surface pressure values measured at various locations on the fire truck were averaged over a 8 min test period and then used to calculate, with the reference total pressure, the value for the coefficient of pressure (Cp) at each tap location. Cp is calculated using the equation from Anderson [2]:

$$C_P = \frac{p_t - p_s}{p_{total} - p_s} \tag{2-2}$$

In this equation:

C_p is the Coefficient of Pressure

p_t is defined as the tap pressure (15 of them) on the model

p_s is the static pressure measured with the Pitot-static tube

p_{total} is the total pressure measured with the Pitot-static tube

The pneumatic pressure scanner has an accuracy of ± 1031 Pa (0.15 psi) when working in a range of less than 17188 Pa (2.5 psi). By taking multiple data readings at one velocity this accuracy can be improved further. The calculated accuracy for coefficient of pressure, when recording data every 3 seconds for 8 minutes at one velocity is ±0.03. This type of accuracy was observed in the results, some of which are seen in Figure 2-6. The following figure is a plot of Cp vs. Velocity for the pressure taps on the windward side of the model during a 90-degree testing (i.e., the side facing the flow). It is observed that the Cp values vary with the tap locations. Despite the changes in velocity it can be seen that the Cp value at each location remains fairly constant. The values for Cp at each location; however, change with changes in the incoming wind direction, with more pressure on the windward side and less on the leeward side. Steep pressure gradients occur at the corners and surface steps. These pressure distributions will be used to calculate the forces acting on the model or the fire truck.

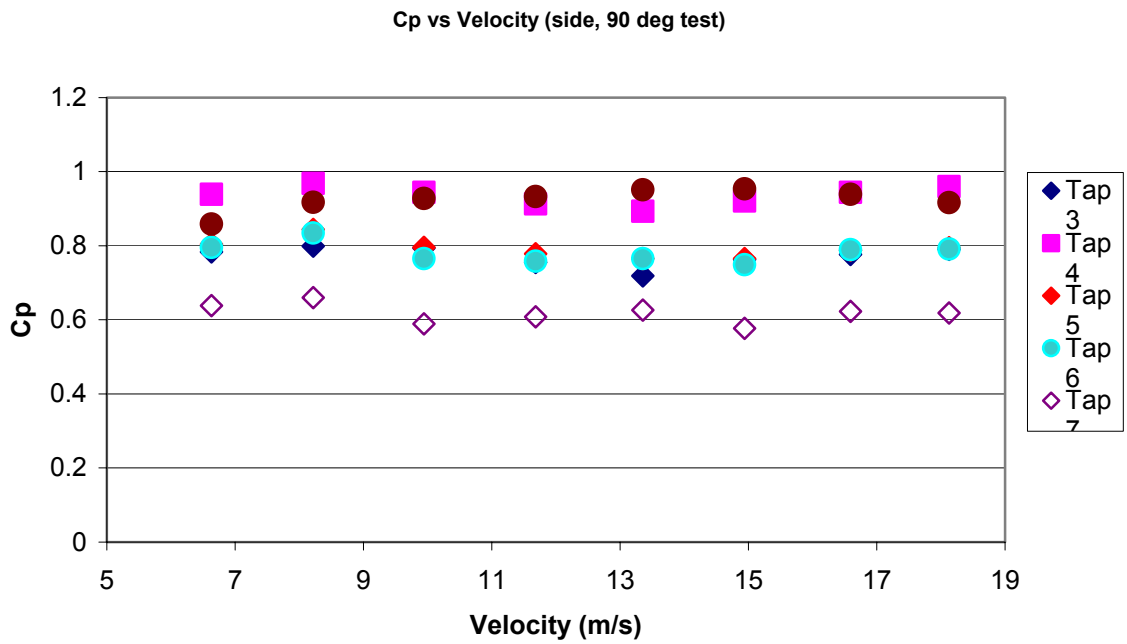

Figure 2-6: Typical Cp vs. velocity distributions at windward tap locations for 90 degrees angle of attack

The complete results for the wind tunnel testing are displayed as Cp vs. velocity for each pressure tap for the various angles tested in Appendix 1B. Figures 2-7 to 2-11 summarize these results. Although the model is instrumented on only one side the argument is made that because the model is symmetric, pressure distributions on one side of the model at a specified angle will be the same as on the opposite side of the model if the angle is negative. Symmetry allows for the combination of the ± orientations to obtain a picture of the pressure distributions about the model at orientations between 0 and 180 degrees. The model is of course not perfectly symmetric. This is particularly true on the top of the model and in addition to other small features there exists a ladder on one side and not the other. Small differences in surface geometry were apparent in the results. Because the pressure taps on the top lie mostly along the line of symmetry they should for either ± orientation (i.e. ±45°) show the same value. In certain cases when the protrusions were windward of the pressure taps the values differed. For purposes of analysis, the values chosen to represent the surface were the condition when there was no interference.

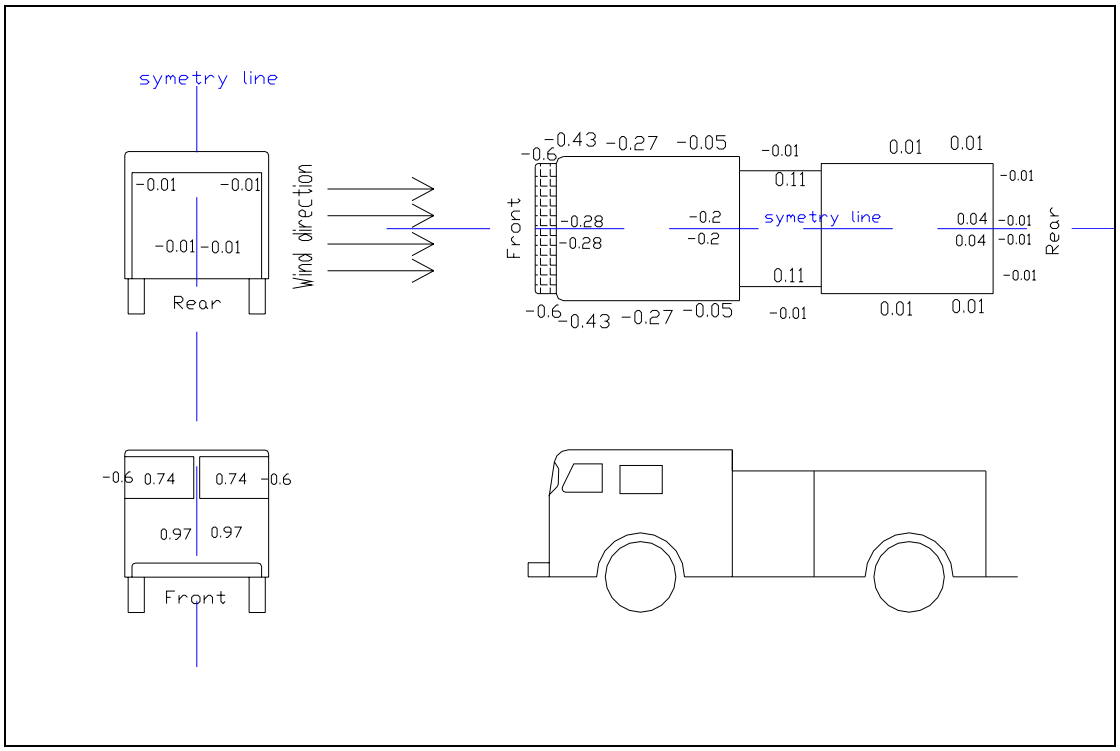

Figure 2-7: 0 degree coefficient of pressure test results

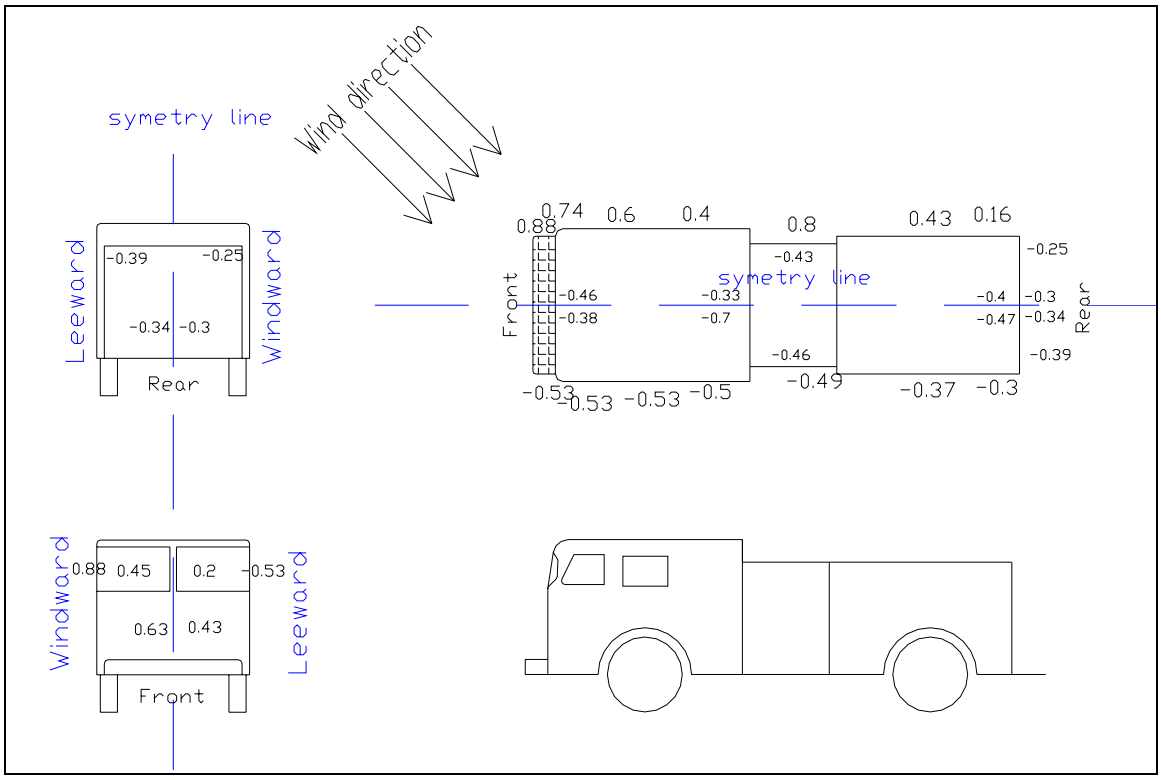

Figure 2-8: 45 degree coefficient of pressure test results

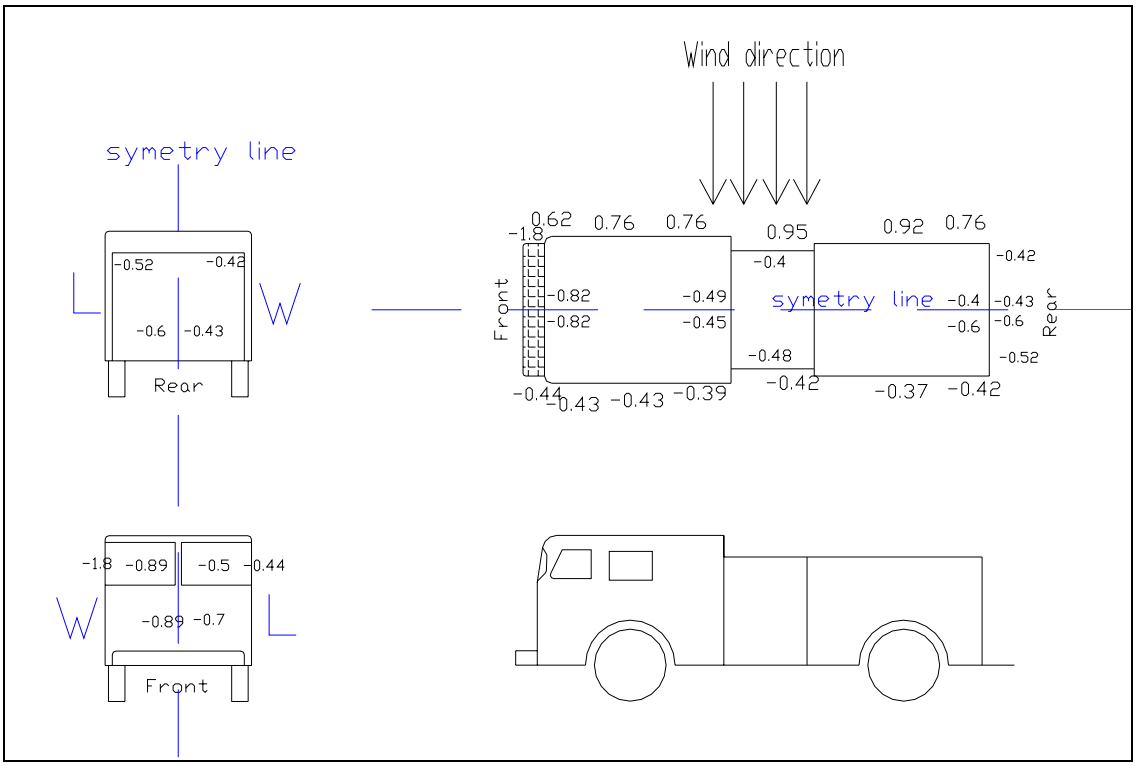

Figure 2-9: 90 degree coefficient of pressure test results

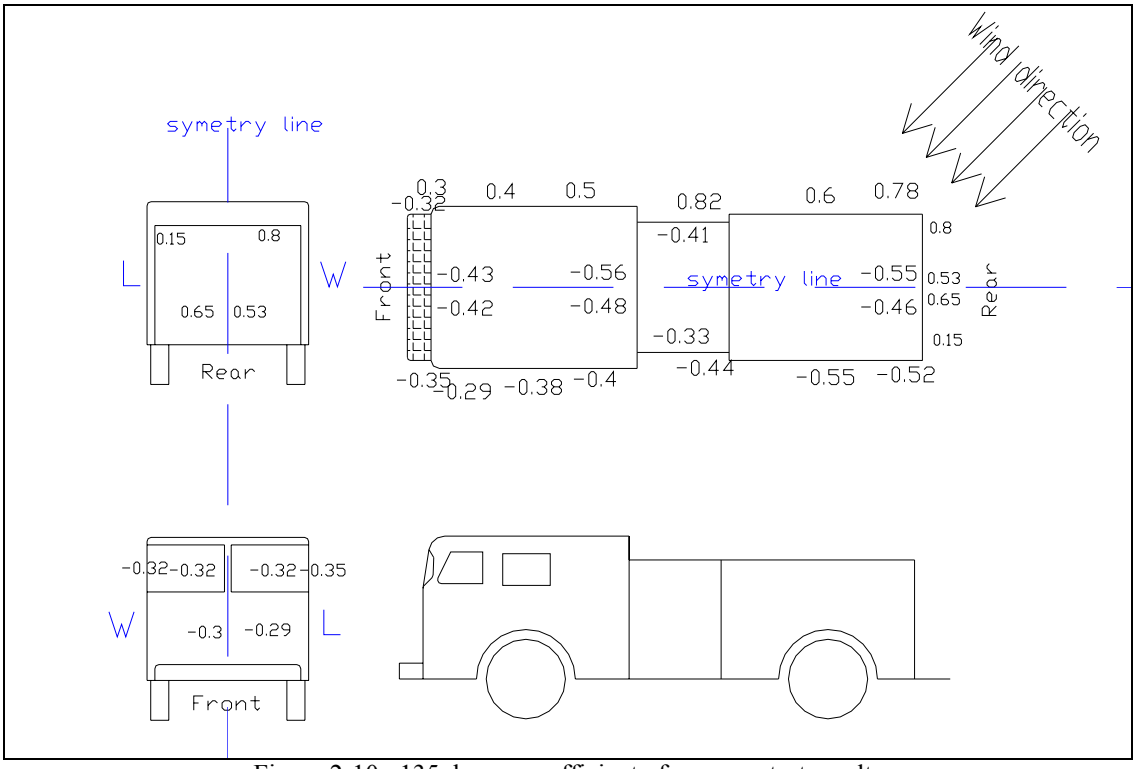

Figure 2-10: 135 degree coefficient of pressure test results

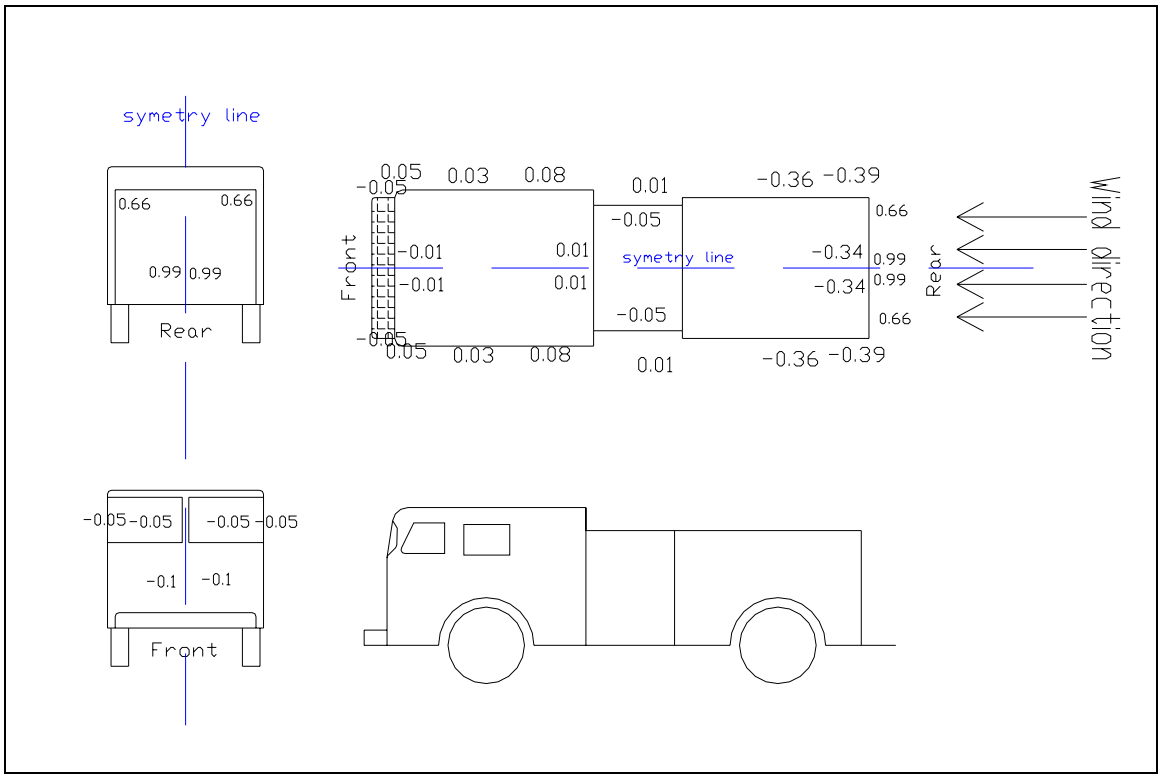

Figure 2-11: 180 degree coefficient of pressure test results

2.3 FULL SCALE FIRE TRUCK – FIELD TEST

2.3.1 Introduction

Testing was also done on a full size fire truck. Testing was done with the help of the Satellite Beach fire department. An Emergency One 1991 Protector series fire truck was used for the field test. The Protector series was manufactured by the company Emergency-One. In recent years E-One has renamed the Protector series as the Cyclone series. Thus the Protector tested has a very similar body styling to the modern Cyclone II X113 Pumper. It is seen in Figure 2-12 below. In addition, the Protector and Cyclone trucks have the same cab and rear compartments as the Typhoon fire truck model, shown in Figure 2-13 below. As mentioned previously, the Typhoon is very similar to the model tested in the wind tunnel. The only difference between the Typhoon and Cyclone vehicles is that the Cyclone has a slightly longer body with an empty gap between the cab and rear compartments. The pumping mechanisms are also slightly larger. This difference can be seen in the figures below.

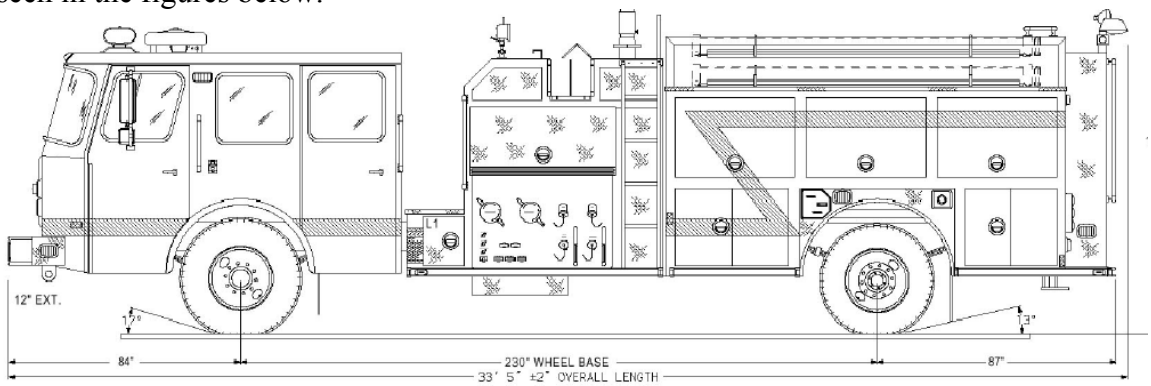

Figure 2-12: Schematic drawing of the E-One Cyclone II X113 Pumper [1]

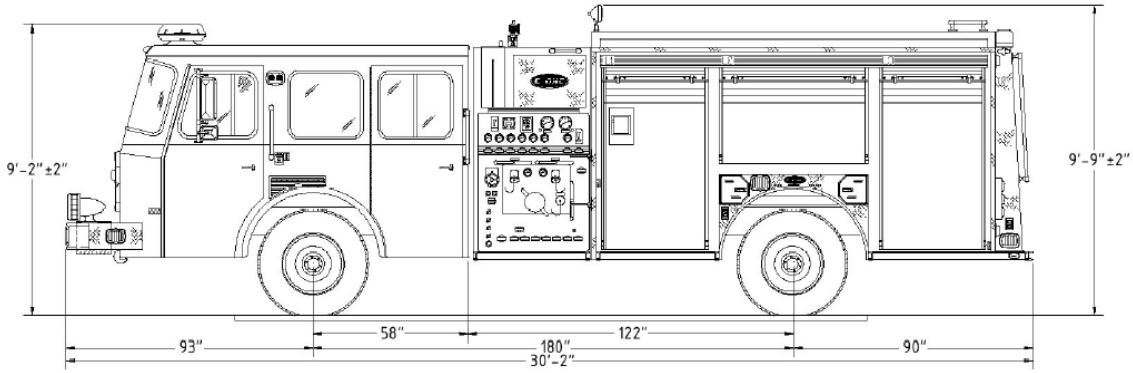

Figure 2-13: Schematic of the E-One Typhoon Pumper [1]

2.3.2 Preliminary Testing

Preliminary testing to validate the instrumentation to be used for testing was done in both the wind tunnel and with a minivan. The minivan was outfitted with an anemometer, Pitot tube, and various pressure taps. During a test drive the anemometer and Pitot tube readings for different velocities were compared to the speedometer of the vehicle. The

instrumented minivan is shown in Figure 2-14 below. The anemometer and aluminum mast are highlighted in white so that they are visible in the picture.

Figure 2-14: Instrumented Minivan for preliminary testing.

The Pitot tube, and Pneumatic Pressure Scanner are the ones used in the wind tunnel and their description can be found in the previous section 3.1.1. The anemometer mounted on the mast over the vehicle is used to obtain velocity and direction of the wind along with temperature. A *weather wizard III* system was used for the data acquisition. Weather wizard III monitors and stores data about the most essential weather conditions: inside and outside temperatures, wind direction, wind speed and wind chill. It was connected to the COM-port of the computer for the first reading and then disconnected from the port. It has the ability to store daily data in its memory. Once the test is finished the acquired data can be downloaded to a computer.

2.3.3 Experimental Setup

The Protector was instrumented similarly to the wind tunnel model, with the exception that holes were not drilled into the surface of the fire truck; rather the brass and Tygon tubing were taped onto the external surface of the vehicle. The brass tubes in this test were connected to the Tygon tubing on one end and sealed at the other end. The brass tubes were 5 cm long, with a 1.6 mm internal diameter, and had a 0.4mm diameter hole drilled in the side to create an opening, and this opening was mounted perpendicular to the surface where it was placed. The tube with the Tygon tubing mounted to the vehicle is shown in Figure 2-15 below. The same Pneumatic pressure scanner as for the wind tunnel tests was used to record the pressure at 15 locations on the fire truck. Pictures of the fire truck instrumentation and the locations where pressure data was recorded are shown in Appendix 1C.

Figure 2-15: Surface pressure brass tube and Tygon tubing mounted to the fire truck

A 0 Degree test was conducted by driving the fire truck down the expressway at various speeds. Vehicle speed was measured with the odometer inside the vehicle. Outside the vehicle wind speed was measured with an anemometer connected to a *Weather Wizard III* and also with a Pitot-static tube. Both anemometer and Pitot static tube were mounted on an aluminum pipe approximately 1.25 m (50 in) above the fire truck. The anemometer was mounted at a height of 3.66 m (144 in) above the ground. The Pitot-static tube was mounted at a height of 4.06 m (160 in) above the ground. This was to ensure that these instruments were exterior to the fire trucks' boundary layer. Figure 2-16 below shows a picture of the instrumented fire truck. Both aluminum pipe and anemometer are visible mounted just aft of the cab.

Figure 2-16: Instrumented Fire Truck

2.3.4 Field Test Results

2.3.4.1 Calculation of wind speeds

The environmental conditions on the day of test were: clear sky with temperature of 75 ^{o}F with relative humidity of 72%. The wind direction was from ESE at 6 mph. The-recorded data from the anemometer before the test run was: temperature 75 ^{o}F; wind direction was from E at 4 mph. The participants in this test drive were Dr. C.S. Subramnanian, Dr. J.P.

Pinelli, research assistant Vidya Chakravarthi, and Captain. James Keating who drove the vehicle during the test. The test was started from the Satellite Beach Fire Department. The Vehicle was driven south on I-95 highway from the Wickham Road to Vero Beach and North on the return trip from Vero Beach to Wickham Road. The truck was driven over distances of roughly 10 miles each at speeds of 20m/s (45mph), 25m/s (55mph) and 30m/s (67mph). The return 30 miles were covered at an average speed of 29 m/s (65mph). The speedometer inside the vehicle determined these speeds.

The Pitot-static tube in conjunction with the Pneumatic Scanner was used to calculate the velocity in the same way it was used to calculate the velocity in the wind tunnel testing. The time history plot of velocity computed from the Pitot-tube readings is shown in Figure 2-17 below. The average computed wind speeds from the Pitot-tube were 24m/s (51mph), 28 m/s (63mph) and 33.0m/s (72mph), and a return speed of 28m/s (63mph).

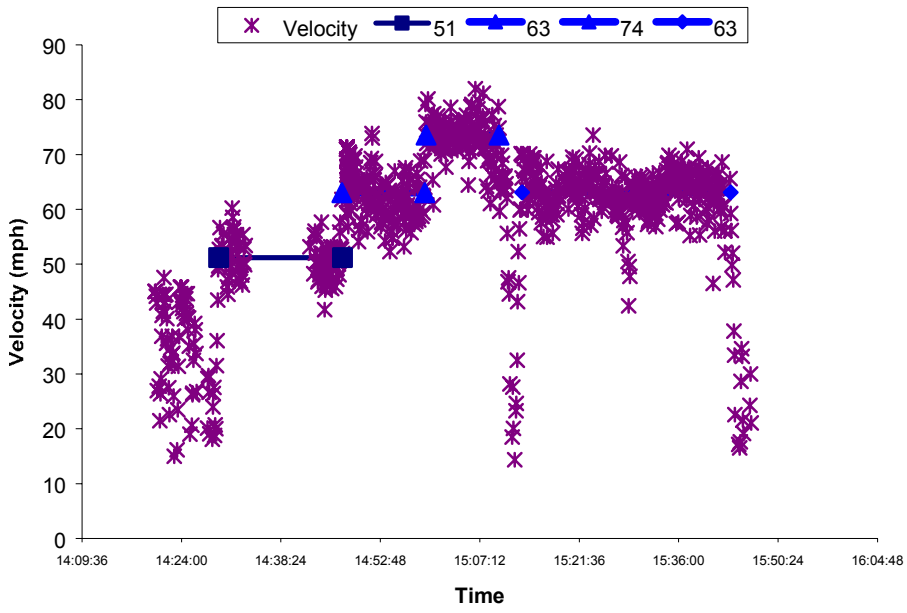

Figure 2-17: Time history plot of velocity measured from Pitot-static tube.

The anemometer acquired wind data on velocity and direction for every one minute. The average measured wind speeds from the anemometer are 24 m/s (51mph), 29.0 m/s (66mph) and 35.0 m/s (78mph). The return speed noted from the anemometer is 29 m/s (65mph). The time history plot of anemometer velocity is shown in Figure 2-18 below. A comparison of the average speeds measured with the three devices is shown in Figure 2-19 below.

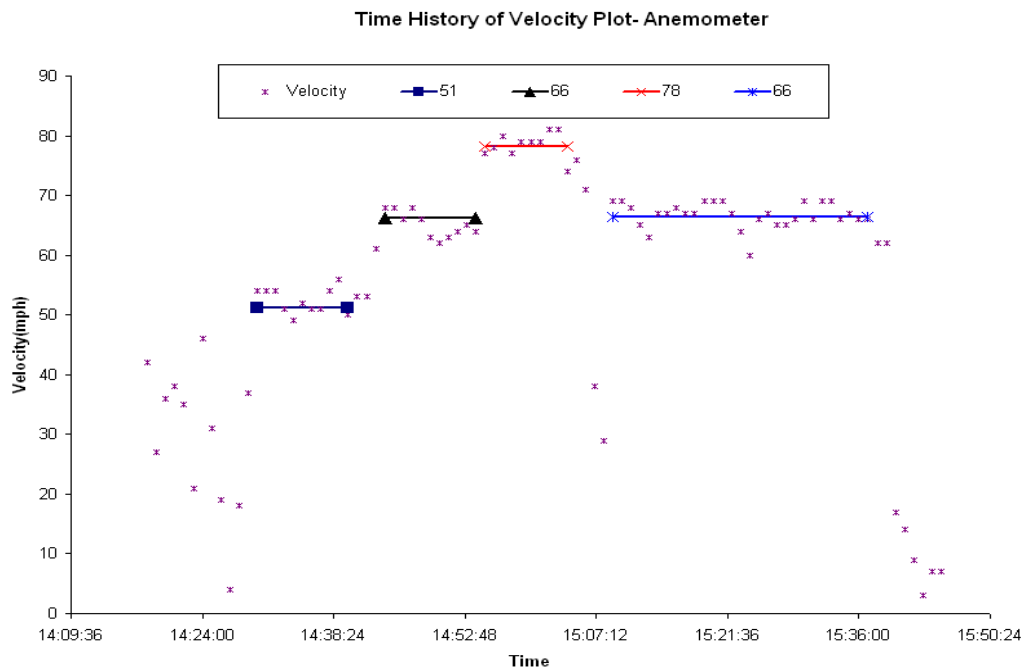

Figure 2-18: Time history plot of velocity measured from Anemometer

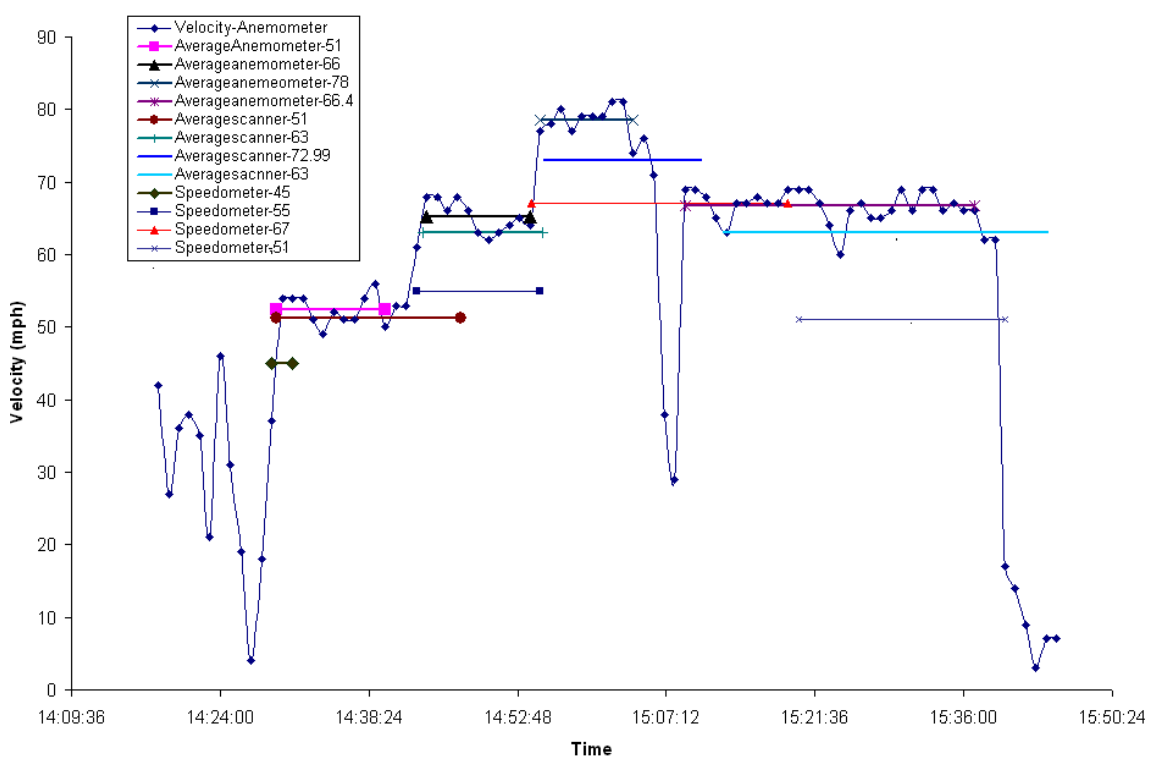

Figure 2-19: Comparison of the average speeds measured from all the 3 instruments

As can be seen in Figure 2-19 above the three measuring devices do not predict the same vehicular speed. This difference is attributed to a small crosswind on the day of testing. The difference in the measured values of velocity from the different instruments is explained with the help of a vector diagram in Figure 2-20 (not to scale) below. AB

represents the air speed resulting from the truck speed (from speedometer). It is opposite to the motion of the truck. AC represents the total wind speed in the direction of the truck (from Pitot-tube). BD represents the free flow wind speed (e.g. from National Weather Service). AD represents the total air speed with respect to the truck (from the anemometer). Figure 2-20 (a) is the vector representation for the truck moving southward on the I-95 highway. Figure 2-20 (b) is the vector representation for the truck moving northward

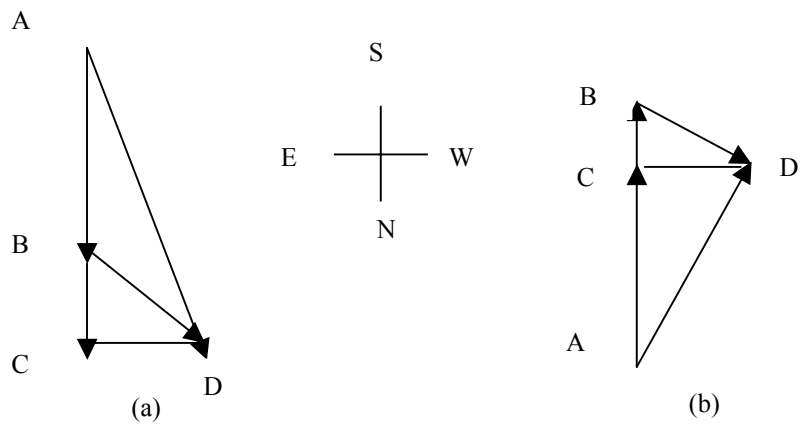

Figure 2-20: Vector representation of the measured speeds

2.3.4.2 Calculation of pressure coefficient Cp values

The dynamic pressure readings of all the taps over the surface of the truck were acquired for every 5 seconds from the pneumatic pressure scanner. As an example of the pressure readings, the time history of pressure tap FC (scanner port 01) is shown in Figure 2-21.

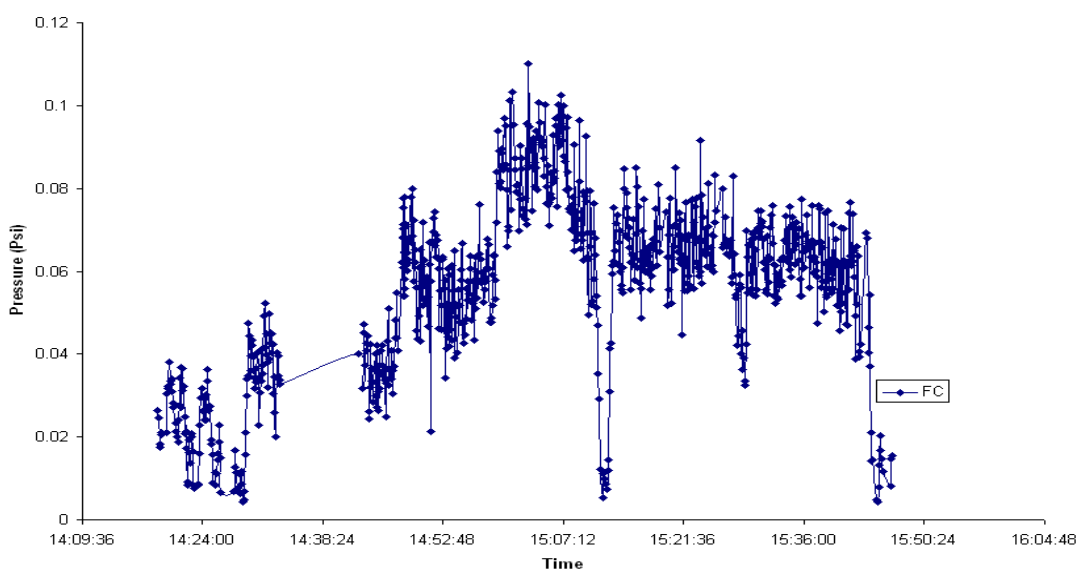

Figure 2-21: Time history of pressure for tap FC on the front face of the fire truck.

From these pressure values, the pressure coefficients Cp were computed at different tap locations using Equation 2-2 presented in the previous chapter. Time history plots of the Cp values for the different tap locations are shown in Appendix 1D.

With this type of experiment there were several sources of error. One is that wind gusts could not be predicted or controlled. In addition, because testing was done on the expressway, passing automobiles were another source of gusting winds. Pressures at the 15 taps were recorded throughout the entire test and significant scatter was seen in the plots for pressure with respect to time. This scatter was attributed to passing vehicles and other unknown anomalies. In order to correct for the scatter, as in the wind tunnel, the pressure at each location was averaged for each velocity to compute the Coefficient of pressure at each location. The plots of Cp Vs wind speed are also shown in Appendix 1D for the different tap locations. The Cp values appear to be constant within the degree of precision for the different velocities tested and these results are summarized in Figure 2-22 below.

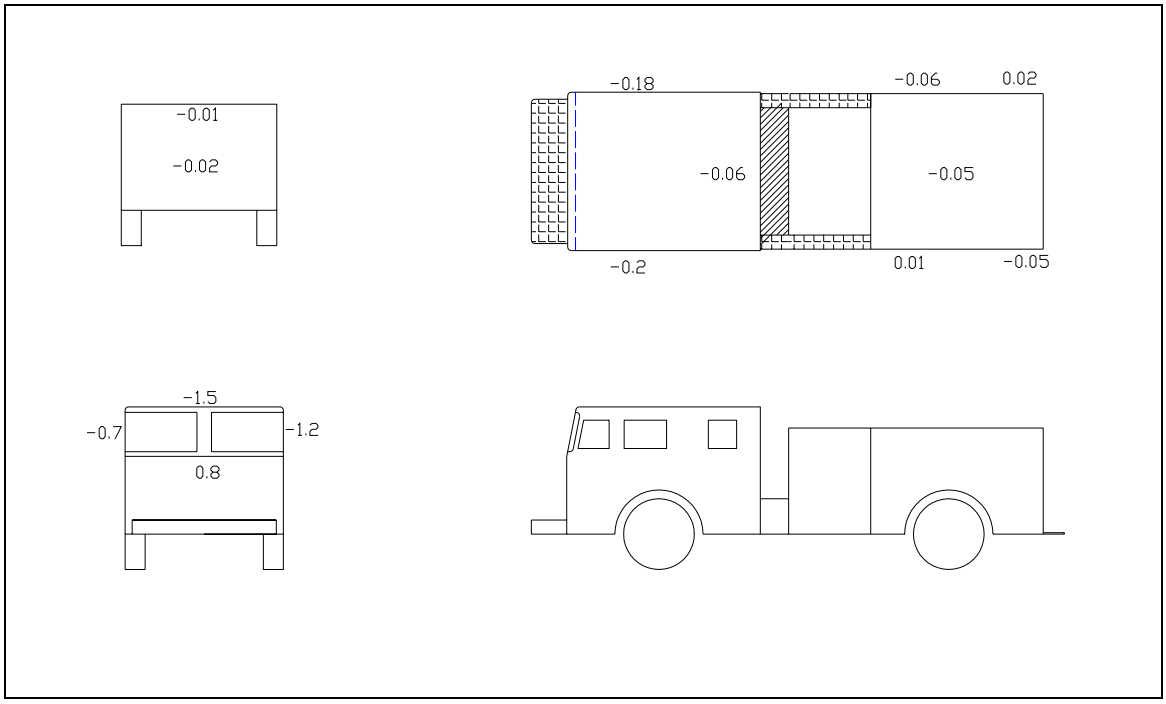

Figure 2-22: 0 Degree Coefficient of Pressure Field Test Results

2.4 COMPUTER SIMULATION

2.4.1 Introduction

The objective of fire truck or any ground-vehicle aerodynamic testing is determination of the aerodynamic characteristics of on-road vehicles during typical modes of operation. To obtain this information most of the aerodynamic testing is conducted in wind tunnels employing scale models. Unfortunately, wind tunnel testing introduces a set of complications. One of these is the constraint imposed on the model flow field by the walls confining the test-section air stream. This constraint can increase the effective free-stream velocity by limiting the available flow-area in the vicinity of the vehicle (blockage effect), alter the flow pattern about the vehicle by intruding into its flow field (wall-effect), or cause a free stream static pressure gradient along the test section because of the growth of boundary layers on its walls (buoyancy effects). To a large degree in practice, wind tunnel design can reduce the flow-quality and tunnel wall effects to small and possibly even negligible magnitudes. However, because of limitations placed on tunnel size by economic considerations, the development of appropriate corrections is often required for tunnel-wall effects. Recognizing limitations of wind tunnel boundary conditions, considerable efforts were made in last decade to study the vehicle aerodynamics computationally. Here, a three-dimensional flow analysis around the fire truck has been performed to understand the airflow characteristics surrounding it. The flow distribution is calculated by solving the Navier-Stokes equation with a two-equation k-ε. This chapter concentrates on how a computational fluid dynamics software, Fluent, was used to obtain the Cp values with emphasis on the grid density and its effect on the results. Similar research was done by Subrato Roy to understand the flow around a truck body and also to see the effect of vehicle design on the drag reduction of the vehicle [4 & 5].

2.4.2 Theory of the CFD model: k-ε model

Turbulent flows are characterized by fluctuating velocity fields. These fluctuations mix transported quantities such as momentum, energy and species concentration, and cause the transported quantities to fluctuate as well. Since these fluctuations can be small scale and high frequency, they are computationally expensive to simulate directly in practical engineering calculations. Instead, the instantaneous (exact) governing equations can be time-averaged, ensemble-averaged, or otherwise manipulated to remove the small scale, resulting in modified equations that are computationally less expensive to solve. The modified equations contain additional unknown variables, and turbulence models are needed to determine these variables in terms of known quantities. There are many different viscous models present in Fluent, which can be used for different types of problems.

1. Sparta-Allamaras model
2. K-ε model
    a. Standard K-ε model
    b. Renormalization-group (RNG) K-ε model

    c. Realized K-ε model
3. K-ω model
    a. Standard K-ω model
    b. Shear-stress transport (SST) K-ω model
4. Reynolds stress model (RSM)
5. Large –eddy simulation (LES) model

The choice of model will depend on considerations such as the physics encompassed in the flow, the established practice for a specific class of problems, the level of accuracy required, the available computational resources and the amount of time available for simulation. While it is impossible to state categorically which model is best for a specific application- general guidelines are presented by the (Fluent) manufacturer. Fluent provides comprehensive modeling capabilities for a wide range of incompressible and compressible, laminar and turbulent fluid flow problems. Steady state or transient analysis can be performed. In Fluent, a broad range of mathematical models for transport phenomenon is combined with the ability to model complex geometry. The flow distribution is calculated by solving the Navier-Stokes equation with a two-equation k-ε. This model is a semi-empirical model based on model transport equations for the turbulence kinetic energy (k) and its dissipation rate (ε). The model transport equation for k is derived from an exact equation, while the model transport equation for ε was obtained using physical reasoning and bears little resemblance to its mathematically exact counterpart**.**

2.4.3 Preliminary Testing

As part of the preliminary testing a 2D model was generated in Gambit.

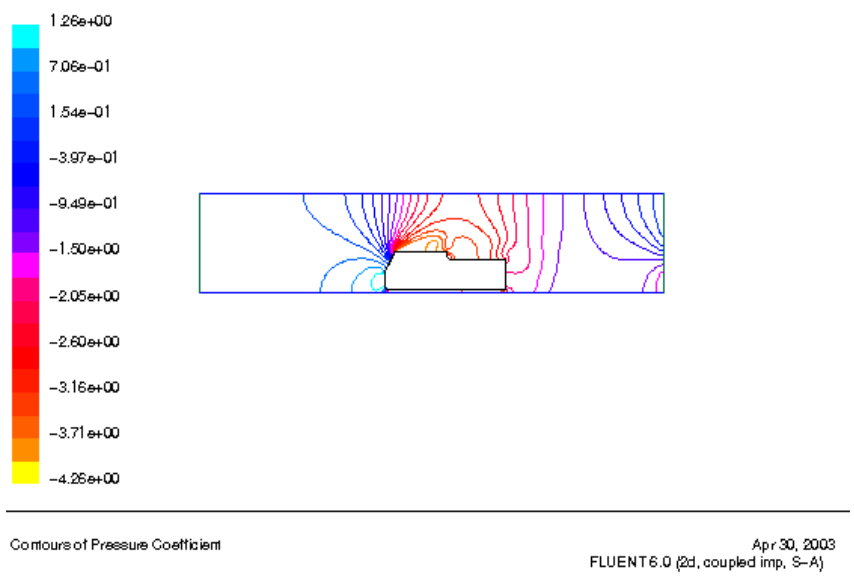

Figure 2-23: 2D-model of truck

From the Figure 2-23 above the stagnation pressure points and low-pressure regions are observed. The front of the face has a stagnation point. Over the top of the body there exists low-pressure regions. The above model resembles the wind tunnel model that was used.

Next a test cube (shown in Figure 2-24) was created in Fluent to see what the procedure should be to obtain symmetry in the flow around the model. By doing this it became clear what should be the boundary conditions used and the solver used. In this test it was observed that the outer block designed near to the cube model created a boundary layer effect. So in later simulation the outer block was placed very far from the truck model.

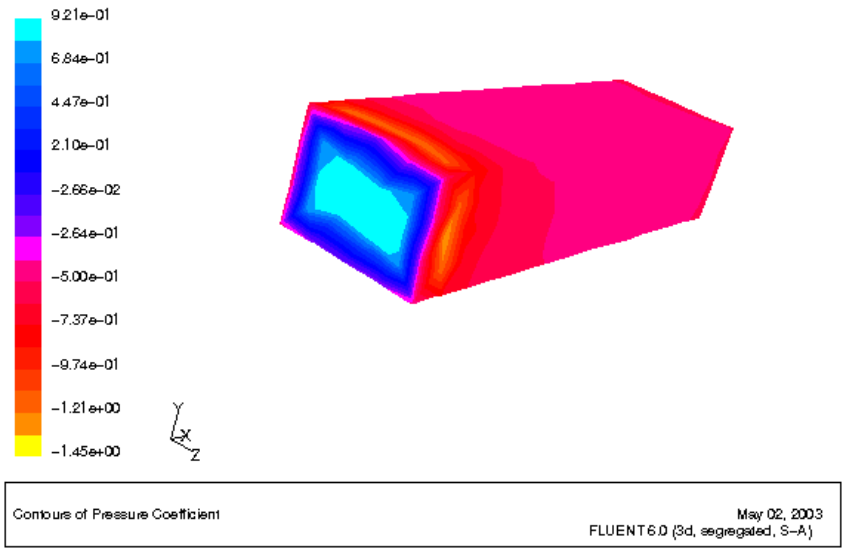

Figure 2-24: Test on a Cube model

2.4.4 Modeling

2.4.4.1 Geometry Construction

GAMBIT was used for the design of the fire truck model that was used for the real time test. The grids can be either structured or unstructured depending on type of discretization, scheme and application. The different schemes available are:

Finite differences: structured
Finite volume or finite element: structured or unstructured.

In this model the grid is generated with the help of the size function. In this size function the growth rate of the mesh size is specified. This creates a mesh, which is refined around the model and grows coarse towards the outer block. By using the size function a non-uniform mesh is created with tetrahedral mesh elements. Figure 2-25 displays the grid density on the vehicle model.

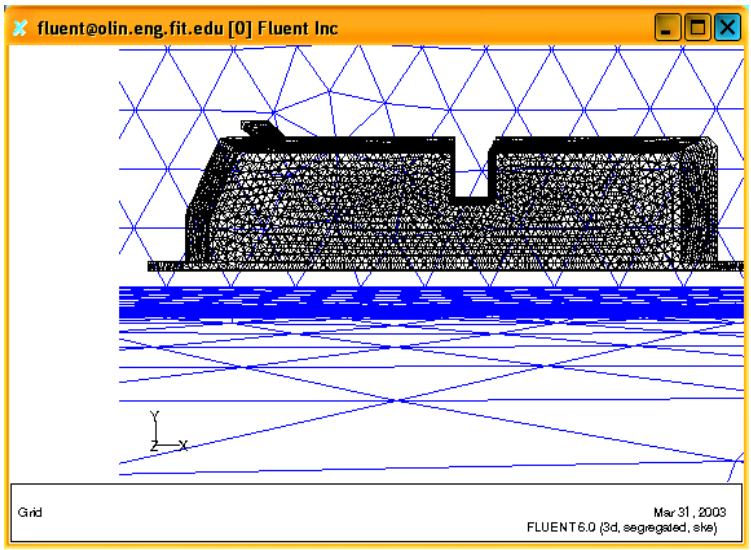

Figure 2-25: Grid display

The boundary zones are specified in Gambit before the mesh is exported to Fluent for further analysis. The boundary zones that are used in Gambit for the model are symmetric on the outer walls and for wall condition around the vehicle. The continuum inside is fluid.

2.4.4.2 Boundary Conditions

The boundary conditions selected for this problem are

1. *Pressure far-field boundary condition: on the front and back faces*
2. *Symmetry condition: on the side faces.*
3. *Wall condition: around the model.*

Pressure far-field conditions are used to model a free-stream compressible flow at infinity, with free-stream Mach number and static conditions specified. When this boundary condition is specified the density is calculated from a temperature dependent calculation method and ideal gas method. This boundary condition is a non-reflecting boundary condition based on the introduction of Rieman invariants for a one-dimensional flow normal to the boundary. To effectively approximate true infinite extent conditions, you must place the far-field boundary far enough from the object of interest. You can define the flow direction by setting the components of the direction vector. Symmetry boundary conditions are used when mirror symmetry is required and to model zero shear slip walls in viscous flows.

After assigning the boundary conditions the solution is to be initialized with the help of pressure-far-field boundary conditions. The speed used for this is analysis is around 20 m/s. After initializing, the problem should be iterated till the solution converges.

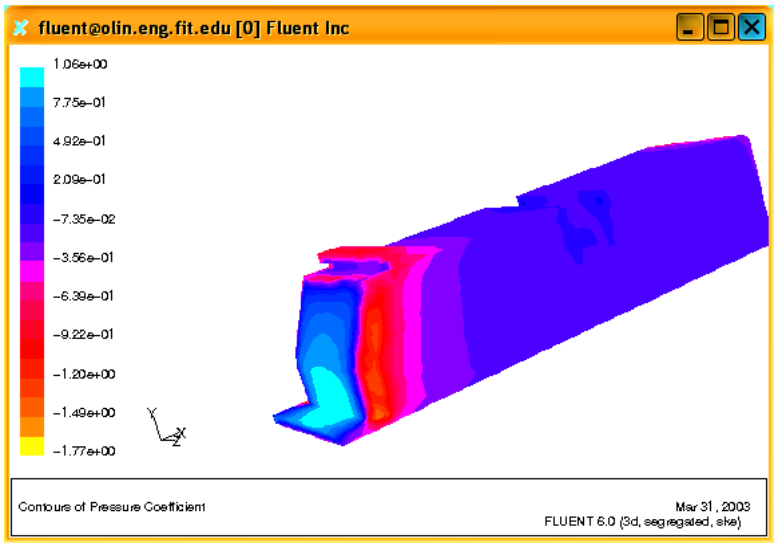

Figure 2-26: Contours of Pressure Coefficient

Figure 2-26 shows the coefficient of pressure distribution around the truck-bluff body. This shows the stagnation points and the low-pressure regions on the vehicle.

2.4.4.3 Grid Adaptation

The grid density and the shape of the vehicle play an important role in the flow characteristics. The solution-adaptive mesh refinement featured in Fluent allows refining or coarsening the grid based on the geometric and numerical solution data. By using this method cells are added where they are needed in the mesh, thus enabling the features of the flow-field to be better resolved. The effect of mesh refinement on the solution can be studied without completely regenerating the mesh. Figure 2-27 shows the grid after the adaptation function is used. The adaptation function that is used is the Y+/Y* function. The change in the pressure coefficient is observed in Figure 2-28 as well as in the comparison graphs.

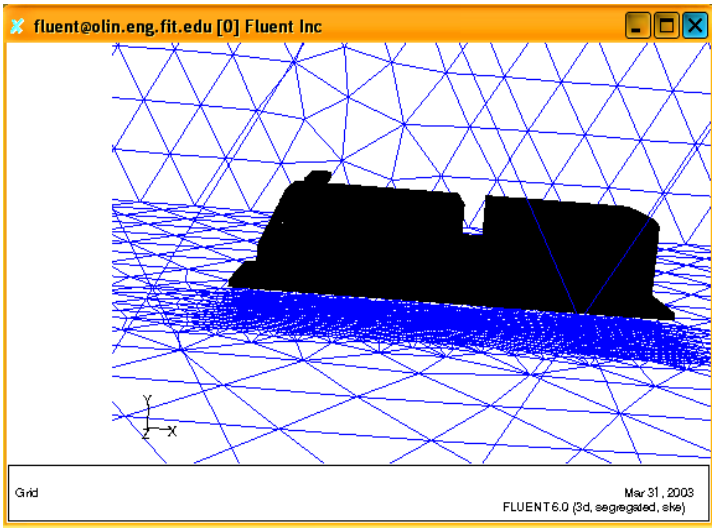

Figure 2-27: After using the Grid adaptation function

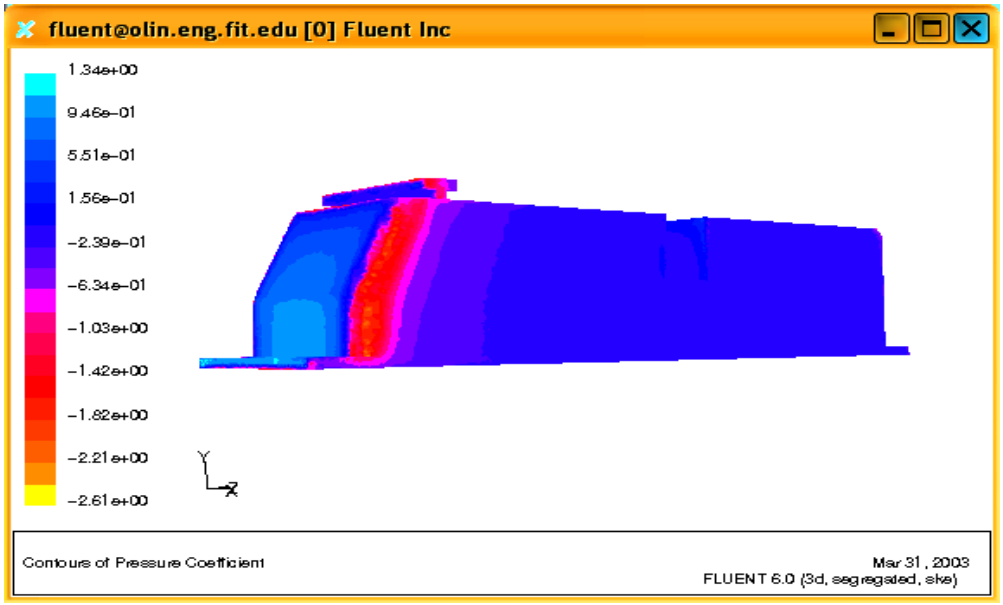

Figure 2-28: The pressure coefficient contours after the grid adaptation

In terms of computation, the Spalart-Allmaras model is the least expensive turbulence model of options provided in Fluent, since only one turbulence transport equation is solved. The standard *K-ε* model clearly requires more computational effort than *S-A* model since an additional transport equation is solved. The complicated model geometry and mesh also govern the computational time. A typical run took 4 hours on a 1.2 GHz PC.

2.5 COMPARISON BETWEEN THE DIFFERENT TESTS AND VALIDATION OF THE RESULTS

2.5.1 Comparison of Results from the Different Tests

As seen from the previous sections, testing and computer modeling was done to determine the coefficients of pressure on different surfaces of a fire truck. The following figures compare the different values of coefficients of pressure measured at different locations from the wind tunnel model, full size fire truck, and the computer simulation. The figures are drawn to scale, and the indicators show the exact location where each coefficient of pressure value was measured.

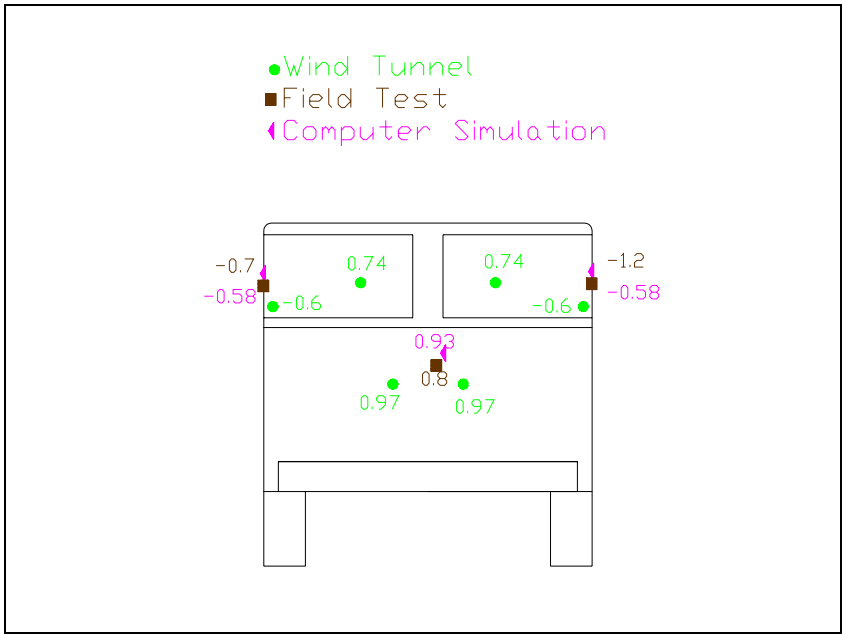

Figure 2-29: Front of Truck Comparisons Between the Field Test, Wind Tunnel testing, and Computer Simulation

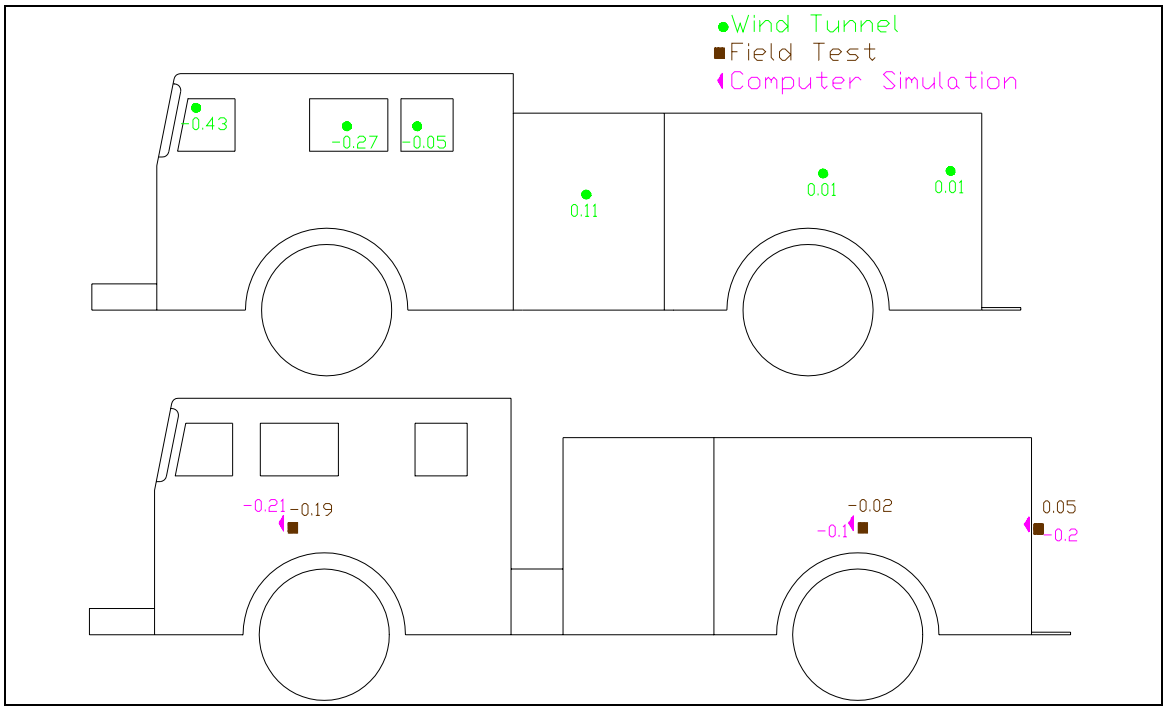

Figure 2-30: Left Side Comparisons between the Field Test, Wind tunnel testing, and Computer Simulation

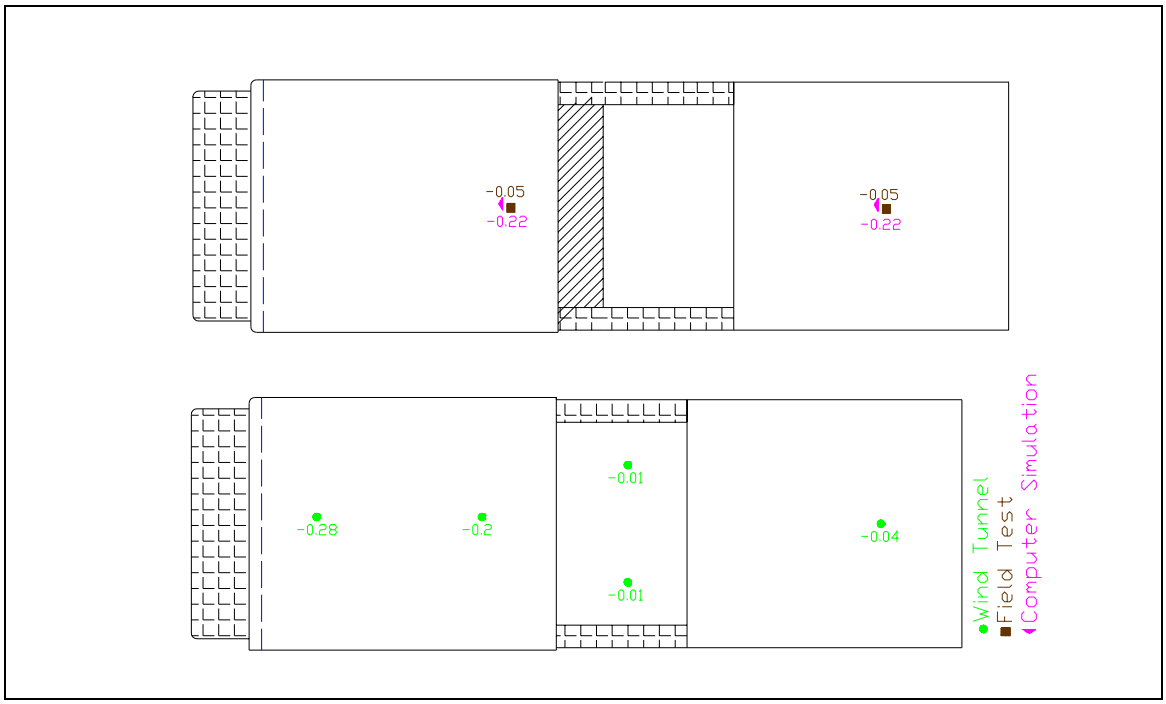

Figure 2-31: Top Side Comparisons between the Field Test, Wind tunnel testing, and Computer Simulation

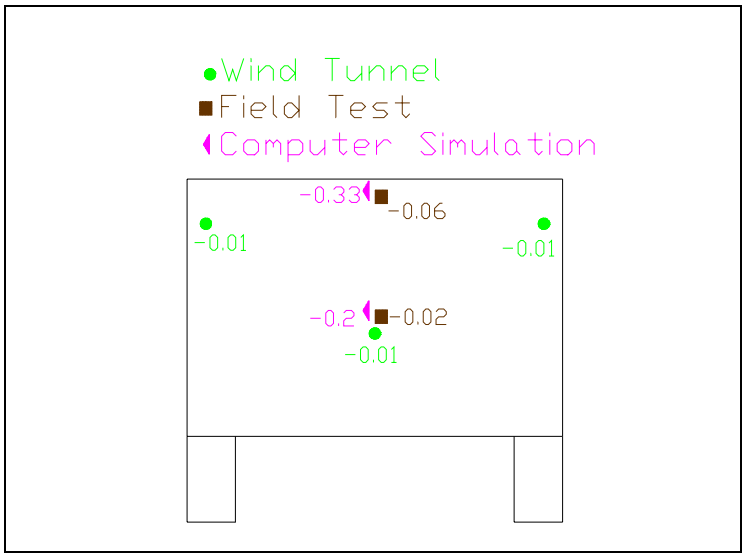

Figure 2-32: Rear of Truck Comparisons between the Field Test, Wind tunnel testing, and Computer Simulation

Comparing the results we see a fair agreement for Cp on the front, sides and rear of the fire truck for the different tests. The locations where more that a few 1/100th of a disagreement are seen are on the leading or trailing edges. In addition the locations of the pressure taps for the wind tunnel model were not exactly the same as for the full size fire truck, so only a comparison to see if the values in the same areas are close can be done. On the front face we can compare 0.8 from the field test to the average of 0.97 and 0.74 on the front of the wind tunnel model. The computer simulation agrees for the most part with the experimental results. The only problem seems to be on the rear of the fire truck where the simulation reports significantly lower values of pressure than was seen in both the wind tunnel and field test.

The values on the right rear side of the full size fire truck are slightly higher than the left side of the same fire truck and the other models but this is attributed to a ladder mounted to the fire truck on that side.

On the top of the cab there is a slightly larger disagreement between the field test and the model. The field test has a much lower value of Cp than the model. The field test had a value of –0.06 in comparison to –0.28 or –0.2 for the wind tunnel model. The explanation is likely due to the differences in surface geometry on the top of the cab. As can be seen in Figures 33 and 34 below the full size fire truck has two very large protrusion in front of the location where pressure was measured, while the model has a virtually no protrusions windward of the pressure taps.

Figure 2-33: Protrusion visible on the top of the Protector Cab

Figure 2-34: Virtually no protrusions windward of the pressure taps on the Wind Tunnel Model in a 0 Degree test

2.5.2 Determination of Forces Acting on the Vehicle

From the wind tunnel tests, coefficients of pressure at various locations and various relative wind directions are known. This information is used to compute the forces acting on a vehicle as a function of wind speed. Coefficient of pressure is defined as local dynamic pressure divided by free stream dynamic pressure. As in the following equation:

$$Cp \equiv \frac{LocalDynamic\,\mathrm{Pr}essure}{FreestreamDynamic\,\mathrm{Pr}essure} \tag{2-3}$$

Pressure is defined as a force over an area. Wind speed is a function of free stream dynamic pressure through the following equation:

$$Vel = \sqrt{\frac{2(p_{Total} - p_{Static})}{\rho}} \tag{2-4}$$

Here ρ is the density of air (assumed to be 1.225 kg/m^3), and $(p_{Total} - p_{Static})$ was measured with the Pitot-static tube and is the free stream dynamic pressure. Rearranging equation 2-3 and combining with 2-4 gives

$$LocalDynamic\,\mathrm{Pr}essure = \frac{1}{2}V^2\rho \times Cp \tag{2-5}$$

Local force can therefore be computed using the local area, $Apanel$, and multiplying it by the local dynamic pressure. Dividing the model into sections or panels on which it is assumed that Cp is constant gives the following equation, which is a function of velocity:

$$Fpanel = V^2(\frac{1}{2} \times \rho \times Cp \times Apanel) \tag{2-6}$$

Summing the forces on all the panels over the fire truck for a certain wind angle and velocity gives the resulting force acting on the model. Some guesswork was used in deciding which area should be used for each panel. For the pressure taps where Cp is determined from symmetry of the fire truck, Cp values are labeled "prime" to indicate that they are a result of symmetry. For the panels on the sides and top of the fire truck the edge of the area was chosen as half the distance between the two pressure taps. For the front and rear of the fire truck the panels where chosen slightly differently. This is shown in the following set of figures (all drawn too scale).

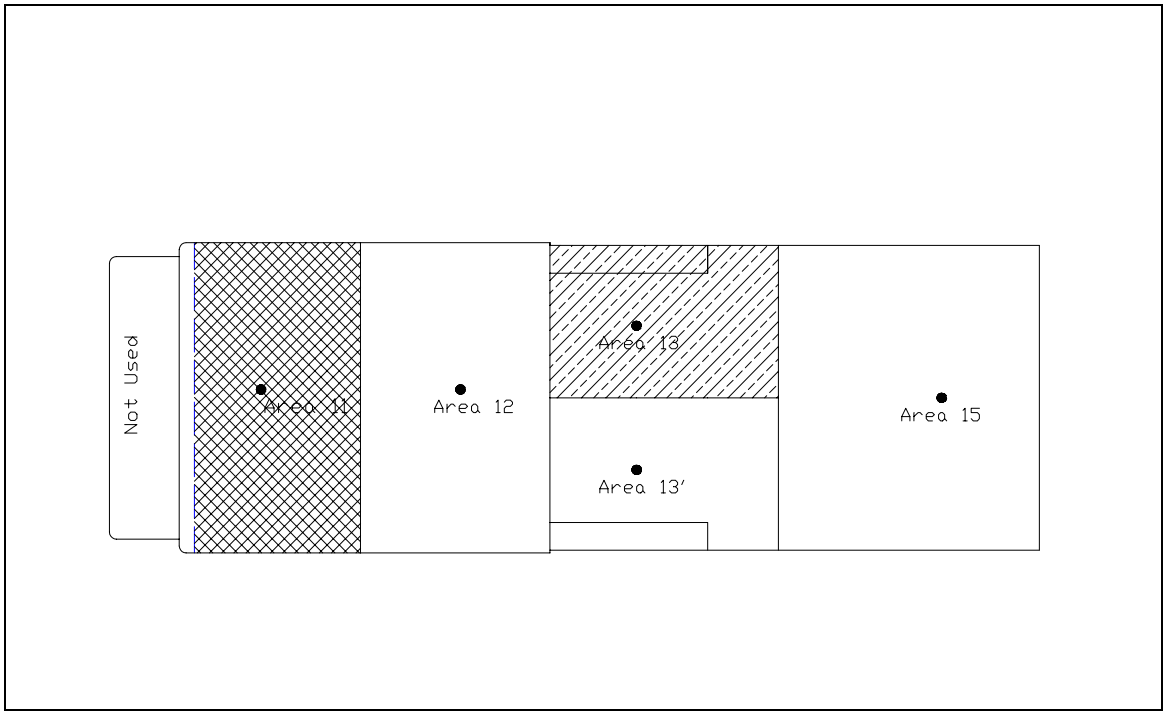

Figure 2-35: Panel division on the top of the fire truck

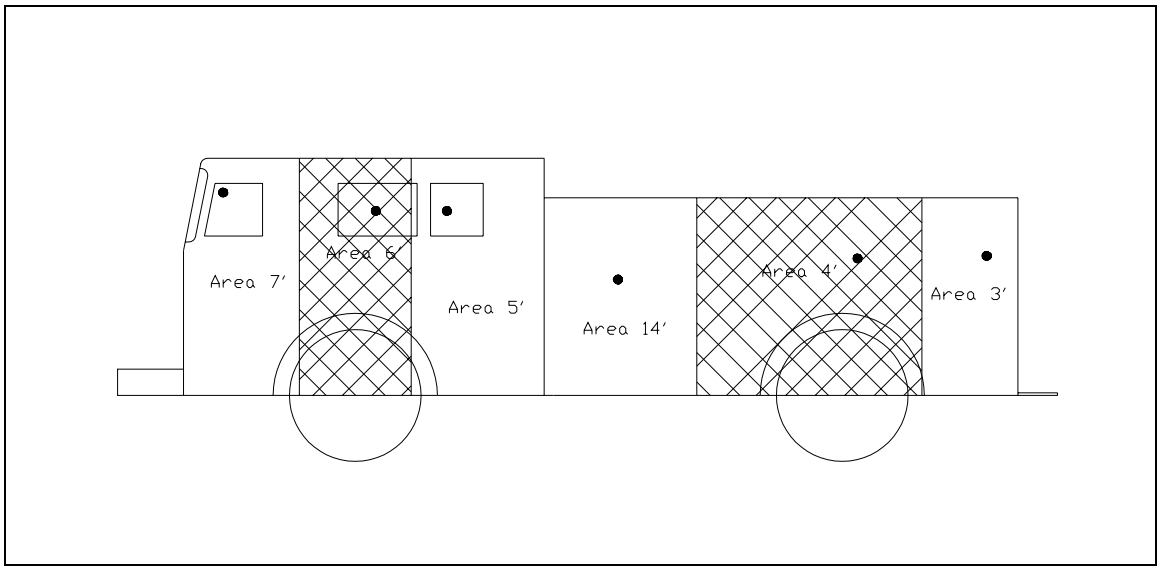

Figure 2-36: Panel division on the sides of the fire truck

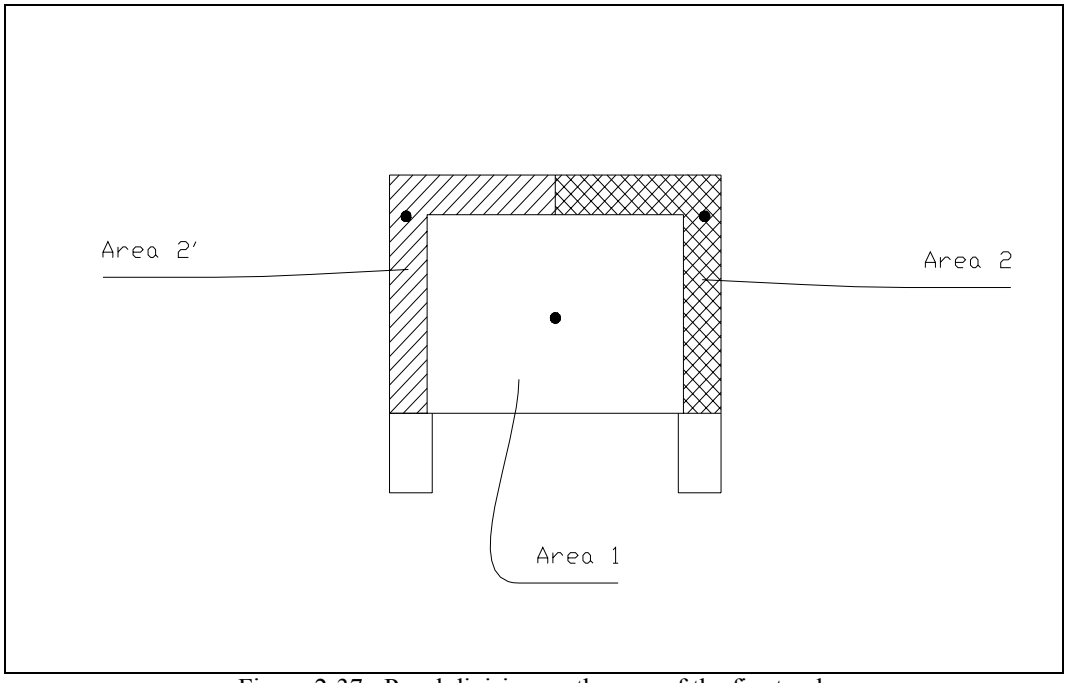

Figure 2-37: Panel division on the rear of the fire truck

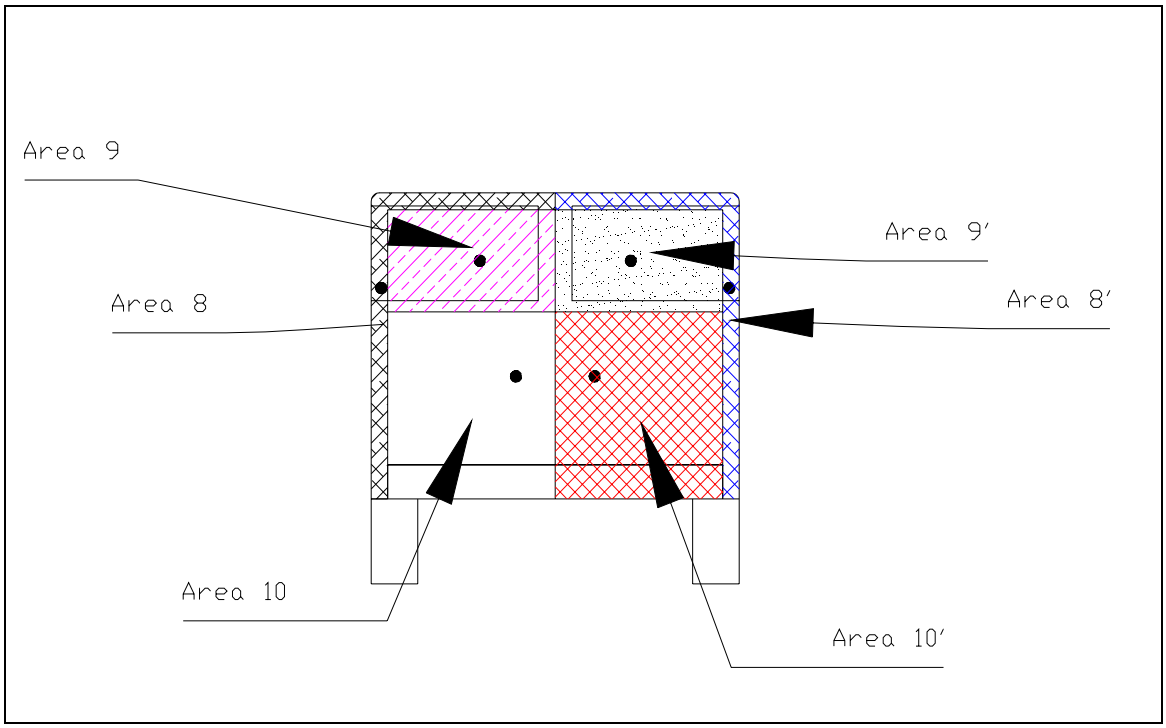

Figure 2-38: Panel Division on the front of the fire truck

2.5.2.1 Comparison between force balance results and measured pressure results

During the tests, the pressures at all locations were collected using a *Pressure Systems Pneumatic Intelligent Pressure Scanner* with piezoresistive pressure sensors capable of measuring an accuracy of ±0.08 % of the full scale. Several steps were followed to ensure that the equipment and methods employed were repeatable. The first was that for several sample velocities and orientations, pressures at different surfaces were measured using a digital manometer rather than the pneumatic scanner. Both methods gave the same results in terms of measured pressure, and the digital manometer in fact displayed larger fluctuations than the Pneumatic scanner. Another step taken was to use a strain gage force balance to measure drag and side force on the model at different orientations and different velocities. The force balance was used to measure drag and sideways force at 0, ±45, and ± 90 degrees. This is compared to the forces resulting from the pressure distributions and is shown in the figures below. Note that the force balance measurements were corrected for stem drag below.

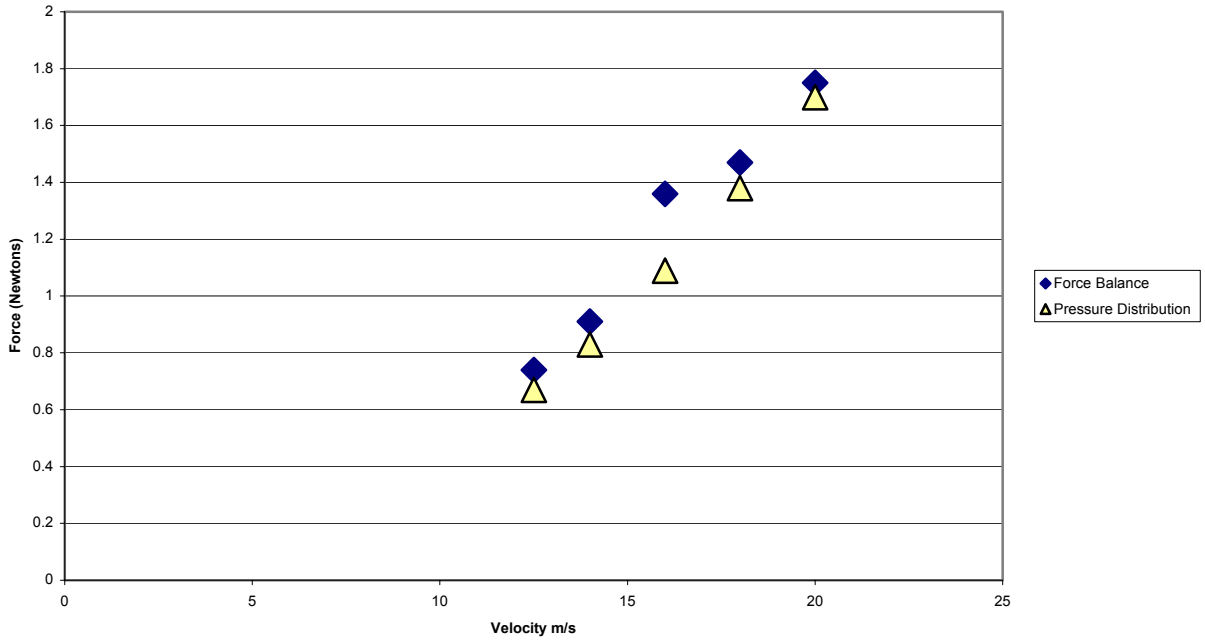

Figure 2-39: Force Balance and Pressure Distribution comparison at 0 Degrees

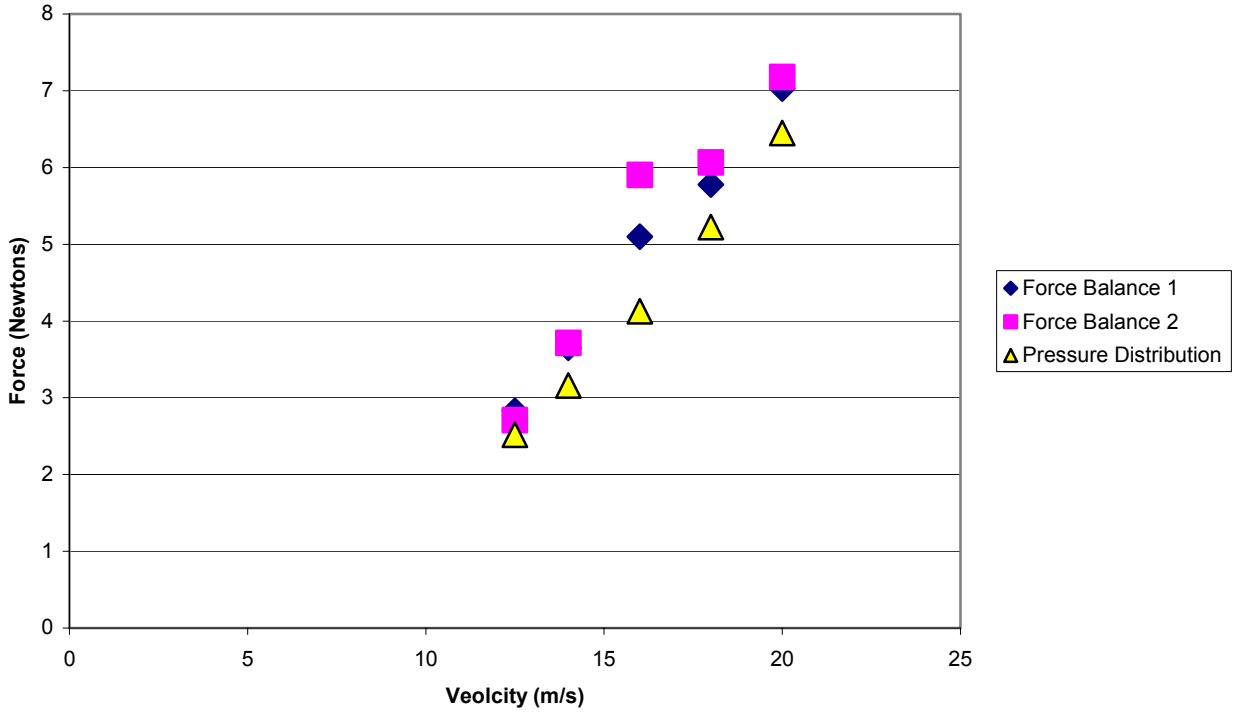

Figure 2-40: Force Balance and Pressure Distribution Comparison at 45 Degrees

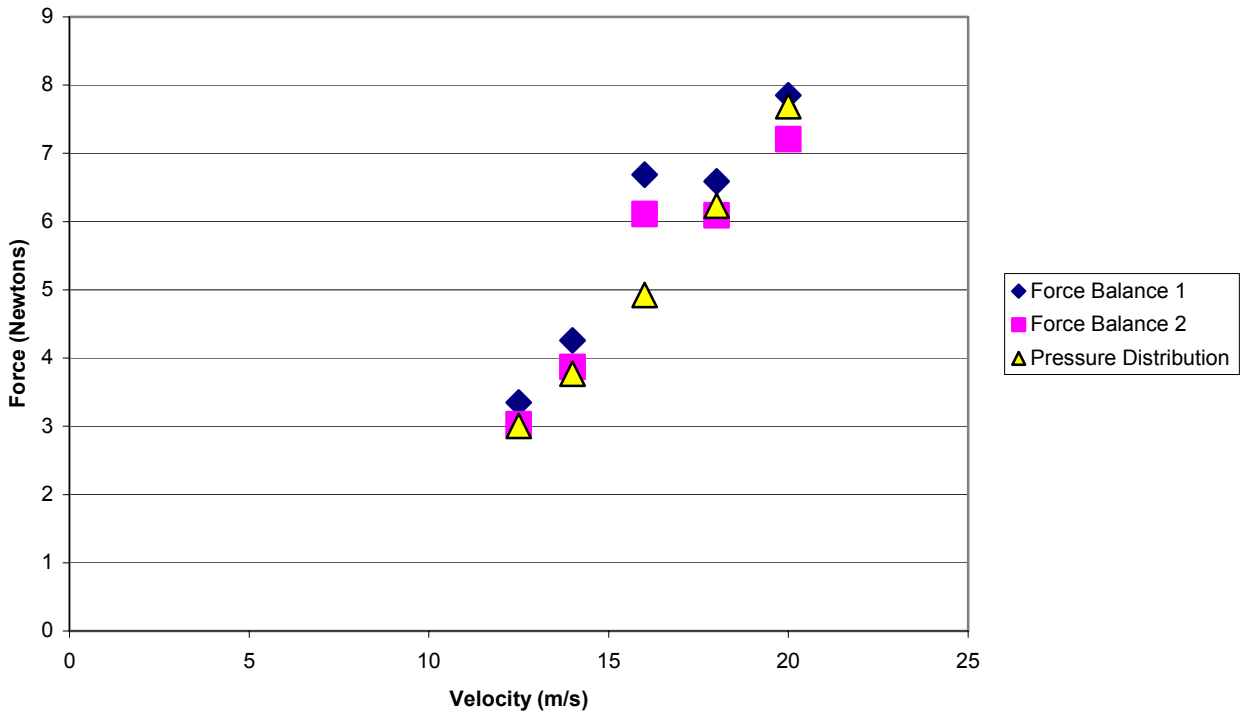

Figure 2-41: Force Balance and Pressure Distribution comparison at 90 Degrees

It is argued that because the fire truck is symmetric about its lengthwise axis that the forces acting on it for a wind angle of +45 degrees will be the same as if the wind were acting at –45 degrees. Therefore in the above plots Force balance 1 represents the force balance measurements at +45 degrees, and force Balance 2 represents the force balance measurements at –45 degrees. Even so, it can be seen that there is about a 10% difference between the two force balance measurements, at some wind speeds. The method discussed in section 5.2 above is the method used for computing force as a result of pressure distribution. The agreement between the force balance and pressure distribution is fairly close for all three angles, it is best for 90 degrees and worst for 0 degrees. The force balance gives the total force on the model, while the pressure measurements are made only at 15 discrete points. Local flow anomalies can alter the pressures at unmeasured locations. The panels are assumed to be flat, and the effects of small inclination of the panel to reference co-ordinates are neglected. The Fluent code gives a more global pressure distribution on the model. So, the force estimation from the Fluent simulation is expected to be in better agreement with the force balance results. Also, the pressure measurements do not include the viscous effects. If skin friction was considered for a turbulent boundary layer the pressure distribution results would be slightly higher, particularly for the 0 degree case.

2.5.2.2 Influence of Reynolds Number

A turbulent boundary layer would explain the scatter seen in tap #10 discussed previously (and all the other taps on the fire truck). A look at the surface of the model shows that it

has a very rough surface and numerous protrusions. Under these conditions turbulence should be expected.

For the model, testing was conducted for a Reynolds number range between 1.5×10^5 and 4.2×10^5. These values come from an equation in Anderson [2] below

$$R_e = \rho_\infty \frac{V_\infty x}{\mu_\infty} \tag{2-7}$$

In this equation:

R_e is Reynolds number

ρ is the density of air

V is the velocity

μ is the viscosity of air

x is the distance from the leading edge.

The subscript infinity defines far upstream from the model. The length of the model is 31 cm long (12.2 in), standard density and viscosity values for air were used at sea level. Velocity was the only parameter that changed giving the stated Reynolds number range.

Reynolds number is one of the simulation requirements Gawthorpe [3] mentions for effective wind tunnel modeling of a vehicle. The other two requirements are simulation of the ground plane, and the same onset of wind characteristics. These two were achieved in the setup. Testing for steady winds was conducted, and these are the same onset characteristics being modeled. The platform simulated the ground plane.

Reynolds number was not completely matched. For a full-scale fire truck Reynolds number would be above $\underline{4.5 \times 10^6}$. The Reynolds number tested with the model was only $\underline{4.2 \times 10^5}$. Both Gawthorpe & Anderson; however, suggest that if the boundary layer is turbulent then the same pressure forces can be generated on the surfaces at lower Reynolds numbers. The additional scatter observed in pressure taps on the model but not the Pitot-static tube indicates a turbulent boundary layer. If the Reynolds numbers were matched then it could be fairly certain that the model correctly mimics the real size vehicle. With a turbulent boundary layer and lower Reynolds number it is likely that the simulation is correct but not certain, therefore a field test and a computer simulation were carried out with a full-scale fire truck and the results were compared to the wind tunnel test results. As seen the results from these comparisons were good.

2.6 CRITICAL WIND SPEEDS

2.6.1 Introduction

In the book *Road Vehicle Aerodynamic Design* [7], Barnard indicates that vehicle accidents due to severe weather can result from overturning, course deviation, or hitting fallen trees and other debris. Course deviation and overturning will be considered in this analysis.

When a vehicle (assumed symmetric about it's centerline) is traveling down the expressway with no crosswind, normal forces acting on the vehicle will only include a Pitching Moment, a Lift force, and a Drag force. In a cross wind the vehicle will experience several additional actions. These actions can be a side force, a yawing moment, and a rolling moment. All the forces acting on a vehicle with a non-zero yaw angle (between vehicle axis and relative wind direction) are shown in Figure 2-42 below.

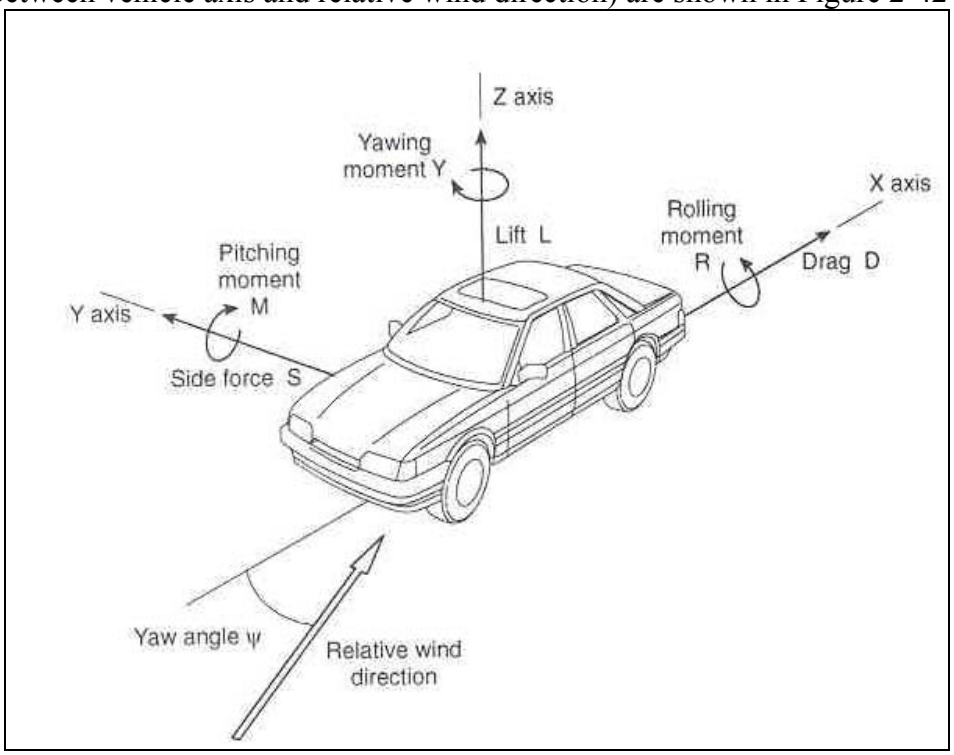

Figure 2-42: Definition of forces and moments acting on a vehicle [7].

2.6.2 Determination of Critical Wind Speeds Due to Course Deviation

2.6.2.1 Definition of Course Deviation

Course deviation occurs when a vehicle is blown off course. An accident as a result of course deviation can occur through a vehicle being blown off the road, into other vehicles, or other obstructions. It is likely that an experienced driver could correct for small course deviations; while violent course deviations will regardless result in an accident.

For this study the critical wind speed due to a course deviation will be defined as the speed at which due to combined forces and moments acting on a vehicle – a course deviation will begin to occur.

2.6.2.2 Calculating Forces and Moments on the Typhoon Fire Truck

A vehicle in a crosswind will have three forces and three moments acting upon it. From the wind tunnel testing the coefficients of pressure at different locations for different wind yaw angles are known. This information was used in conjunction with equation (5-4) to calculate the forces acting on the different panels of the model. The wind tunnel model, as stated earlier, closely resembles the E-One Typhoon Pumper. In terms of scaling factors between the two: it is a 1:25th scale for the wheelbase, a 1:27th scale for the length, a 1:26th scale for the height, and a 1:23rd scale for the width. In order to extrapolate the forces acting on the wind tunnel model to a full size Typhoon Pumper a 1:25th scale was used for all the dimensions.

2.6.2.3 Vehicle Weight and Center of Gravity

For their Typhoon Pumper, E-one [1] lists it as having a Gross Vehicle Weight Rating (G.V.W.R.) of 18,050 kg (39,800lbm) with 7,250 kg on the front axle and 10,796 kg on the rear axle. The company E-One defines G.V.W.R., for Pumpers, as 5% above the weight the vehicle is expected to carry. For Ladder trucks this is 10% above the expected weight. E-one estimates their vehicles as having 1600 lbm of people (200 lbm/person), 2000 lbm of gear, and 8000 lbm of water in the tank.

For this study analysis will be conducted for a full fire truck, and an empty one. An empty one being defined as the condition when the fire truck has an empty water tank. The Water tank is assumed to be 1000 gallons (8000lbm/ 3784 kg), and symmetric above the rear axle. So that for the empty analysis the weight acting upon the rear axle will be reduced.

In order to compute yawing and pitching moment acting on a vehicle it is necessary to reduce the forces acting on the vehicle to some arbitrary point. When this point coincides with the center of rotation, the resultant is a force. Otherwise, the resultant is a force and a moment. Some studies, [7] for example, use the midpoint between the front and rear axle. In this study, the forces are reduced to the center of gravity of the truck on the X-axis. With the argument that the vehicle is symmetric about its centerline, or X-axis (see Figure 2-42 for a definition of the X-axis), the location of the center of gravity on the X-axis can be computed by knowing the gravity forces on each axle. This is demonstrated in Figure 2-43 below.

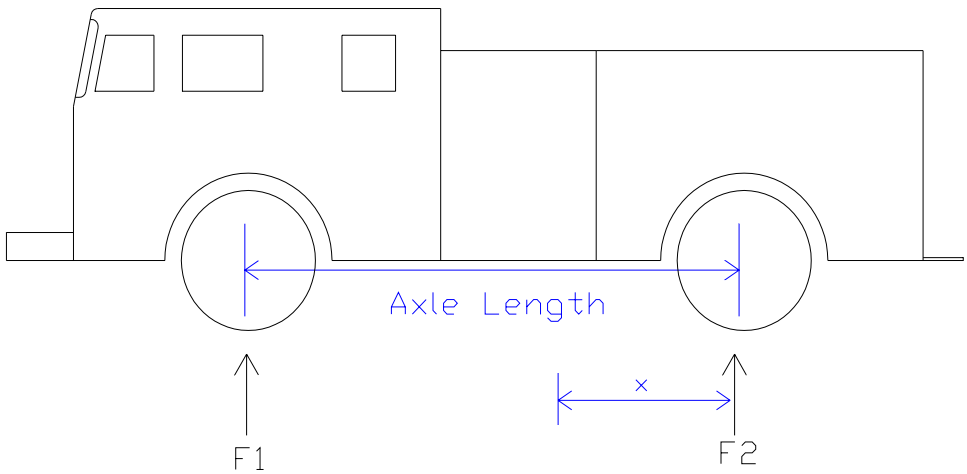

Figure 2-43: Center of Gravity of a Truck

In Figure 2-43 the distance x to the center of gravity can be calculated if F_1, F_2, and the total axle length, L, are known. This is done through the following equation, where L is the total length, F_1 and F_2 are the weight on each axle:

$$x = \frac{F_1(L)}{F_2 + F_1} \tag{2-8}$$

The weight and center of gravity information used in this analysis is summarized in the table 2-1. In this table x is defined as the Center of Gravity distance forward from the rear axle. The weights reported are 5% less than the Gross Vehicle Weight Rating.

Full			Empty		
Axle Weight (kg)		x (meters)	Axle Weight (kg)		x (meters)
Front	Rear		Front	Rear	
6895 kg	10256 kg	1.84m	6895	6472	2.417
The Total Distance Between the axles is 4.57 meters					

Table 2-1: Center of gravity of the Typhoon truck

2.6.2.4 Lift, Drag and Side Forces

Lift, drag and side forces are defined as shown in Figure 2-42. The side force is computed by summing the forces acting on both sides of the fire truck. The drag force is computed by summing the forces on the front and rear of the fire truck. The lift force is computed by summing the forces acting on the roof of the fire truck. In reality there are forces acting underneath the fire truck and these should be accounted for in the lift force. But the pressure forces were not measured underneath the model, because the moving road condition could not be modeled. This will contribute an amount of uncertainty to the final results.

2.6.2.5 Pitching and Yawing Moments

The moments are computed by summing the wind forces acting about the center of gravity of the fire truck. The yawing moment is computed from forces acting in the X-Y plane, and the pitching moment is computed from the forces acting in the Z-X plane. This is demonstrated for the yawing moment in Figure 2-44. Knowing the forces on each panel, and the distance from the center of each panel to the origin of the X-Y axis, the moment contribution from each force about the axis is known. Summing the total moments about the axis gives a single yawing moment about the origin. The whole system of forces can therefore be reduced to a resultant force and moment shown in Figure 2-45.

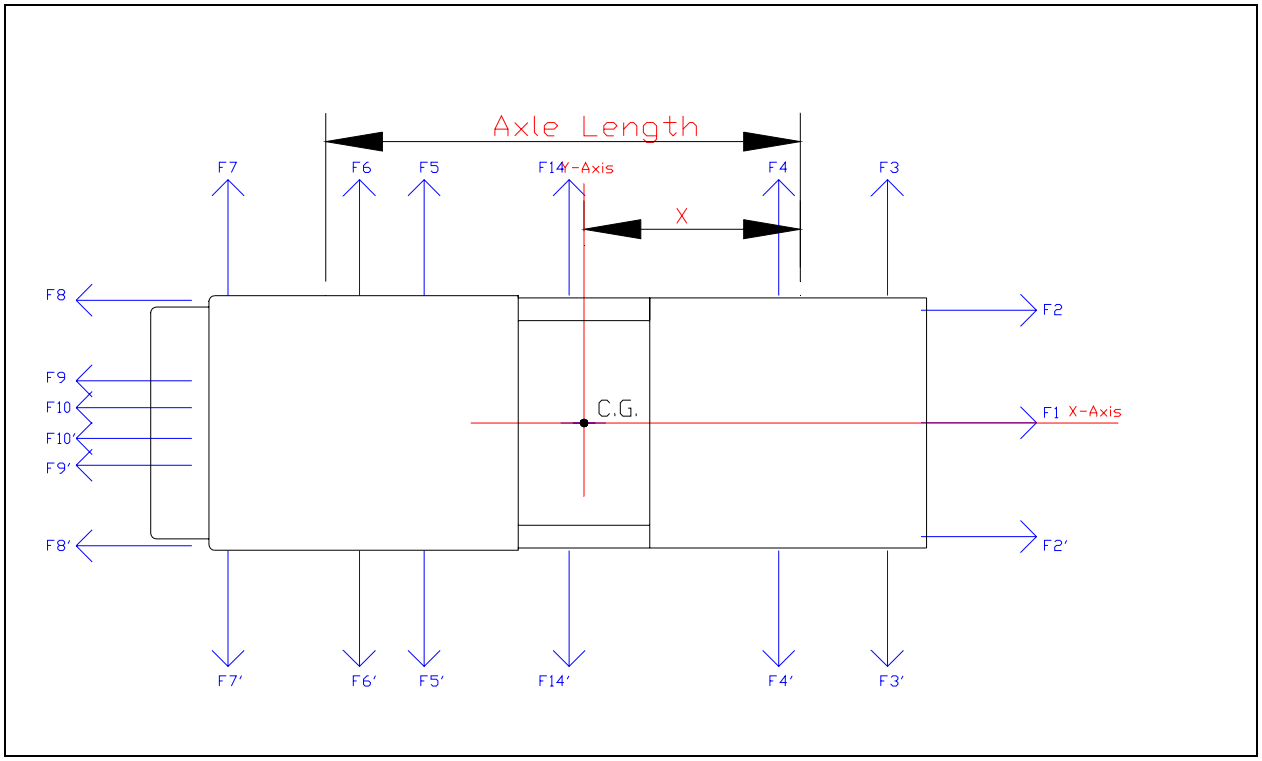

Figure 2-44: The Forces acting in the X-Y plane which create a yawing moment and resultant force.

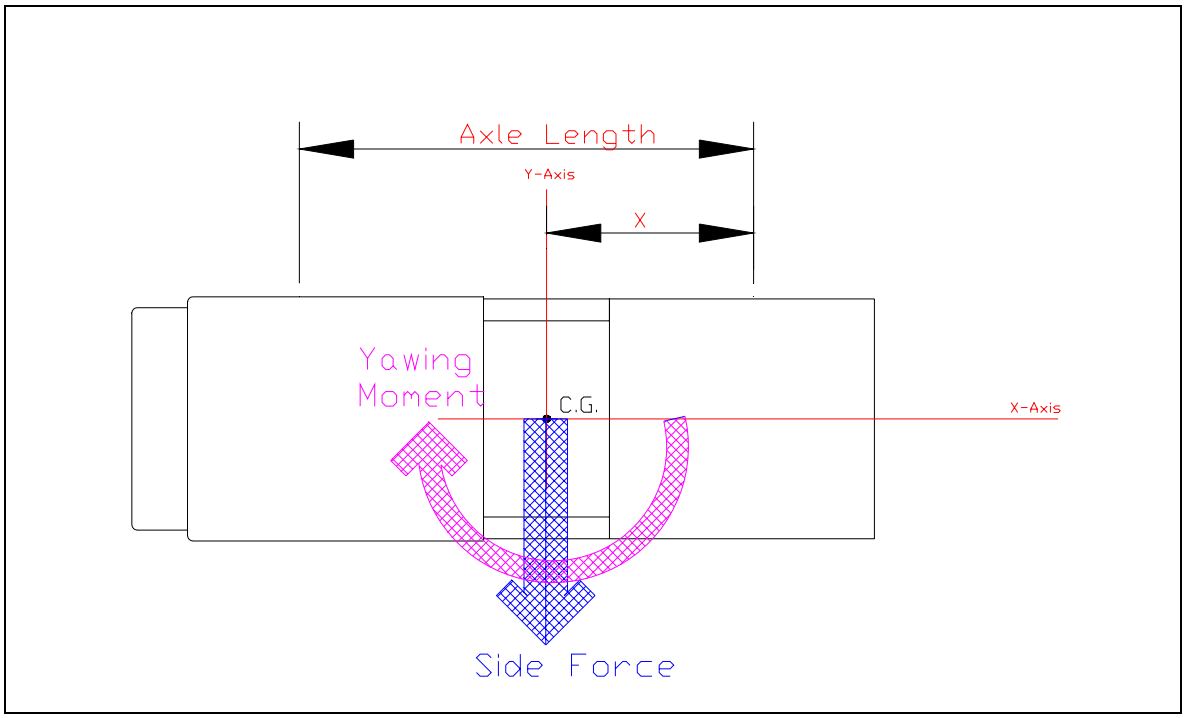

Figure 2-45: Reduction of forces in the X-Y plane to a single yawing moment and side force about the center of gravity

2.6.2.6 Combination of Moments and Forces to Determine Course Deviation

Using equation 5-4 and the summation of forces and moments method discussed in the previous two sections for any vehicle speed the forces on the fire truck can be predicted. In terms of course deviation analysis the side force and yawing moment can be balanced against the resistive force of the vehicle weight. This is shown in Figure 2-46 below.

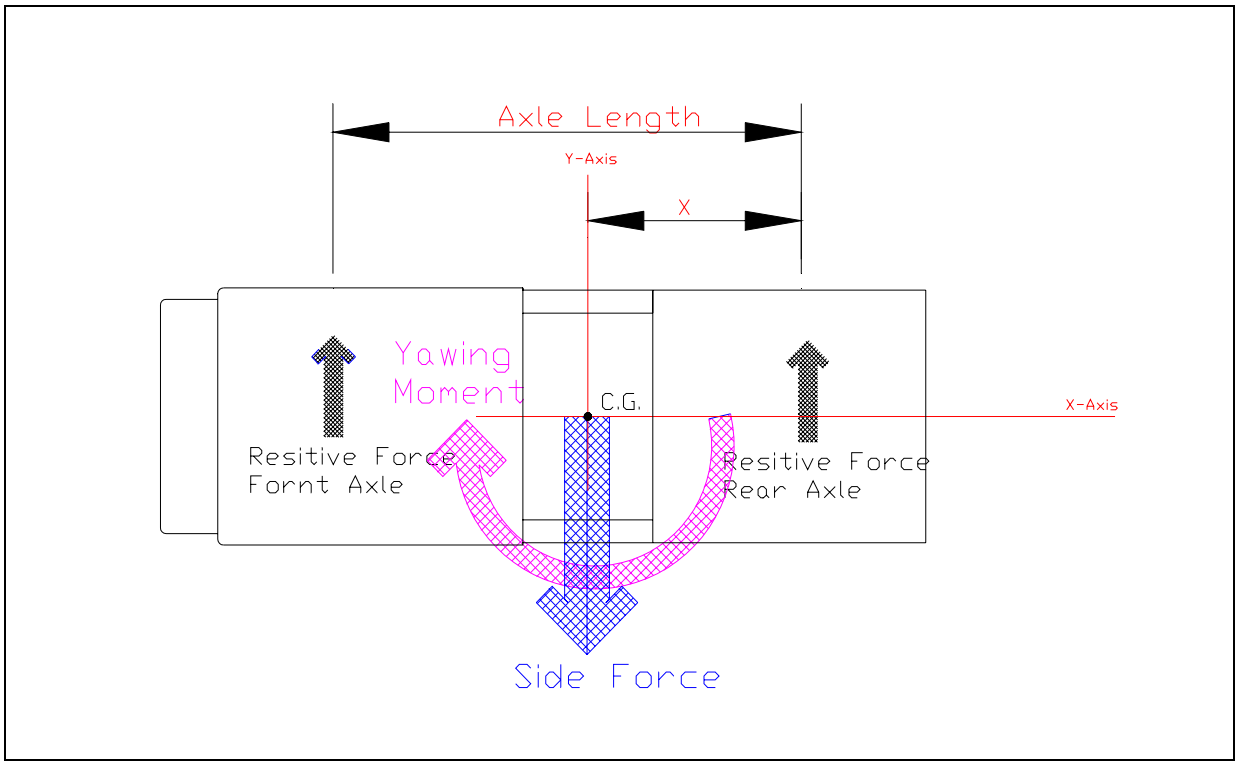

Figure 2-46: Balancing yawing moment and side force against the resistive force per axle.

In Figure 2-46 the yawing moment and side force are known as a function of velocity. The resistive force per axle depends upon vehicle weight per axle and the coefficient of friction between the tires and the roads. If two objects are being held together by some force (wheels on pavement, held together by gravity) the coefficient of friction tells what ratio of the force holding the objects together must be used to begin to slide one object over another.

In the above figure, the yawing moment, side force, and distance from each axle to the center of gravity are used to determine the side force acting on each axle. The equilibrium equations for each axle are shown below.

$$WindforceFrontAxle = \frac{YawingMoment + Sideforce * X}{AxleLength} \tag{2-8}$$

$$Windforce\,\mathrm{Re}\,arAxle = \frac{-YawingMoment + Sideforce * (Axlelength - X)}{AxleLength} \tag{2-9}$$

In these equations X is the previously defined distance from the center of gravity to the rear axle. The yawing moment and side force are calculated as a function of wind angle, and vehicle speed. The moment is defined as positive counterclockwise, and negative clockwise. In order for a course deviation to be avoided the forces per axle must be less than the resistive force available on that axle.

The resistive force on each axle depends upon the coefficient of static friction between the tires and the road, and the weight acting on each axle. Due to the pitching moment and lift (see Figure 2-47) the weight per axle will differ with wind speed and yaw angle. The result is an effective weight per axle.

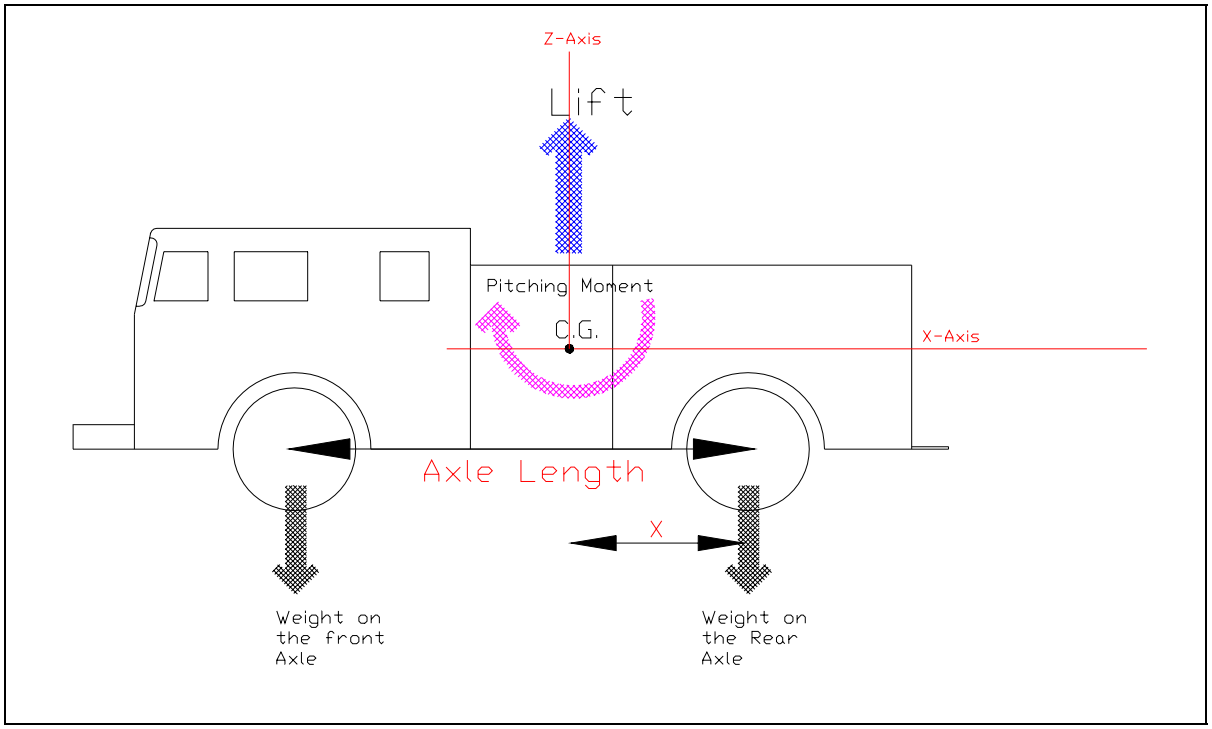

Figure 2-47: Lift and Pitching Moment affect weight

The following are the equations relating the effective weight per axle to the lift, pitching moment, and the G.V.W.R per axle.

$$E_f = G_f - \frac{Lift * X + PitchingMoment}{AxleLength} \tag{2-10}$$

In this equation E_f is the effective weight on the front axle, and G_f is the weight on the front axle based upon the gross vehicle weight rating, plus any adjustments due to an empty or full condition. X is the previously defined distance from the center of gravity to the rear axle. Similarly an equation can be defined for the rear axle:

$$E_R = G_R - \frac{Lift * (Axlelength - X) - PitchingMoment}{AxleLength} \tag{2-11}$$

In this equation E_R is the effective weight on the rear axle, and G_R is the weight on the rear axle based upon the gross vehicle weight rating, plus any adjustments due to an empty or full condition.
In terms of course deviation analysis the resistive force per axle can now be defined.

$$R_{force} = E\mu \tag{2-12}$$

In Equation 2-12 E is the effective weight for the front or rear axle from equation 2-11 or 2-12, μ is the coefficient of static friction, and R_{force} is the resistive force provided by that axle.

2.6.2.7 The Importance of the Coefficient of Static Friction

The coefficient of static friction (μ) is defined as the ratio of frictional force to the normal force pressing two surfaces together. It can also be known as the coefficient of adhesion. For some surfaces this value is known very well.

For galvanized rubber on different road surfaces this is a value that is not very well documented because it depends upon numerous variables. For example it is assumed that for racing slicks on dry pavement the coefficient of static friction (μ) will be approximately 0.9 or more, and for wet pavement about 0.1 or less (if hydroplaning occurs). This is why certain types of car races are not conducted in the rain.

For automobiles the coefficient of static friction (μ) will usually be somewhere between 0.1 and 0.9. These are unsubstantiated numbers, but in the National Highway Traffic Safety Administrations "Rating System for Rollover Resistance" [8] it states that "For a good dry paved surface, μ may be in the neighborhood of 0.9. But for wet, icy roads, μ is considerably less." There are several reasons for this broad uncertainty. The first is that this value depends upon the chemical composition of the tire and the road. Another factor is the tire pattern and the tire pressure. And finally, it depends upon the conditions of the road. For a hot, dry day μ will be highest. For a cold wet day μ will be considerably lower.

One of the worst-case scenarios for μ would be immediately after it begins to rain. Most roads are porous, and they absorb the oil and other products from the cars. When it rains, oil being less dense that water is displaced and a thin film of oil is produced on the surface road – this inevitably leads to slipperiest conditions. The only case where μ *might* be reduced more is when a road is covered in a sheet of ice. (See reference [14] for an in-depth discussion of force and motion, and what creates friction.)

2.6.3 Course Deviation For the Typhoon Pumper

Gawthorpe [3] states that the shape of a vehicle largely fixes proneness of road vehicles to course deviation in a crosswind in addition to its weight distribution. Rear-engine cars with low tails are more prone than front-engine cars with high tails. For the wet road analysis a coefficient of static friction of 0.2 was used. For the dry road analysis a coefficient of static friction of 0.8 was used.

Wind Speed to Cause a Course Deviation, m/s (mph)				
	Full		Empty	
Wind Angle	Dry Roads	Wet Roads	Dry Roads	Wet Roads
0	__	__	__	__
45	71 (159)	40 (90)	71 (159)	40 (90)
90	65 (145)	38 (85)	65 (145)	38 (85)
135	77 (173)	45 (100)	76 (170)	45 (100)
180	__	__	__	__

Table 2-2: Wind speed to cause a static course deviation-Typhoon -The fire truck is not moving.

Table 2-2 shows the static results. The first number has the units of meters per second and the number in parenthesis has the units of miles per hour. This information only indicates at which cross wind speed a parked fire truck will begin to move in its parking space.

From the table, it can be noticed that for 0 and 180 degrees the analysis was left blank. At this wind angles, because the vehicle is symmetric, a course deviation will technically not occur. But this will still affect the vehicle safety in an unknown way. This is particularly true for a tail wind. A strong tail wind will increase the stopping distance by an undocumented amount.

From the table it can also be seen that the speed at which a course deviation will occur doesn't change much between and empty and a full fire truck. A course deviation occurs as a result of the front of the fire truck slipping sideways. The weight on the front axle doesn't change and the pressure distribution around the fire truck does not change with a change in weight. Because of this the front of the fire truck will slide sideways at the same wind speed regardless of whether the tank above the rear axle is full or empty.

Nevertheless, the static analysis cannot be considered by itself. When traveling down the highway, the vehicle speed in addition to the wind speed must be considered to determine the speed at which a course deviation will occur. This creates a resultant wind speed that for wind Yaw angles between 0 and 90 degrees will be higher than just the wind relative to the road. This is demonstrated in Figure 2-48 below:

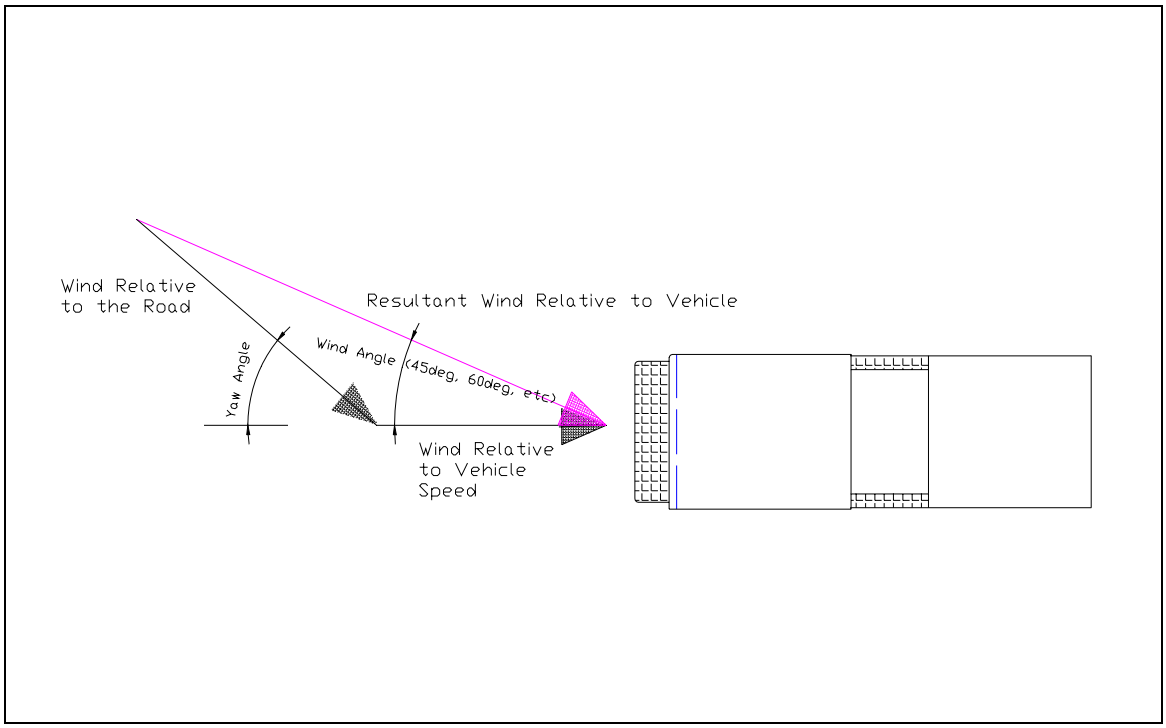

Figure 2-48: The Difference between Relative Wind and Resultant wind

The law of cosines must be used with vehicle speed, the resultant wind speed and the resultant wind angle to compute the crosswind speed; which will result in a course deviation. The law of cosines rearranged for this use is:

$$c = \sqrt{vs^2 + rs^2 - 2(vs)(rs)\cos 45} \tag{2-13}$$

In this equation c is defined as the crosswind speed, vs is defined as the vehicle speed, and rs is defined as the resultant wind speed. Taking vehicle speed into consideration the table 2-3 demonstrates vehicle speed and necessary cross wind speed to create a 45 deg wind resulting in a course deviation. This analysis was done for wet roads.

Vehicle Speed	Crosswind to cause a Course Deviation	Yaw Angle (Degrees)
16m/s (35mph)	31m/s (70mph)	72
20m/s (45mph)	30m/s (66mph)	81
25m/s (55mph)	29m/s (**64mph**)	83

Table 2-3: Typhoon vehicle speed and necessary crosswind speed to cause a resultant wind speed of 40m/s at 45degrees.

2.6.4 Extrapolating the Typhoon data to the Cyclone II X-113

From the field test and wind tunnel tests it was seen that the Typhoon model and Cyclone II have very similar pressure distributions at 0 degrees. Because of their similarity in the Cab and the Rear storage compartments it is argued that the pressure distributions at other

angles will be similar too. The major difference between the two models is a gap between the cab and rear compartments (see figures 2-12 and 2-13), and the pumping mechanism is slightly longer in the Cyclone model.

For extrapolation purposes areas 14 and 14' will be enlarged to account for the difference in size of the pumping mechanism. The assumption will be made that the Cp values on the different surfaces remain the same from the Typhoon to the Cyclone model. Although, it is realized that this is not true, it can be argued that because the changes take place close to the center of gravity, any error in the force will make very little difference to the total yawing moment; which is one of the driving factors in determining course deviation. The data used for analysis are presented in the following table. The equations from the previous sections can easily be used to determine course deviation for the Cyclone model. The same coefficient of static friction was used as in the previous analysis. The results are presented below in Tables 2-4 to 2-6.

Full			Empty		
Axle Weight (kg)		X (meters)	Axle Weight (kg)		X (meters)
Front	Rear		Front	Rear	
6895 kg	10256 kg	2.35m	6895	6472	3.013m
The Total Distance Between the axles is 5.842meters					

Table 2-4: Center of Gravity of the Cyclone II X113

Wind Speed to Cause a Course Deviation, m/s (mph)				
	Full		Empty	
Wind Angle	Dry Roads	Wet Roads	Dry Roads	Wet Roads
45	74.5 (167)	41.5 (93)	74.5 (167)	41.5 (93)
90	68.5 (153)	39.5 (88)	68.5 (153)	39.5 (88)
135	80.5 (180)	45 (104)	80.5 (180)	45 (104)

Table 2-5: Wind Speed to Cause a Static Course Deviation-Cyclone.

Vehicle Speed	Crosswind to cause a Course Deviation	Yaw Angle (Degrees)
16m/s (35mph)	32m/s (72mph)	66
20m/s (45mph)	31m/s (69mph)	72
25m/s (55mph)	30m/s (**66mph**)	81

Table 2-6: Cyclone Vehicle speed and necessary crosswind speed to cause a resultant wind speed of 40m/s at 45degrees.

2.6.5 Determination of Critical Wind Speeds Due to Overturning

Overturning of a vehicle as defined by Gawthorpe [3] is when "generation by wind flows, in combination with vehicle speed, of rolling moments taken about the leeward side tire contact point, which are in excess of the restoring moment provided by the mass of the vehicle acting thorough it's center of gravity (G.G.)". This rolling moment defined in Figure 2-42 results from the side force acting on the vehicle and the lift. This analysis is simpler than the course deviation analysis, in that the moment about the tire edge

produced by the side and lift forces must be simply balanced against the weight of the vehicle. This is shown in the Figure 2-49.

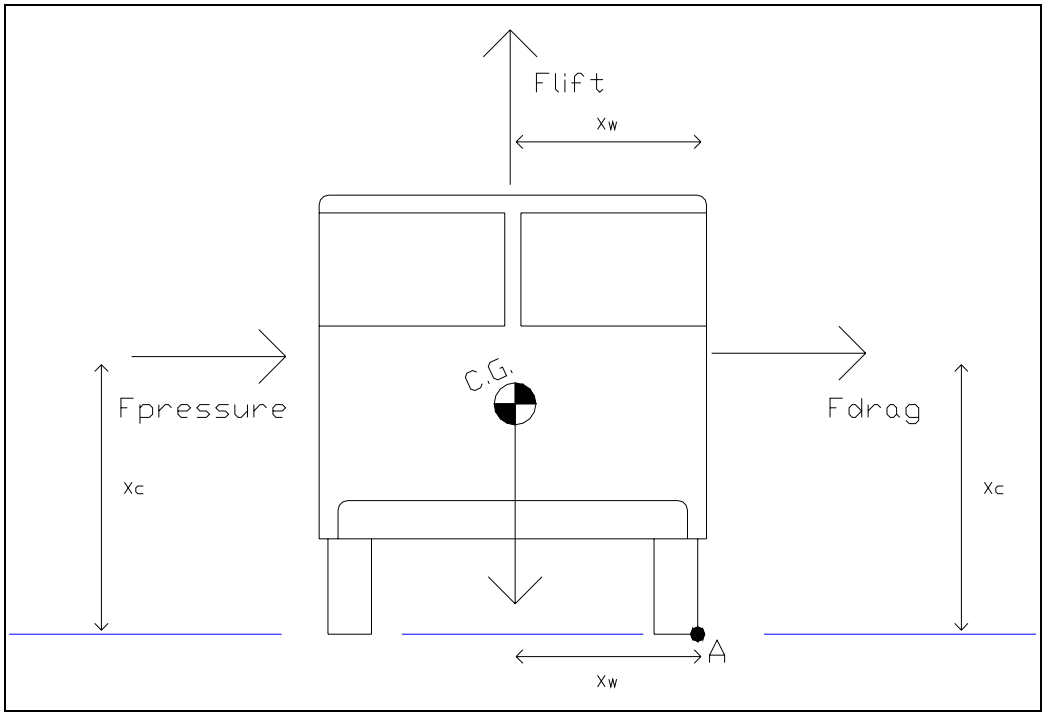

Figure 2-49: Generation of rolling moments pitched against the weight stabilizing moment.

Defining overturning as the case when the rolling moment exceeds the moment provided by the mass of the vehicle, a wind speed can be defined to cause overturning for different yaw angles of incoming wind. This is shown in Tables 2-7 and 2-8. This analysis was done for the Typhoon with empty water tanks.

Yaw Angle	Wind Speed to result in overturning
45°	87m/s (195mph)
90°	78m/s (174mph)
135°	87m/s (195mph)

Table 2-7: Wind speeds to cause static overturning at different yaw angles

Vehicle Speed	Crosswind to cause Overturning	Yaw Angle (Degrees)
16m/s (35mph)	77m/s (172mph)	53
20m/s (45mph)	74m/s (166mph)	56
25m/s (55mph)	72m/s (160mph)	59

Table 2-8: Vehicle speed and necessary crosswind speed to cause a resultant wind speed of 87m/s at 45degrees.

As can be seen, static overturning due to high wind speeds is unlikely to occur. These wind speeds fall into those for a Category Five Hurricane (greater than 155mph). Based upon the Course Deviation analysis the vehicle would start sliding sideways before these wind speeds were ever reached. Overturning may still occur, however, as a result of a violent course deviation. There are numerous likely scenarios where this could occur.

A possible way overturning might result is through overcompensation by the driver to a gust of wind. Or a course deviation may lead to the vehicle hitting a curb, in which case the vehicles momentum would likely lead to a rollover. It is also possible that in a turn, a strong crosswind may induce a rollover. Crosswinds in a turn were not studied for this report. If such a study was conducted information such as road curvature, vehicle speed, and height of the vehicles center of gravity would be needed to predict the strength of a cross wind that would lead to a rollover while turning.

3 AMBULANCE TESTING

3.1 WIND TUNNEL EXPERIMENTATION

3.1.1 Wind Tunnel Experimentation

3.1.1.1 Experimental Setup

Testing was conducted at Florida Tech's Low Speed Wind Tunnel facility with a test chamber section 54 cm x 54 cm. An ambulance model 36 cm long, 15 cm wide, and 16 cm tall was tested for pressure distributions on its surfaces at various incoming wind angles. The model tested was a generic toy ambulance manufactured by Tonka™, this model resembles the Type I ambulance manufactured by companies such as Wheeled Coach Industries [10].

Figure 3-1: Experimental setup with the ambulance at a 25 degrees orientation

Figure 3-1 above is a picture of the ambulance supported in the center of the test chamber. The wooden platform serves the purposes of dampening vibrations and mimicking the ground effect a vehicle experiences. A Pitot-static tube above the model gives the reference dynamic pressure by measuring the free stream total and static pressures. The Pitot-static tube is 61cm long (24 inches) constructed from stainless steel. Located on the front, sides, top, and rear of the fire truck are fifteen pressure taps, which

are used to surface pressure at their respective locations. These pressure taps are constructed from holes drilled into the model at certain locations. The holes have a 1.6 mm diameter with a 5 cm length brass tube mounted flush with the outer surface and held in place with a strong epoxy. Inside the model these brass tubes are attached to flexible 1.6 mm diameter Tygon tubing that runs out of a hole cut in the bottom of the model, through stiff cardboard tubing underneath the platform and attaches to a *Multiple Port Pneumatic Intelligent Pressure Scanner* (Model 9010). The cardboard tubing underneath the platform protects the tubing from flapping at higher wind speeds. The location of the pressure taps and numbering convention can be seen in the pictures displayed in Appendix 2A.

The Model 9010 Pneumatic Intelligent Pressure Scanner is manufactured by Pressure Systems and is a completely self–contained pressure acquisition module for multiple measurements of dry, non-corrosive gases. The scanner can be easily interfaced with an RS-232 serial port on any personal computer. The start up software runs through MS-DOS and allows for the collection of data at a specified interval of time. There are 16 pressure input channels, in addition to a run-reference channel and a calibration-reference channel. Dynamic pressures up to 5 psi can be read between the run-reference channel and any of the 16 input channels. Compressed air is used at 85 psi during startup of the equipment to calibrate and re-zero the system. During testing dynamic pressures from 15 locations on the model and one from the Pitot tube are recorded through the 16 channels on the scanner.

3.1.2 Experimental Procedure

For varying velocities up to 20 m/s, surface pressures at the 15 tap locations were recorded. The pressure data was recorded every 3 seconds for a total time of 5 minutes. Prior to data acquisition at least two minutes were allowed for the wind tunnel to settle at each velocity. Another parameter tested was pressure distribution as a function of incoming wind angle. This was done by repeating the test for all velocities at yaw angles of 0, ±25, ± 45, ±65, ± 90, ± 135, and ±180 degrees. 0 degrees is defined as the condition where the front of the fire truck faces the oncoming wind. Viewed from above: positive angles were defined in the clockwise direction and negative angles were defined as counter clockwise. This is shown in Figure 3-2 below. Note that this experimental procedure is slightly different than the one used for the fire truck. The sample rate was increased from every 5 seconds to every 3 seconds. This and other improved testing procedures saved time during testing and allowed testing to be conducted at additional wind angles- specifically ±25 and ± 65 degrees. The reason for this was to allow further studying of combining vehicle speed with crosswind speed.

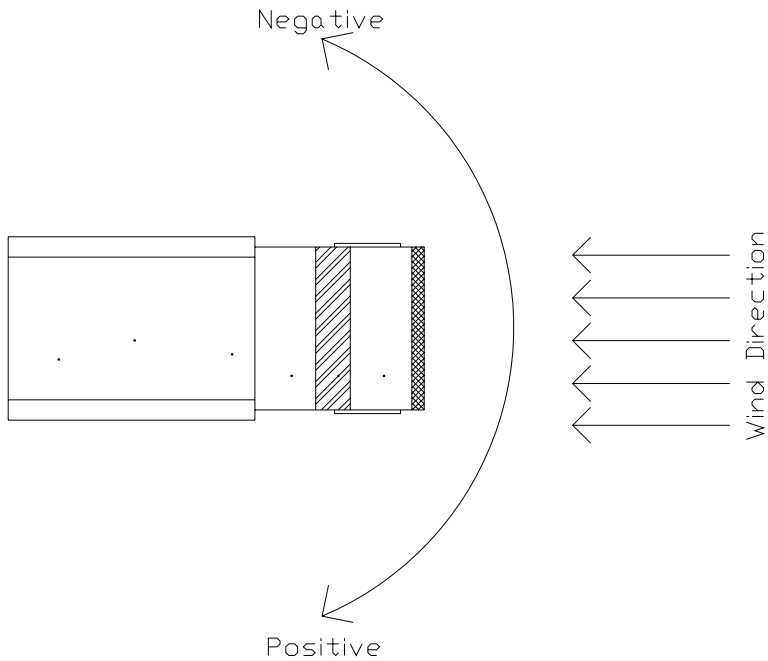

Figure 3-2: Convention used to define the Yaw angle with respect to incoming wind

3.2 WIND TUNNEL RESULTS

3.2.1 Scatter in Measurements

From previous testing of the fire truck model in the wind tunnel, methods were developed and used to reduce the observed scatter in pressure measurements as wind tunnel velocity was increased. These methods were followed during the ambulance testing in the wind tunnel. The steps taken were to:

- Shield the electronics to ensure that electro-magnetic field created by wind tunnel's 15 kW electric motor were not causing interference
- Check the connections for each pressure tap to ensure that there were no leaks.
- Use the rigid wooden platform to ensure that vibrations would be dampened. The platform served the dual purpose of mimicking a ground effect.
- Use a stiff cardboard piping system beneath the platform to protect the thin Tygon tubing from vibrations at higher wind tunnel velocities.

3.2.2 Wind Tunnel Testing Results

The surface pressure values measured at various locations on the ambulance were averaged over the 5 min test period (~100 data points) and then used to calculate, with the reference pressures, the value for the coefficient of pressure (Cp) at each tap location. Cp is calculated using the equation from Anderson [2]:

$$C_P = \frac{p_t - p_s}{p_{total} - p_s} \tag{3-1}$$

In this equation:

C_p *is the Coefficient of Pressure*

p_t *is defined as the tap pressure (15 of them) on the model*

p_s *is the static pressure measured with the Pitot-static tube*

p_{total} *is the total pressure measured with the Pitot-static tube*

For each test run the dynamic pressure from the pitot static tube is used to compute velocity with the use of Bernoulli's equation [2]:

$$V = \sqrt{\frac{2(p_{total} - p_{static})}{\rho_{air}}} \tag{3-2}$$

In this equation

ρ is the density of air

V is the velocity

pstatic is the static pressure measured with the Pitot-static tube

ptotal is the total pressure measured with the Pitot-static tube

The pneumatic pressure scanner has an accuracy of ± 1031 Pa (0.15 psi) when working in a range of less than 17188 Pa (2.5 psi). By taking multiple data readings at one velocity this accuracy can be improved further. The calculated accuracy for coefficient of pressure, when recording data every 3 seconds for 5 minutes at one velocity is ±0.05. This type of accuracy was observed in the results for most of the pressure taps at almost every wind orientations. Despite changes in velocity it can be seen that the Cp value at each location remains fairly constant. The values for Cp at each location also change with change in the incoming wind direction with more pressure on the windward side and less on the leeward side. There are some exceptions steep pressure gradients occur at the corners and surface steps. And for some wind orientations certain taps displayed irregularities in Cp as velocity was increased. This was observed during the +90degree test and the +45degree test on taps close to a smooth leading edge. An example of this is seen in Figure 3-3 below. Tap #10 in particular displays a large irregularity in Cp as velocity is increased. This tap is on the windshield of the model and very close to the incoming wind edge (see figure 4 Appendix 2A).

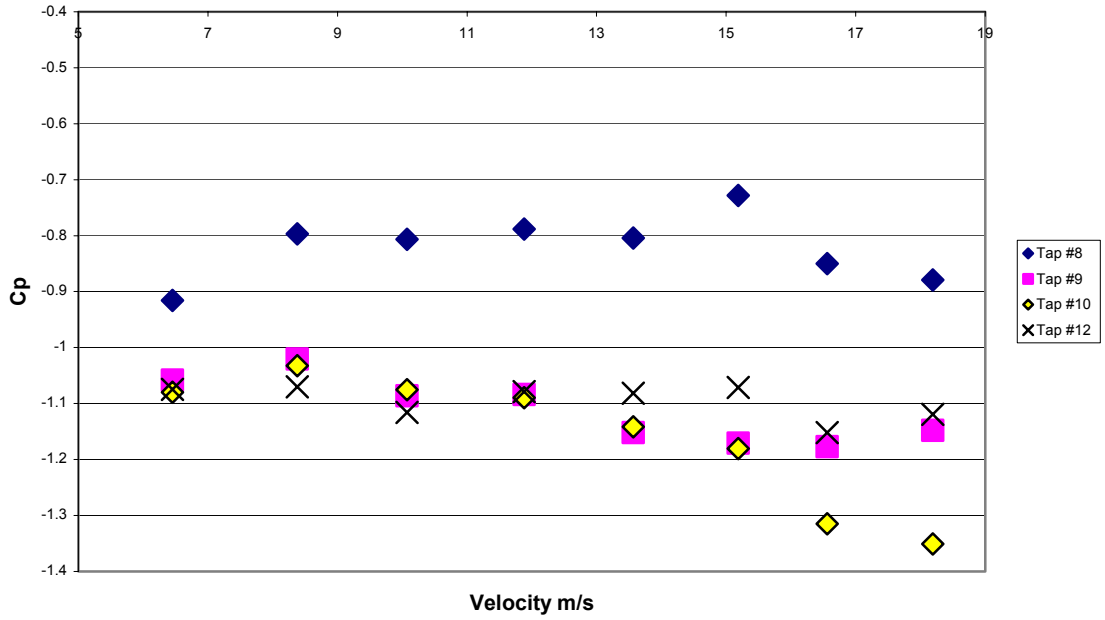

Figure 3-3: Ambulance Cp vs. Velocity distributions for 90 degrees angle of attack

For the tests where discrepancies such as the one displayed in Figure 3-3 were observed the test was repeated twice, one to prove repeatability and the second time after the surface windward of the pressure tap was roughened with sandpaper to help create turbulence in the boundary layer and reduce the severity of boundary layer separation. This is discussed in many texts on controlling boundary layer separation. For example, Schlicting [12] mentions that "Separation can only be avoided when the flow in the boundary layer is turbulent. A laminar boundary layer can support only a very small pressure rise so that separation would occur with even very slender bodies".

The combination of retests and original test is shown in Figure 3-4 below. The retests in combination with the original tests and the complete results for the wind tunnel testing are displayed as Cp vs. velocity for each pressure tap for the various angles tested in Appendix 2B. These results are summarized in figures 3-5 through 3-11 below. As with the fire truck model the symmetry argument is used to combination of the ± testing orientations to obtain a picture of the pressure distributions about the model at orientations between 0 and 180 degrees. For the cases with a retest where there is a difference between measured Cp values the mean between the tests was used as the Cp value for that tap at that orientation. (This only had to be done for a few cases, notably those displayed in Figure 3-4 below).

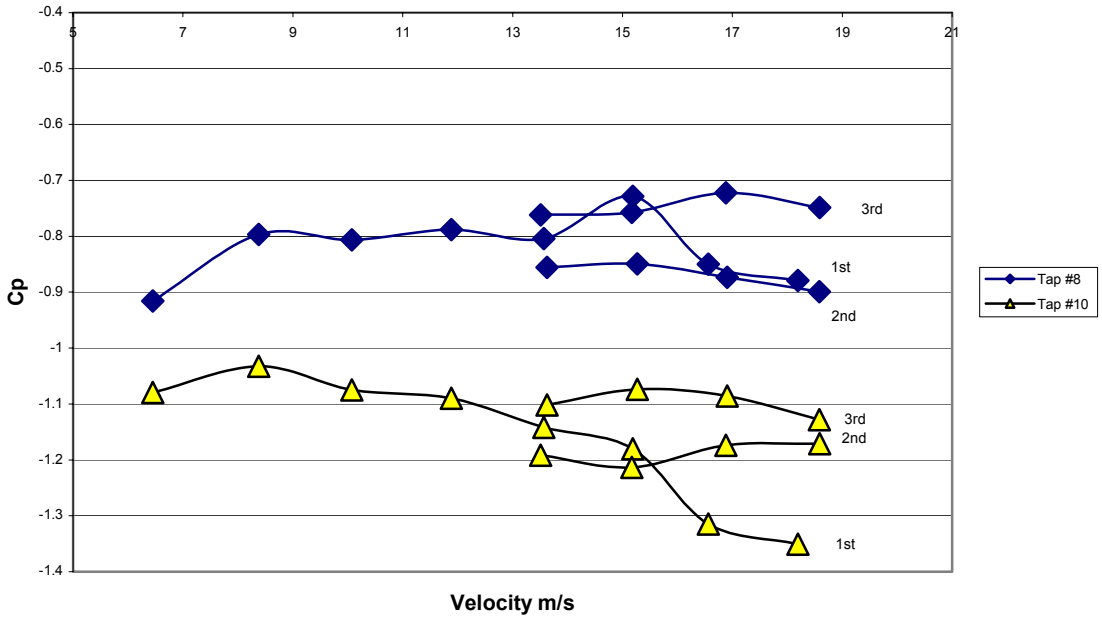

Figure 3-4: Ambulance Cp vs. Velocity distributions for 90 degrees angle of attack including retests (Note: lines were drawn through the experimental data to help differentiate between the different test runs.)

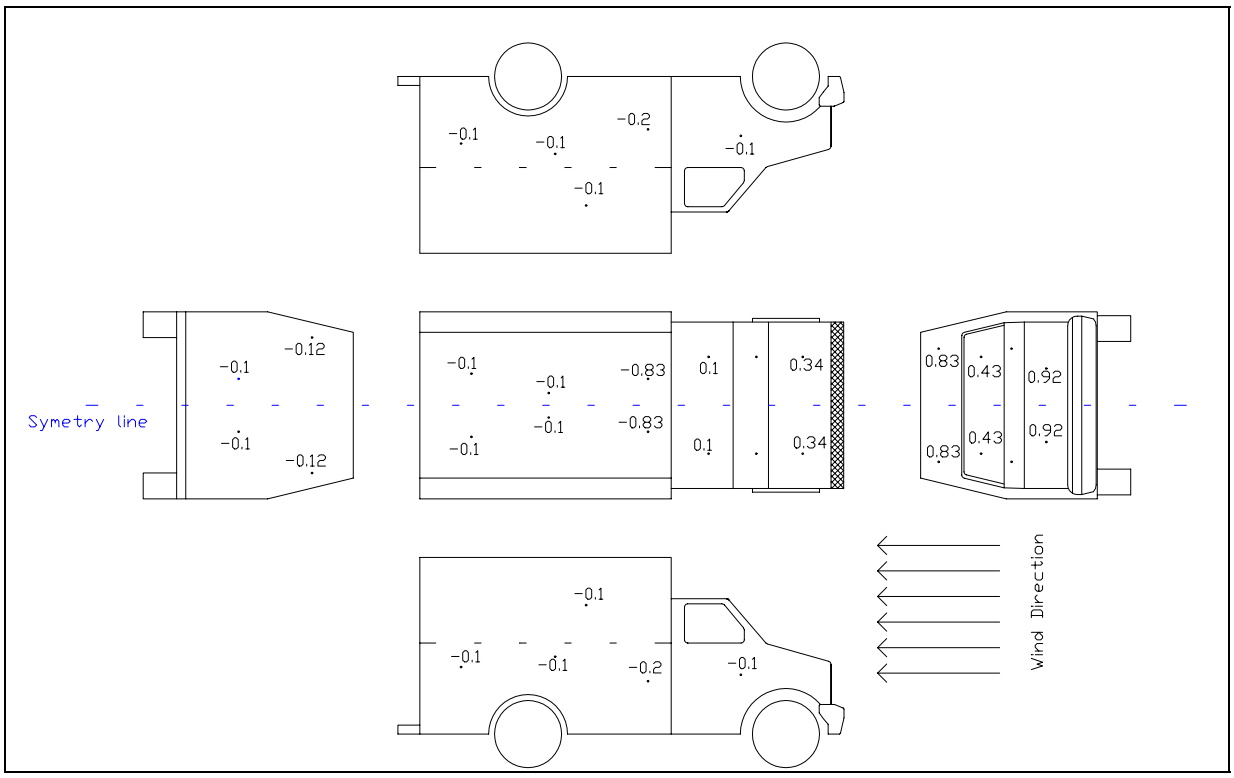

Figure 3-5: 0 Degree Coefficient of Pressure Test results

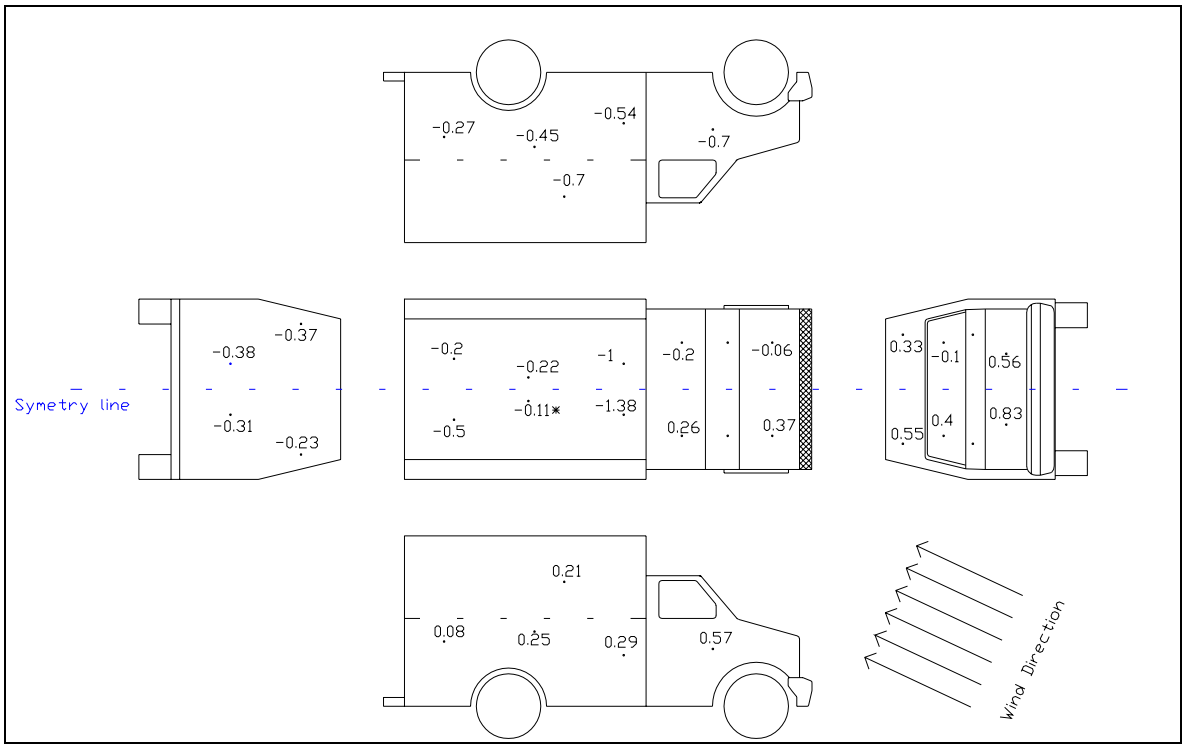

Figure 3-6: 25 Degree Coefficient of Pressure Test results

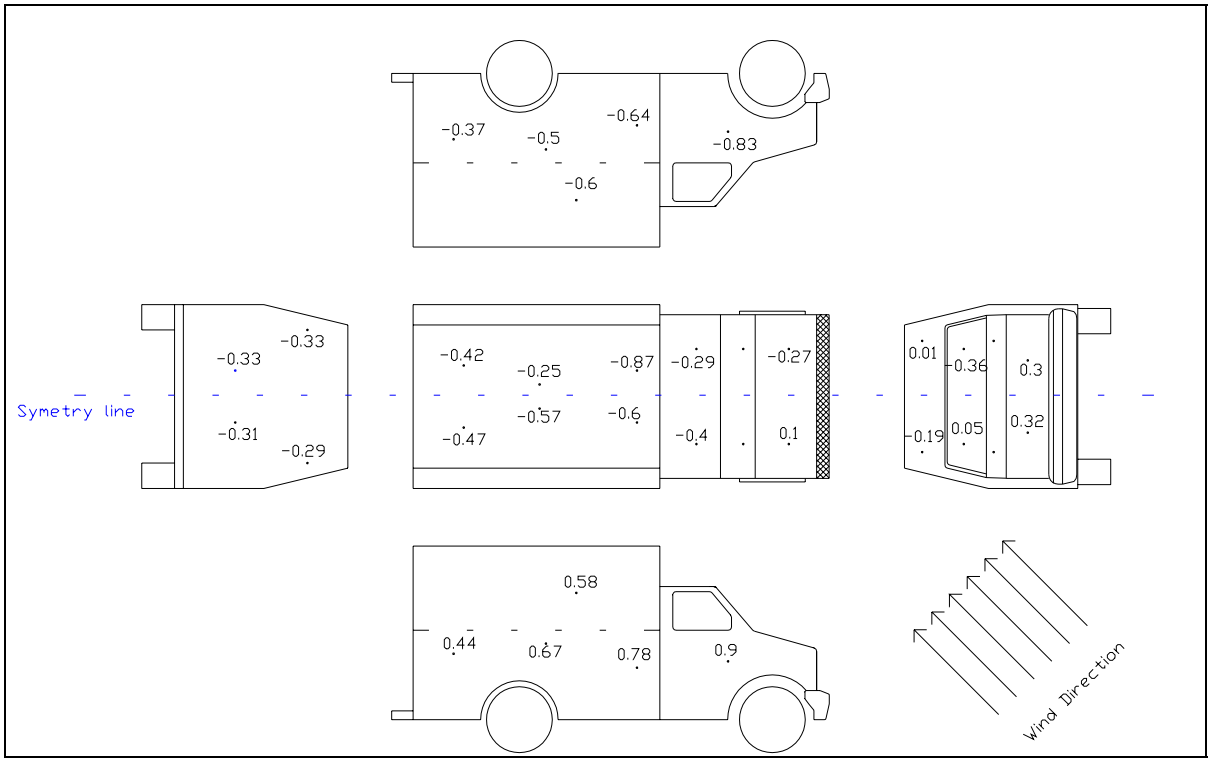

Figure 3-7: 45 Degree Coefficient of Pressure test results

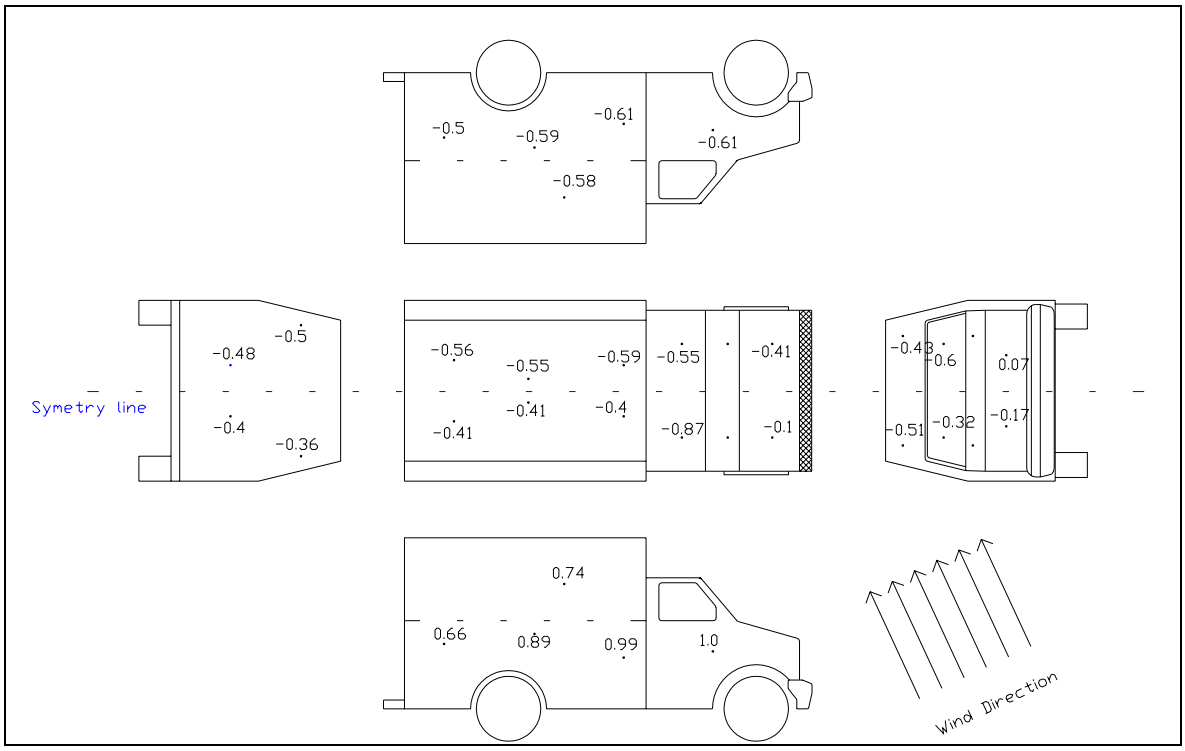

Figure 3-8: 65 Degree Coefficient of Pressure Test results

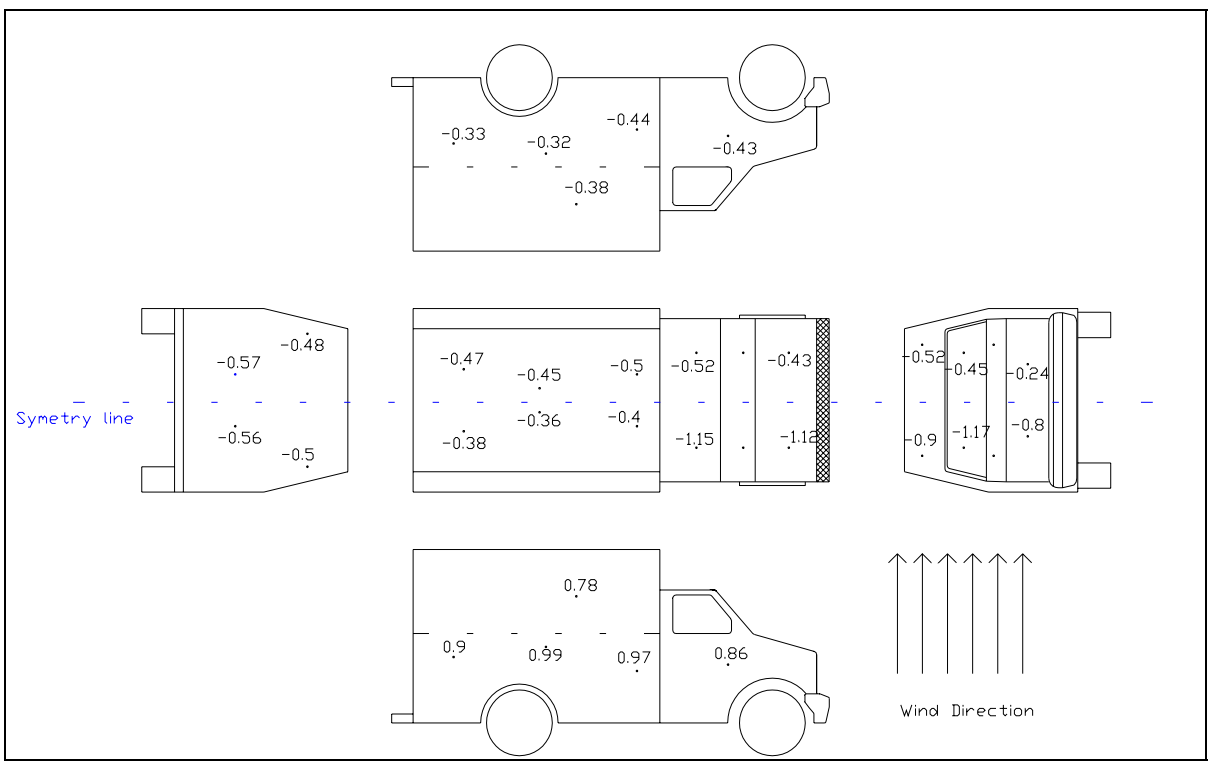

Figure 3-9: 90 Degree Coefficient of Pressure Test results

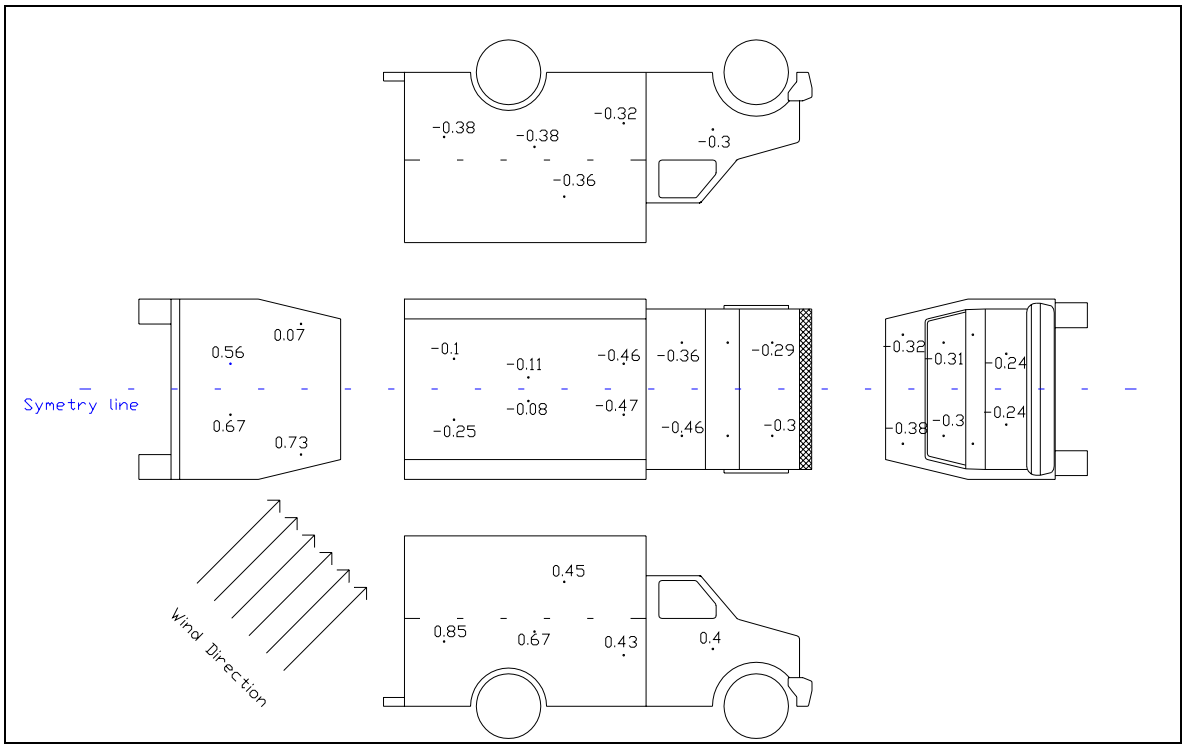

Figure 3-10: 135 Degree Coefficient of Pressure Test results

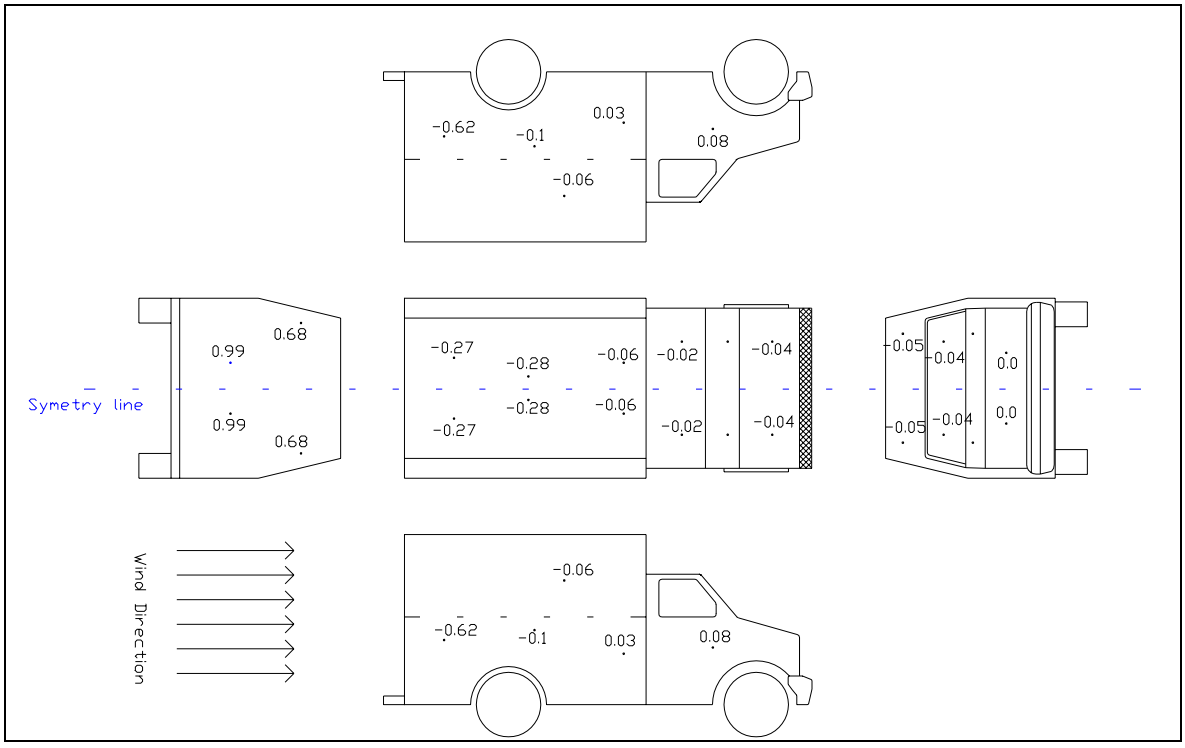

Figure 3-11: 180 Degree coefficient of pressure test results

3.3 COMPARISON BETWEEN THE FORCE BALANCE AND PRESSURE DISTRIBUTION - VALIDATION OF THE RESULTS

3.3.1 Determination of Forces Acting on the Vehicle

(*Note this description for determining the forces acting on the vehicle was given in the fire truck section of the report but is repeated here as a reminder.)* From the wind tunnel tests, coefficients of pressure at various locations and various relative wind directions are known. This information is used to compute the forces acting on a vehicle as a function of wind speed. Coefficient of pressure is defined as local dynamic pressure divided by freestream dynamic pressure. As in the following equation:

$$Cp \equiv \frac{LocalDynamic\,\mathrm{Pr}essure}{TotalDynamic\,\mathrm{Pr}essure} \tag{3-3}$$

Pressure is defined as a force over an area. Wind speed is a function of freestream dynamic pressure through the following equation:

$$Vel = \sqrt{\frac{2(p_{Total} - p_{Static})}{\rho}} \tag{3-4}$$

Here ρ is the density of air (assumed to be 1.225 kg/m^3), and $(p_{Total} - p_{Static})$ was measured with the Pitot-static tube and is the freestream dynamic pressure. Rearranging equation 3-3 and combining with 3-4 gives

$$LocalDynamic\,\mathrm{Pr}essure = \frac{1}{2}V^2\rho \times Cp \tag{3-5}$$

Local force can therefore be computed using the local area, $Apanel$, and multiplying it by the local dynamic pressure. Dividing the model into sections or panels on which it is assumed that Cp is constant gives the following equation, which is a function of velocity:

$$Fpanel = V^2(\frac{1}{2} \times \rho \times Cp \times Apanel) \tag{3-6}$$

Summing the forces on all the panels over the vehicle for a certain wind angle and velocity gives the resulting force acting on the model. Some guesswork was used in deciding which area should be used for each panel. For the pressure taps where Cp is determined from symmetry of the vehicle, Cp values are labeled “prime” to indicate that they are a result of symmetry. For the panels on the sides and top of the vehicle the edge of the area was chosen as half the distance between the two pressure taps. For the front and rear of the fire truck the panels where chosen slightly differently. This is shown in the following set of figures (all drawn too scale).

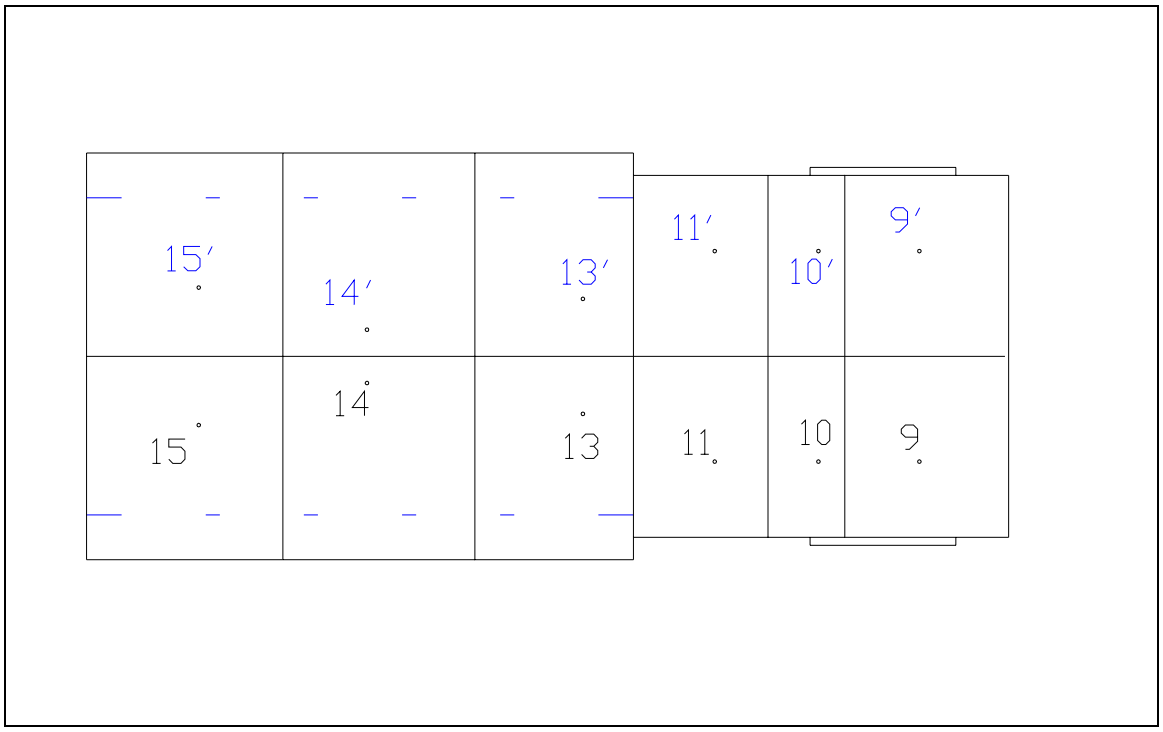

Figure 3-12: Panel division on the top of the ambulance

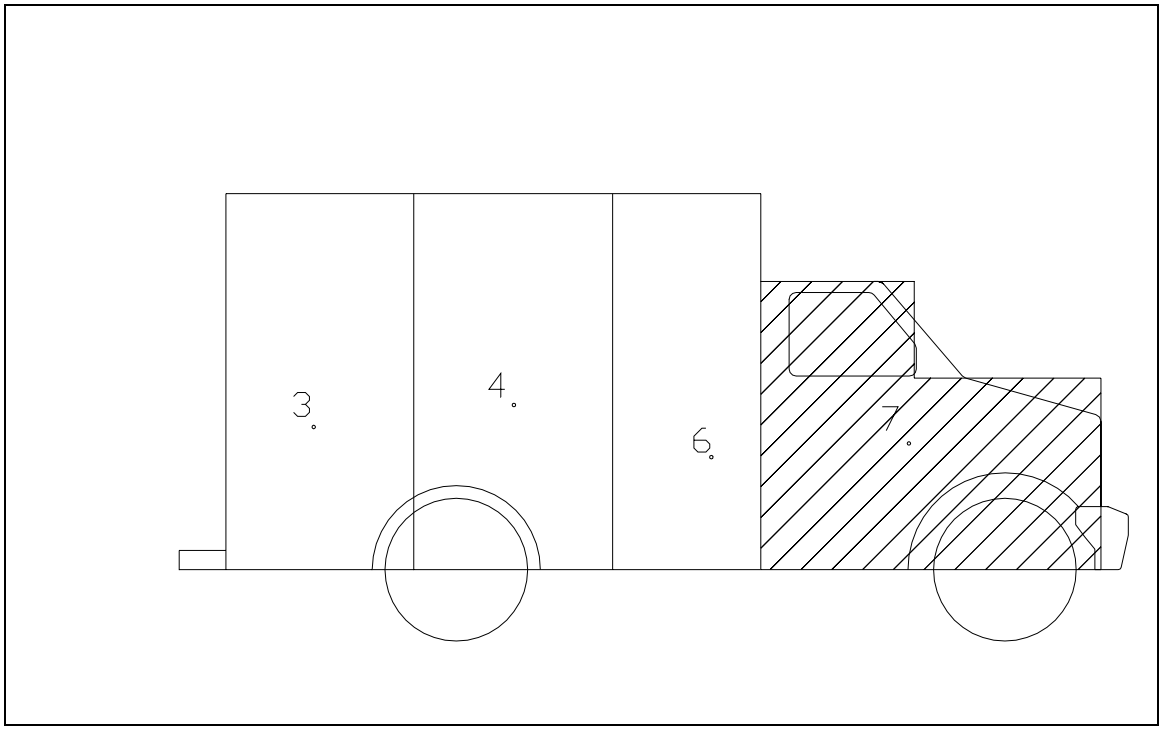

Figure 3-13: Panel division on the sides of the ambulance

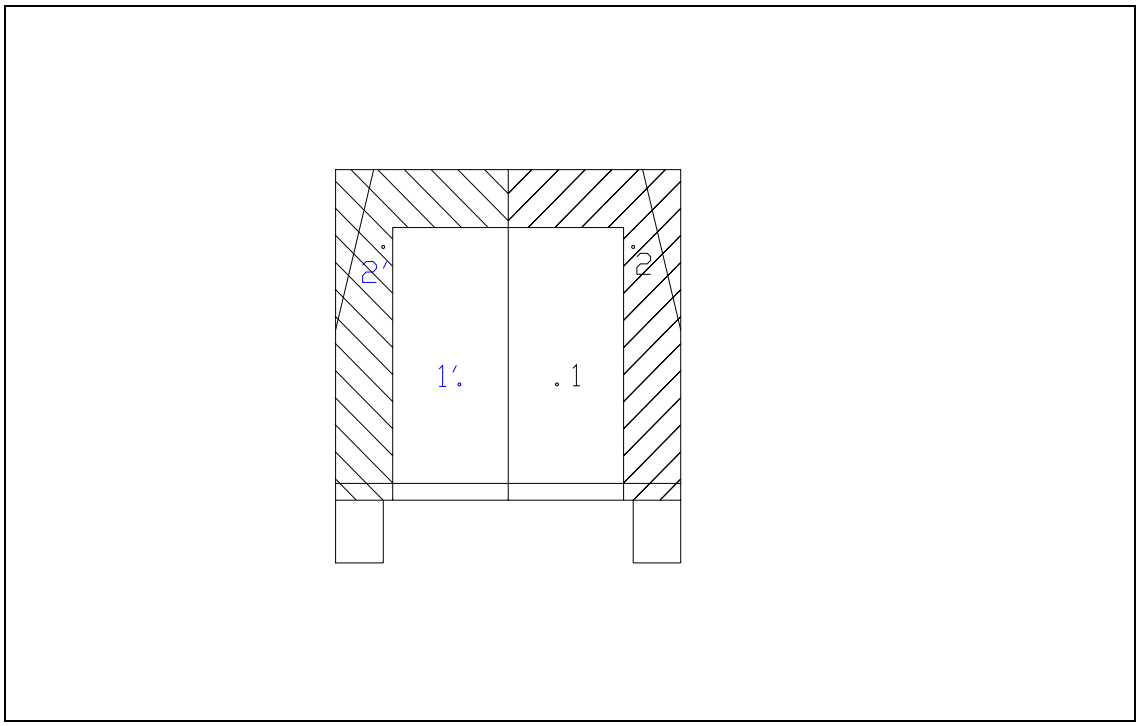

Figure 3-14: Panel division on the rear of the ambulance

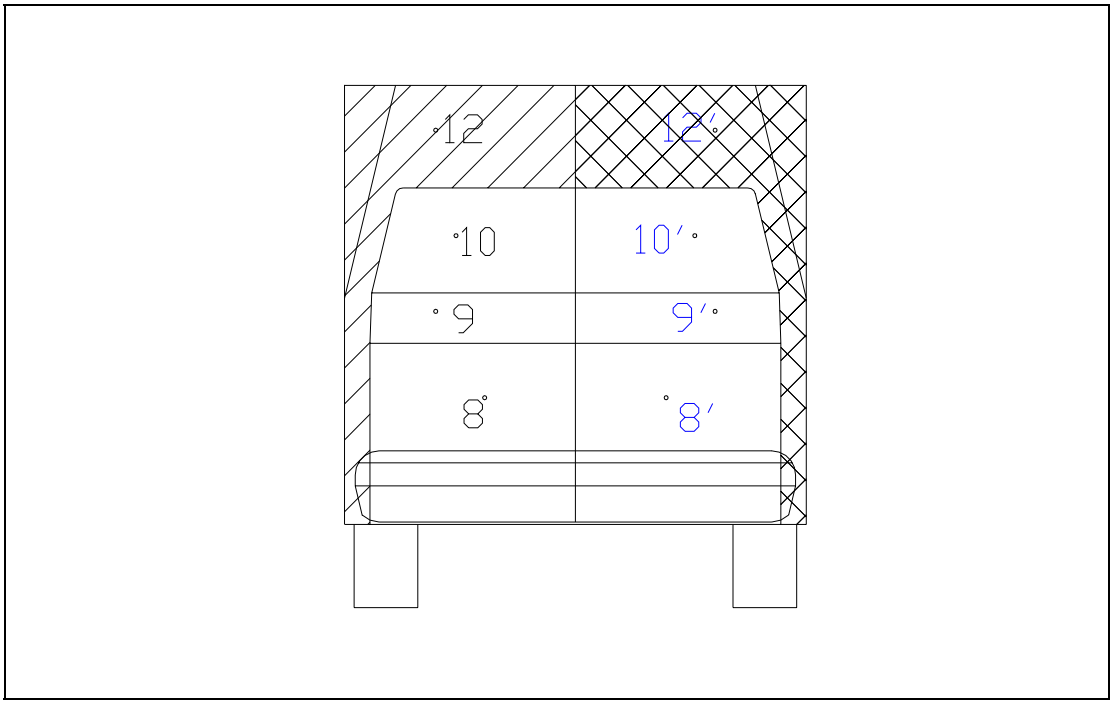

Figure 3-15: Panel Division on the front of the ambulance

Geometrically the ambulance model construct by Tonka toys and used for testing in the wind tunnel is very similar to the full scale Type I ambulance used by fire departments. There are; however, slight differences. One difference is that the side of the Tonka model has a slight curvature the real model does not. To account for this tap #5, which resides

on this curvature is not used in the full-scale analysis because the measured Cp on that surface was lower than the Cp values on flat surfaces near it. The panel division was modified from the wind tunnel model to account for this, as shown in the previous figures. As can be seen the patient module is assumed square. This modification; however, was not used for the following comparison between the force balance readings and the pressure forces on the model in the wind tunnel.

3.3.2 Comparison between force balance results and measured pressure results

To help ensure the accuracy of the results a strain gage force balance was used to measure drag and side force on the model at different orientations and different velocities. The force balance was used to measure drag and sideways force at 0, ±45, and ± 90 degrees. This is compared to the forces resulting from the pressure distributions and is shown in the figures below, not that the force balance measurements are corrected for stem drag.

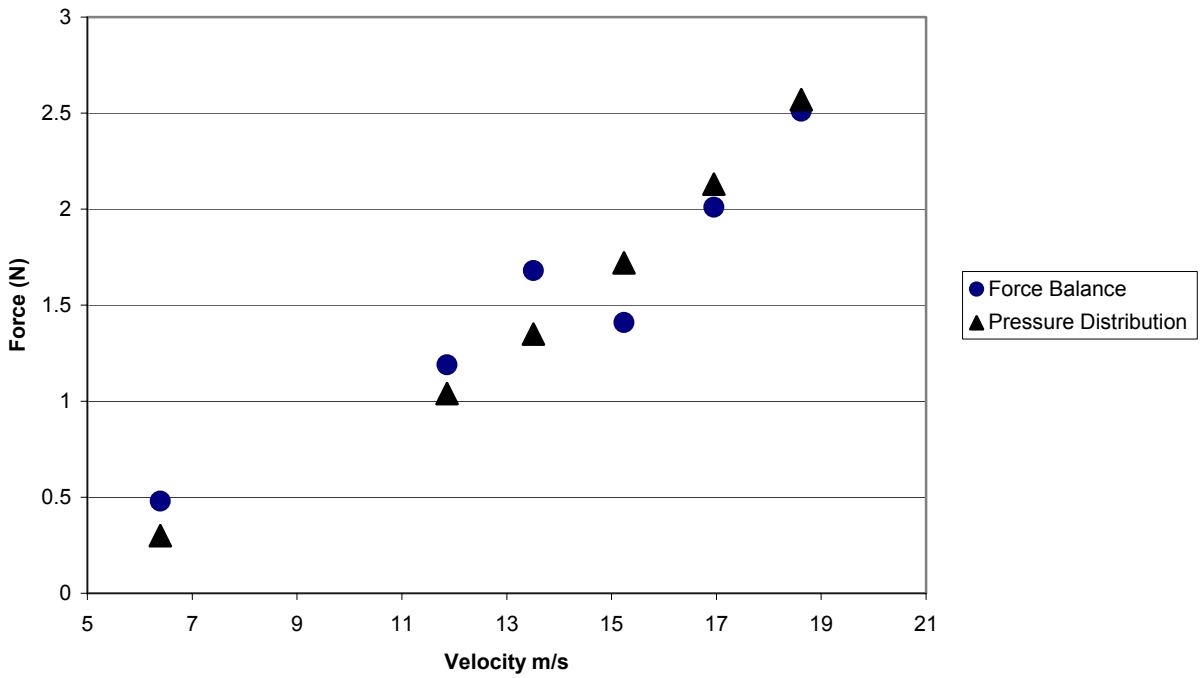

Figure 3-16: Force Balance and Pressure Distribution comparison at 0 Degrees

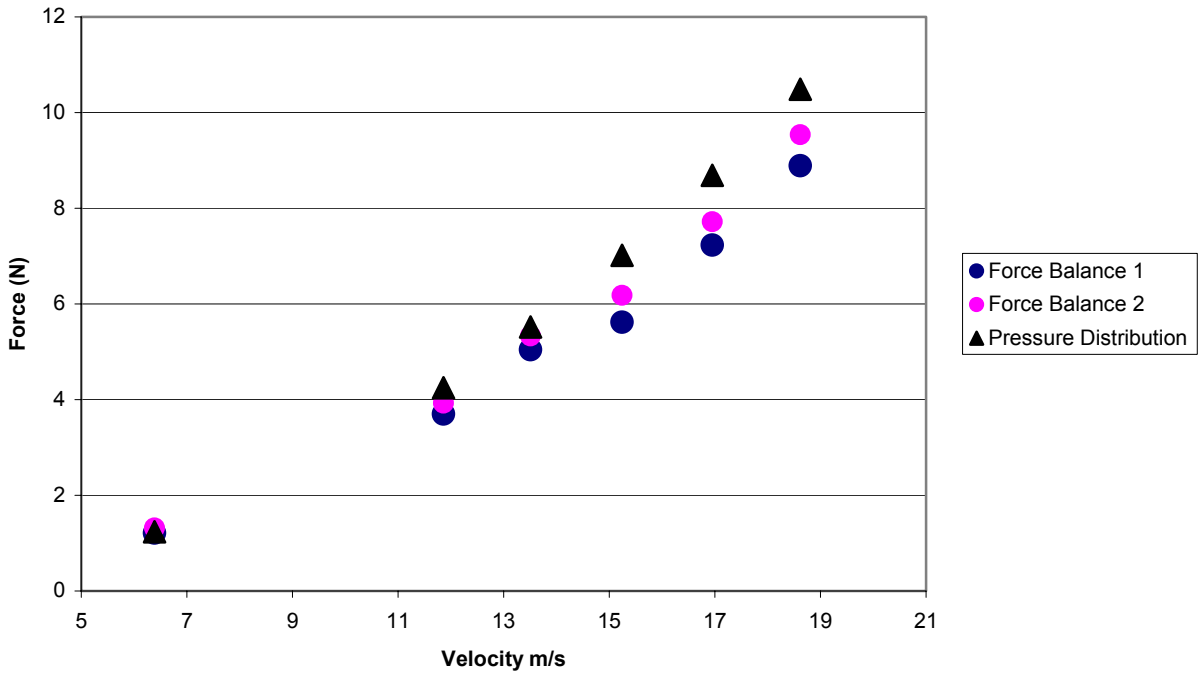

Figure 3-17: Force Balance and Pressure Distribution Comparison at 45 Degrees

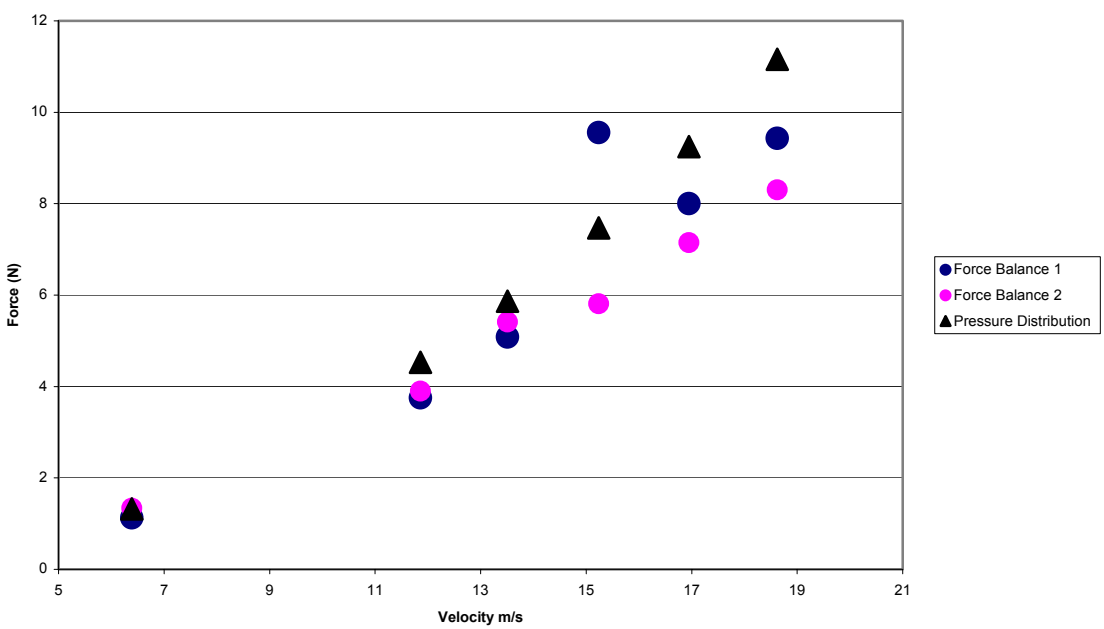

Figure 3-18: Force Balance and Pressure Distribution comparison at 90 Degrees

Using the symmetric argument about the vehicles lengthwise axis it is assumed that the forces acting on it for a wind angle of +45 degrees will be the same as if the wind were acting at –45 degrees. Therefore in the above plots Force balance 1 represents the force

balance measurements at +45 degrees, and force Balance 2 represents the force balance measurements at –45 degrees. Even so, it can be seen that there is about a 10% difference between the two force balance measurements, at some wind speeds. The method discussed in section 2 above is the method used for computing force as a result of pressure distribution. As can be seen the agreement between the force balance and pressure distribution fairly close for all three angles.

3.3.3 Influence of Reynolds Number

For the model, testing was conducted for a Reynolds number range between 1.75×10^5 and 4.9×10^5. These values come from an equation in Anderson [2] below

$$R_e = \rho_\infty \frac{V_\infty x}{\mu_\infty} \tag{3-7}$$

In this equation:

R_e is Reynolds number
ρ is the density of air
V is the velocity
μ is the viscosity of air
x is the distance from the leading edge.

The subscript infinity defines far upstream from the model. The length of the model is 36 cm long (13.8 in), standard density and viscosity values for air were used at sea level. Velocity was the only parameter that changed giving the stated Reynolds number range.

Reynolds number is one of the simulation requirements Gawthorpe [3] mentions for effective wind tunnel modeling of a vehicle. The other two requirements are simulation of the ground plane, and the same onset of wind characteristics. These two were achieved in the setup. Testing is concerned with steady winds not gusting, and steady winds were modeled. The platform simulated the ground plane. Although it was not a moving ground plane which would have given a better simulation.

Reynolds number was not completely matched. For a full-scale vehicle Reynolds number would be above $\underline{4.5 \times 10^6}$. The largest Reynolds number tested with the model was only $\underline{4.9 \times 10^5}$. Both Gawthorpe & Anderson; however, suggest that if the boundary layer is turbulent then the same pressure forces can be generated on the surfaces at lower Reynolds numbers. From what was seen in the fire truck testing, it is assumed that there is a turbulent boundary layer for this model also. This is supported by the fact that scattering was observed at each pressure tap at every velocity and orientation.

3.4 CRITICAL WIND SPEEDS

3.4.1 Introduction

(*Note: this description for determining the forces acting on the vehicle was given in the fire truck section of the report but is repeated here for completeness.)* In the book *road vehicle Aerodynamic Design* [7], Barnard indicates that vehicle accidents due to severe weather can result from overturning, course deviation, or hitting fallen trees and other debris. Course deviation and overturning will be considered in this analysis.
When a vehicle (assumed symmetric about it's centerline) is traveling down the expressway with no crosswind, normal forces acting on the vehicle will only include a Pitching Moment, a Lift force, and a Drag force. In a cross wind the vehicle will experience several additional actions. These actions can be a side force, a yawing moment, and a rolling moment. All the forces acting on a vehicle with a non-zero yaw angle (between vehicle axis and relative wind direction) are shown in Figure 3-19 below.

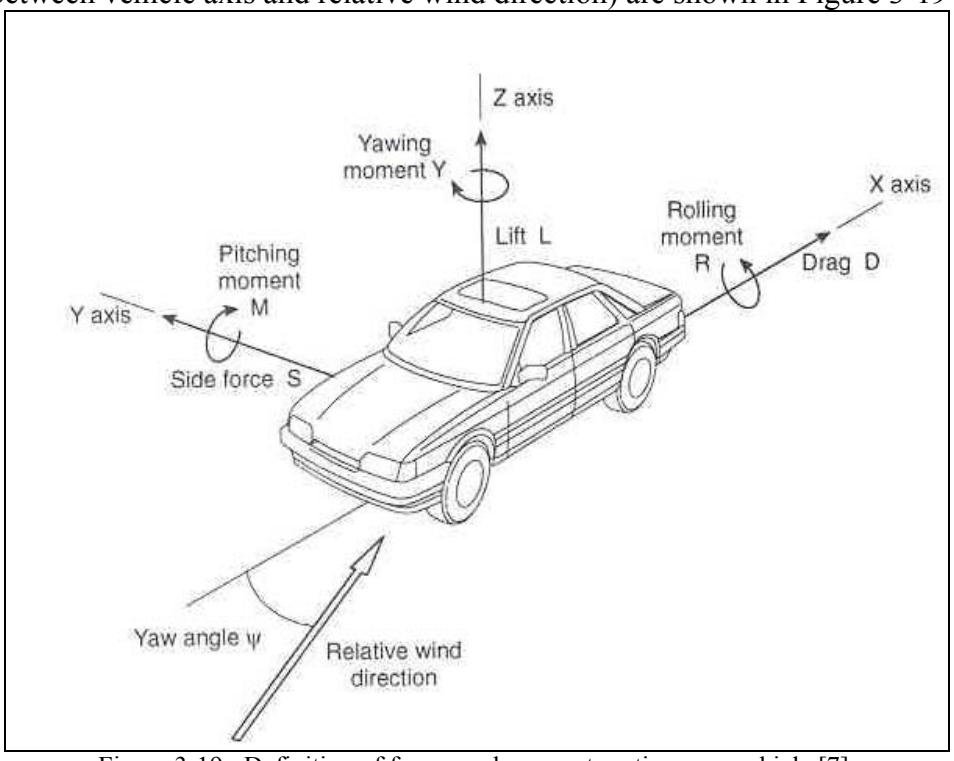

Figure 3-19: Definition of forces and moments acting on a vehicle [7].

3.4.2 Determination of Critical Wind Speeds Due to Course Deviation

3.4.2.1 Definition of Course Deviation

Course deviation occurs when a vehicle is blown off course. An accident as a result of course deviation can occur through a vehicle being blown off the road, into other vehicles, or other obstructions. It is likely that an experienced driver could correct for small course deviations; while violent course deviations will regardless result in an accident.

For this study the critical wind speed due to a course deviation will be defined as the speed at which due to combined forces and moments acting on a vehicle – a course deviation will begin to occur.

3.4.2.2 Calculating Forces and Moments on the Ambulance

A vehicle in a crosswind will have three forces and three moments acting upon it. From the wind tunnel testing the coefficients of pressure at different locations for different wind yaw angles are known. This information was used in conjunction with equation (2-4) to calculate the forces acting on the different panels of the model. The wind tunnel model, as stated earlier, closely resembles a F-350 Type I ambulance. In terms of scaling factors between the two: it is a 1:21th scale along the wheelbase. This is the scale used for analysis.

3.4.2.3 Vehicle Weight and Center of Gravity

For the F-450 Type I ambulance, Wheeled Coach Industries [10] lists this vehicle as having a Gross Vehicle Weight Rating (G.V.W.R.) of 6,600 kg (14,500lbm) with 2200kg on the front axle and 4400kg on the rear axle. (This information was collected from Rusty Bollock a representative of Wheeled Coach Industries through a phone interview) As is usual GVWR is defined as 5% minimum above the actual weight the vehicle is expected to carry.

In order to compute yawing and pitching moment acting on a vehicle it is necessary to reduce the forces acting on the vehicle to some arbitrary point. When this point coincides with the center of rotation, the resultant is a force. Otherwise, the resultant is a force and a moment. Some studies, [7] for example, use the midpoint between the front and rear axle as the point for the reduction of forces. In this part of the study, the forces are also reduced to the midpoint between the front and rear axle.

3.4.2.4 Lift, Drag and Side Forces

Lift, drag and side forces are defined as shown in Figure 3-22. The side force is computed by summing the forces acting on both sides of the vehicle. The drag force is computed by summing the forces on the front and rear of the vehicle. The lift force is computed by summing the forces acting on the roof of the vehicle. In reality there are forces acting underneath the vehicle and these should be accounted for in the lift force. But the pressure forces were not measured underneath the model, because the moving road condition could not be modeled. This will contribute an amount of uncertainty to the final results.

3.4.2.5 Pitching and Yawing Moments

The moments are computed by summing the wind forces acting about the midpoint between the vehicle axles. The yawing moment is computed from forces acting in the X-Y plane, and the pitching moment is computed from the forces acting in the Z-X plane. Knowing the forces on each panel, and the distance from the center of each panel to the origin of the X-Y axis, the moment contribution from each force about the axis is known. Summing the total moments about the axis gives a single yawing moment about the

origin. The whole system of forces can therefore be reduced to a resultant force and resultant moment.

3.4.2.6 Combination of Moments and Forces to Determine Course Deviation

Using equation 2-4 and the summation of forces and moments method discussed in the previous two sections for any vehicle speed the forces on the vehicle can be predicted. In terms of course deviation analysis the side force and yawing moment can be balanced against the resistive force of the vehicle weight. This is shown in Figure 3-20 below.

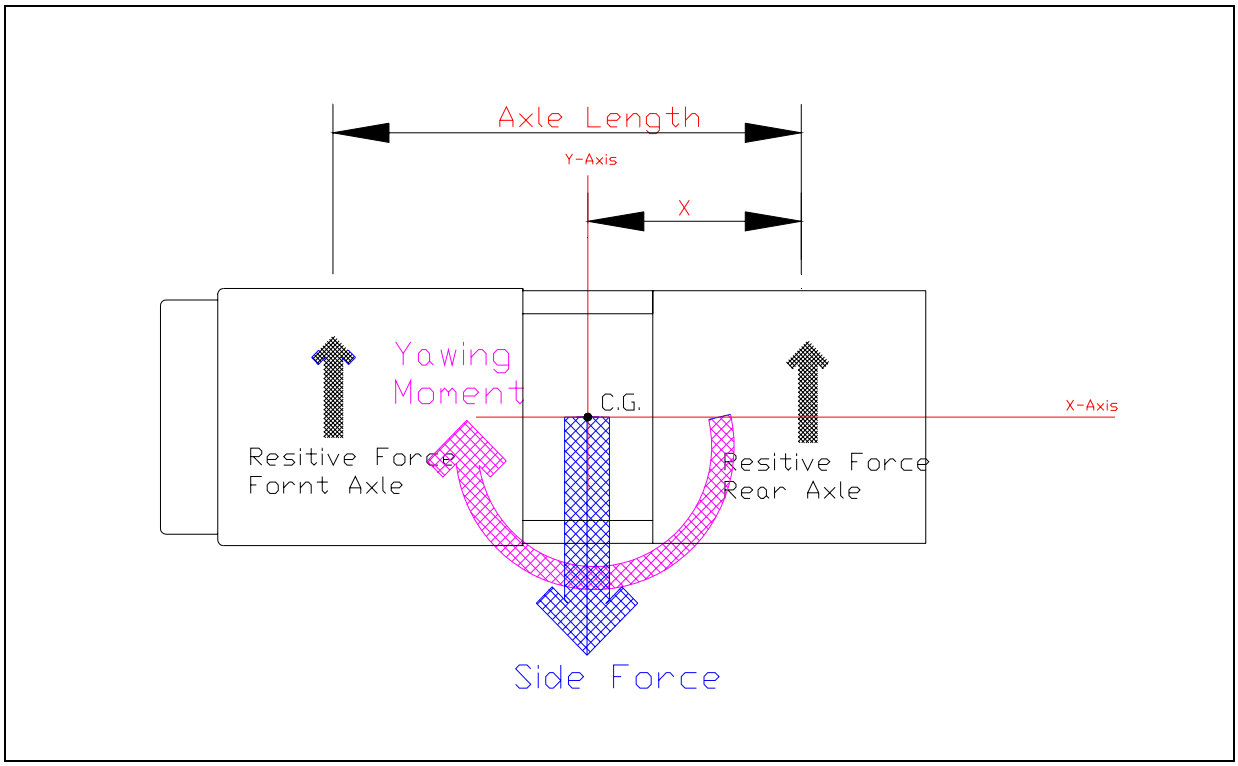

Figure 3-20: Balancing yawing moment and side force against the resistive force per axle.

In Figure 3-20 the yawing moment and side force are known as a function of velocity. The resistive force per axle depends upon vehicle weight per axle and the coefficient of friction between the tires and the roads. If two objects are being held together by some force (wheels on pavement, held together by gravity) the coefficient of friction tells what ratio of the force holding the objects together must be used to begin to slide one object over another (see reference 14 for more details).

In the above figure, the yawing moment, side force, and distance from each axle to the center of gravity are used to determine the side force acting on each axle. The equilibrium equations for each axle are shown below.

$$WindforceFrontAxle = \frac{YawingMoment + Sideforce * X}{AxleLength} \tag{3-8}$$

$$Windforce\,\mathrm{Re}arAxle = \frac{-YawingMoment + Sideforce * X}{AxleLength} \tag{3-9}$$

In these equations X is half the axle length (Recall that the fire truck the forces and moments were reduced to the center of gravity, here they are reduced to the center between the two axles). The yawing moment and side force are calculated as a function of wind angle, and vehicle speed. The moment is positive counterclockwise, and negative clockwise. In order for a course deviation to be avoided the forces per axle must be less than the resistive force available on that axle.

The resistive force on each axle depends upon the coefficient of static friction between the tires and the road, and the weight acting on each axle. Due to the pitching moment and lift the weight per axle will differ with wind speed and yaw angle. The result is an effective weight per axle.

The following are the equations relating the effective weight per axle to the lift, pitching moment, and the G.V.W.R per axle.

$$E_f = G_f - \frac{Lift * X + PitchingMoment}{AxleLength} \tag{3-10}$$

In this equation E_f is the effective weight on the front axle, and G_f is the weight on the front axle based upon the gross vehicle weight rating, plus any adjustments due to an empty or full condition. X is half the distance between the axles. Similarly an equation can be defined for the rear axle:

$$E_R = G_R - \frac{Lift * (X) - PitchingMoment}{AxleLength} \tag{3-11}$$

In this equation E_R is the effective weight on the rear axle, and G_R is the weight on the rear axle based upon the gross vehicle weight rating, plus any adjustments due to an empty or full condition.
In terms of course deviation analysis the resistive force per axle can now be defined.

$$R_{force} = E\mu \tag{3-12}$$

In Equation 3-12 E is the effective weight for the front or rear axle from equation 3-11 or 3-10, μ is the coefficient of static friction, and R_{force} is the resistive force provided by that axle.

3.4.2.7 The Importance of the Coefficient of Static Friction

The coefficient of static friction (μ) is defined as the ratio of frictional force to the normal force pressing two surfaces together. It can also be known as the coefficient of adhesion. For some surfaces this value is known very well.

For galvanized rubber on different road surfaces this is a value that is not very well documented because it depends upon numerous variables. For example it is assumed that for racing slicks on dry pavement the coefficient of static friction (μ) will be

approximately 0.9 or more, and for wet pavement about 0.1 or less (if hydroplaning occurs). This is why certain type of car races are not conducted in the rain.

For automobiles the coefficient of static friction (μ) will usually be somewhere between 0.1 and 0.9. These are unsubstantiated numbers, but in the National Highway Traffic Safety Administrations "Rating System for Rollover Resistance" [8] it states that "For a good dry paved surface, μ may be in the neighborhood of 0.9. But for wet, icy roads, μ is considerably less." There are several reasons for this broad uncertainty. The first is that this value depends upon the chemical composition of the tire and the road. Another factor is the tire pattern and the tire pressure. And finally, it depends upon the conditions of the road. For a hot, dry day μ will be highest. For a cold wet day μ will be considerably lower.

One of the worst-case scenarios for μ would be immediately after it begins to rain. Most roads are porous, and they absorb the oil and other products from the cars. When it rains, oil being less dense that water is displaced and a thin film of oil is produced on the surface road – this inevitably leads to slipperiest conditions. The only case where μ *might* be reduced more is when a road is covered in a sheet of ice.

3.4.3 Course Deviation

Gawthorpe [3] states that the shape of a vehicle largely fixes proneness of road vehicles to course deviation in a crosswind in addition to its weight distribution. Rear-engine cars with low tails are more prone than front-engine cars with high tails. For the wet road analysis a coefficient of static friction of 0.2 was used. For the dry road analysis a coefficient of static friction of 0.8 was used.

	Course Deviation Speed	
Wind Angle	Dry Roads	Wet Roads
25	66 (148)	34.1(76)
45	53 (119)	28.3(63)
65	51.2(115)	28.4 (64)
90	49.8 (112)	29.8 (67)
135*	63.5(142)	33.8(76)

Table 3-1: Wind Speed to Cause a Static Course Deviation-Ambulance-The vehicle is not moving.
*Denotes instability in the rear axle.

Table 3-1 shows the static results. The first number has the units of meters per second and the number in parenthesis has the units of miles per hour. This information only indicates at which cross wind speed a parked vehicle will begin to move in its parking space. Note also that for all wind angles except 135 degrees the vehicle displays instability on its front axle. For 135 degree the vehicles rear axle is the axle which will begin to move first.

Also note that course deviation analysis was not computed for 0 or 180 degree angles. This is because a course deviation will not occur for winds acting on these angles, but they will affect the vehicle in other ways. For example a strong tail wind will increase the stopping distance by an undocumented amount.

Nevertheless, the static analysis cannot be considered by itself. When traveling down the highway, the vehicle speed in addition to the wind speed must be considered to determine the speed at which a course deviation will occur. This creates a resultant wind speed that for wind angles between 0 and 90 degrees will be higher than just the wind relative to the road.

The law of cosines must be used with vehicle speed, the resultant wind speed and the resultant wind angle to compute the crosswind speed; which will result in a course deviation. The law of cosines rearranged for this use is:

$$c = \sqrt{vs^2 + rs^2 - 2(vs)(rs)\cos 45} \tag{3-13}$$

In this equation *c* is defined as the crosswind speed, *vs* is defined as the vehicle speed, and *rs* is defined as the resultant wind speed. Taking vehicle speed into consideration the following tables demonstrates vehicle speed and necessary cross wind speed to create a resulting wind angle course deviation. This analysis was done for wet roads.

Vehicle Speed	Crosswind to cause a Course Deviation	Yaw Angle (Degrees)
12m/s (27mph)	24m/s (53mph)	37
16m/s (35mph)	21m/s (46mph)	44
20m/s (45mph)	18m/s (40mph)	53
25m/s (55mph)	16m/s (**34mph**)	68

Table 3-2: Ambulance vehicle speed and necessary crosswind speed to cause a resultant wind speed of 34m/s at 25degrees.

Vehicle Speed	Crosswind to cause a Course Deviation	Yaw Angle (Degrees)
12m/s (27mph)	21.5m/s (48mph)	68
16m/s (35mph)	20.4m/s (46mph)	79
20m/s (45mph)	20.0m/s (45mph)	90
25m/s (55mph)	20.6m/s (46mph)	104

Table 3-3: Ambulance vehicle speed and necessary crosswind speed to cause a resultant wind speed of 28.m/s at 45degrees.

Vehicle Speed	Crosswind to cause a Course Deviation	Yaw Angle (Degrees)
12m/s (27mph)	26m/s(58mph)	90
16m/s (35mph)	26m/s (58mph)	99
20m/s (45mph)	27m/s (60mph)	107
25m/s (55mph)	29m/s (64mph)	117

Table 3-4: Ambulance vehicle speed and necessary crosswind speed to cause a resultant wind speed of 28.4m/s at 65degrees.

The above tables must be looked at with a little interpretation. In table 3-3 we see that as the vehicles speed increases the crosswind speed which will cause a course deviation will decrease but then it actually increases past a certain vehicle speed. The explanation for this stems from the summation of vectors. The resultant speed and angle is held constant, but as vehicle speed increases the crosswind speed decreases to a certain point (until the Yaw angle reaches 90 degrees) and then the crosswind speed will increase because past this point the vehicle speed no longer sums with the crosswind speed, it actually acts to subtract from it. Therefore one see a deceiving situation when looking at resultant wind angles of 65degrees, and for high vehicle speeds at 45degrees.
The most important result that can be seen is that for a resultant wind angle of 45 degrees the crosswind speed to cause a course deviation is fairly independent of vehicle speed. But for a resultant wind angle of 25 degrees the crosswind speed is fairly dependent upon vehicle speed. Nevertheless, if one is driving an ambulance at 35 or 40 mph there is a strong risk of course deviation if the crosswind speed is 45mph or above for both 25 and 45 degrees. Below this, crosswind speed course deviation will depend more upon Yaw angle of the incoming wind and the speed at which the vehicle is being driven.

3.4.4 Determination of Critical Wind Speeds Due to Overturning

As with the fire truck analysis for the ambulance overturning is defined as the case when the rolling moment exceeds the moment provided by the mass of the vehicle. Statically for different resulting wind angle the speeds to result in overturning are as follows.

Wind Angle	Wind Speed to result in overturning
25°	68m/s (152mph)
45°	54m/s (121mph)
65°	50m/s (112mph)
90°	50m/s (112mph)
135°	62m/s (139mph)

Table 3-5: Ambulance wind speeds to cause static Overturning at different Yaw Angles

Vehicle Speed	Crosswind to cause Overturning	Yaw Angle (Degrees)
16m/s (35mph)	53m/s (120mph)	32
20m/s (45mph)	51m/s (113mph)	35
25m/s (55mph)	47m/s (104mph)	38

Table 3-6: Vehicle speed and necessary crosswind speed to cause a resultant wind speed of 68m/s at 25degrees.

Vehicle Speed	Crosswind to cause Overturning	Yaw Angle (Degrees)
16m/s (35mph)	44m/s (99mph)	60
20m/s (45mph)	42m/s (95mph)	65
25m/s (55mph)	40m/s (90mph)	71

Table 3-7: Vehicle speed and necessary crosswind speed to cause a resultant wind speed of 54m/s at 45degrees.

Vehicle Speed	Crosswind to cause Overturning	Yaw Angle (Degrees)
16m/s (35mph)	47m/s (102mph)	84
20m/s (45mph)	45m/s (101mph)	89
25m/s (55mph)	46m/s (102mph)	95

Table 3-8: Vehicle speed and necessary crosswind speed to cause a resultant wind speed of 50m/s at 65degrees.

Unlike the fire truck, static overturning due to high wind speeds is a real possibility. Wind speeds for this to occur fall into those for a Category Two Hurricane (96-110mph). Based upon the Course Deviation analysis the vehicle would start sliding sideways before these wind speeds were ever reached. But as with the fire truck overturning may still occur as a result of a violent course deviation at a lower crosswind speed.

4 SPORTS UTILITY VEHICLE SECTION

4.1 WIND TUNNEL EXPERIMENTATION

4.1.1 Experimental Setup

Testing was conducted at Florida Tech's Low Speed Wind Tunnel facility with a test chamber section 54 cm x 54cm. For the SUV study, a 2001 Chevrolet Suburban model, 28 cm long, 10 cm wide, and 8.5 cm tall was tested for pressure distributions on its surfaces at various incoming wind angles. The model tested was an exact replica manufactured by Wally™ Die-Cast Models.

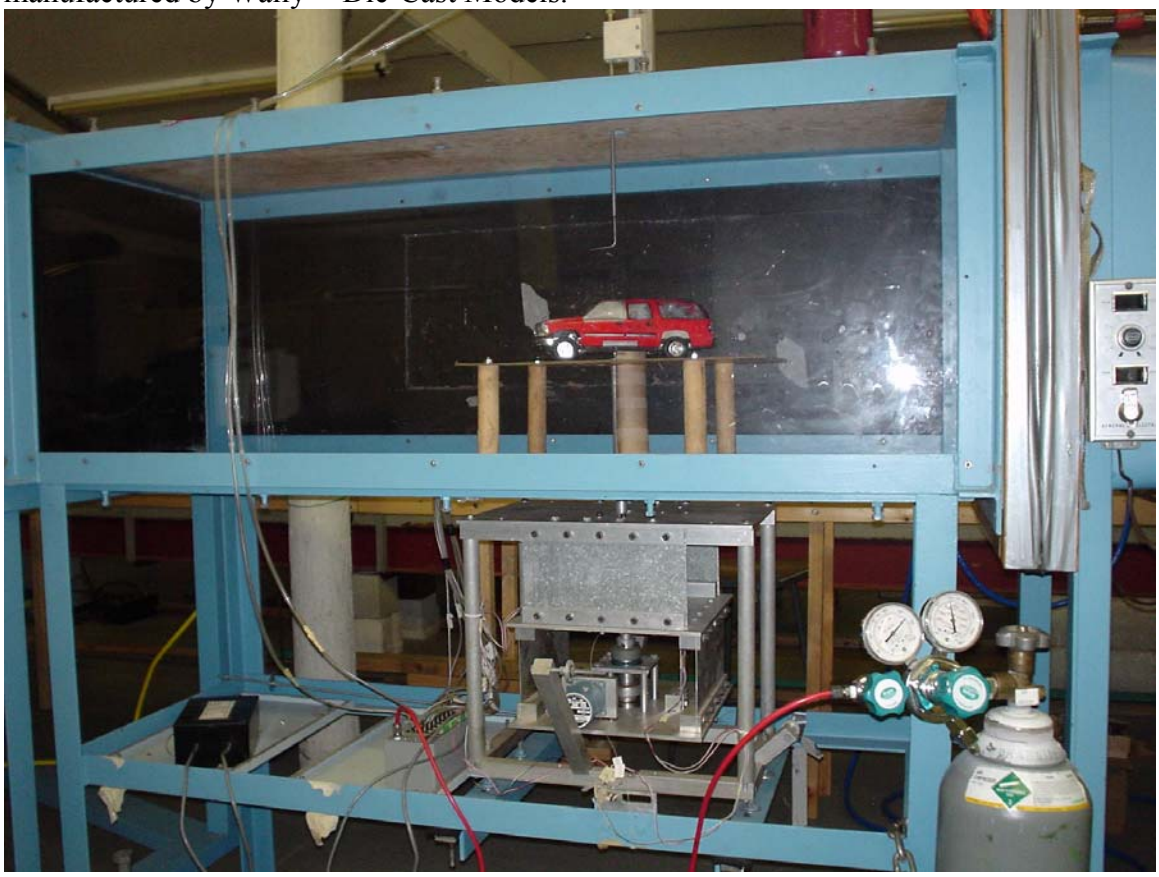

Figure 4-1: Experimental setup with the SUV at a 25 degrees orientation

Figure 4-1 above is a picture of the SUV supported in the center of the test chamber. The wooden platform serves the purposes of dampening vibrations and mimicking the ground effect a vehicle experiences. A Pitot-static tube above the model gives the reference dynamic pressure by measuring the free stream total and static pressures. The Pitot-static tube is 61cm long (24 inches) constructed from stainless steel Located on the front, sides, top, and rear of the fire truck are fifteen pressure taps, which are used to measure surface pressure at their respective locations. These pressure taps are constructed from holes drilled into the model at certain locations. The holes have a 1.6mm diameter with a 5cm length brass tube mounted flush with the outer surface and held in place with a

strong epoxy. Inside the model these brass tubes are attached to flexible 1.6mm diameter Tygon tubing that runs out of a hole cut in the bottom of the model, through stiff cardboard tubing underneath the platform and attaches to a *Multiple Port Pneumatic Intelligent Pressure Scanner* (Model 9010). The cardboard tubing underneath the platform protects the tubing from flapping at higher wind speeds. The location of the pressure taps and numbering convention can be seen in the pictures displayed in Appendix 3A.

The Model 9010 Pneumatic Intelligent Pressure Scanner is manufactured by Pressure Systems and is a completely self–contained pressure acquisition module for multiple measurements of dry, non-corrosive gases. The scanner can be easily interfaced with an RS-232 serial port on any personal computer. The start up software runs through MS-DOS and allows for the collection of data at a specified interval of time. There are 16 pressure input channels, in addition to a run-reference channel and a calibration-reference channel. Dynamic pressures up to 5 psi can be read between the run-reference channel and any of the 16 input channels. Compressed air is used at 85 psi during startup of the equipment to calibrate and re-zero the system. During testing dynamic pressures from 15 locations on the model and one from the Pitot tube are recorded through the 16 channels on the scanner.

4.1.2 Experimental Procedure

The experimental procedure for the SUV was exactly the same as that for the ambulance. For varying velocities up to 20 m/s, surface pressures at the 15 tap locations were recorded. The pressure data was recorded every 3 seconds for a total time of 5 minutes. Prior to data acquisition at least two minutes were allowed for the wind tunnel to settle at each velocity. Another parameter tested was pressure distribution as a function of incoming wind angle. This was done by repeating the test for all velocities at yaw angles of 0, ±25, ± 45, ±60, ± 90, ± 135, and ±180 degrees. 0 degrees is defined as the condition where the front of the vehicle faces the oncoming wind. The definition of yaw angle is the same as previously defined.

4.2 WIND TUNNEL RESULTS

4.2.1 Scatter in Measurements

Steps, similar to the ones implemented for the ambulance, were taken to reduce the possibility of scatter in the results. The steps taken were to:

- Shield the electronics to ensure that electro-magnetic field created by the wind tunnel's 15 kW electric motor were not causing interference.
- Check the connections for each pressure tap to ensure that there were no leaks.
- Use the rigid wooden platform to ensure that vibrations would be dampened. The platform served the dual purpose of mimicking a ground effect.

- Use a stiff cardboard piping system beneath the platform to protect the thin Tygon tubing from vibrations at higher wind tunnel velocities.

4.2.2 Wind Tunnel Testing Results

The surface pressure values measured at various locations on the ambulance were averaged over a 5 min test period (~100 data points) and then used to calculate, with the reference total pressure, the value for the coefficient of pressure (Cp) at each tap location. Cp is calculated using the equation from Anderson [2]:

$$C_P = \frac{p_t - p_s}{p_{total} - p_s} \tag{4-1}$$

In this equation:

C_p *is the Coefficient of Pressure*

p_t *is defined as the tap pressure (15 of them) on the model*

p_s *is the static pressure measured with the Pitot-static tube*

p_{total} *is the total pressure measured with the Pitot-static tube*

For each test run the data from the pitot static tube is used to compute velocity with the use of Bernoulli's equation [2]:

$$V = \sqrt{\frac{2(p_{total} - p_{static})}{\rho_{air}}} \tag{4-2}$$

In this equation

ρ is the density of air

V is the velocity

pstatic is the static pressure measured with the Pitot-static tube

ptotal is the total pressure measured with the Pitot-static tube

The pneumatic pressure scanner has an accuracy of ± 1031 Pa (0.15 psi) when working in a range of less than 17188 Pa (2.5 psi). By taking multiple data readings at one velocity this accuracy can be improved further. The calculated accuracy for coefficient of pressure, when recording data every 3 seconds for 5 minutes at one velocity is ±0.05. This type of accuracy was observed in the results for most of the pressure taps at almost every wind orientations. Despite changes in velocity it can be seen that the Cp value at each location remains fairly constant. The values for Cp at each location also change with change in the incoming wind direction with more pressure on the windward side and less

on the leeward side. The results for the SUV can be seen in Appendix 3B. Figures 4-2 to 4-8 summarize these results. The Cp's for each velocity and orientation were more consistent than those measured for the ambulance, therefore retesting at any angle was deemed unnecessary. From previous analysis for the ambulance and fire truck it was seen that testing at 180 degrees was unnecessary and at 65 degrees less critical. But for completeness the SUV was tested for coefficient of pressure at these angles. In order to reduce the number of hours required for testing, however, these angles were only tested at higher velocities (i.e. greater than 12 m/s).

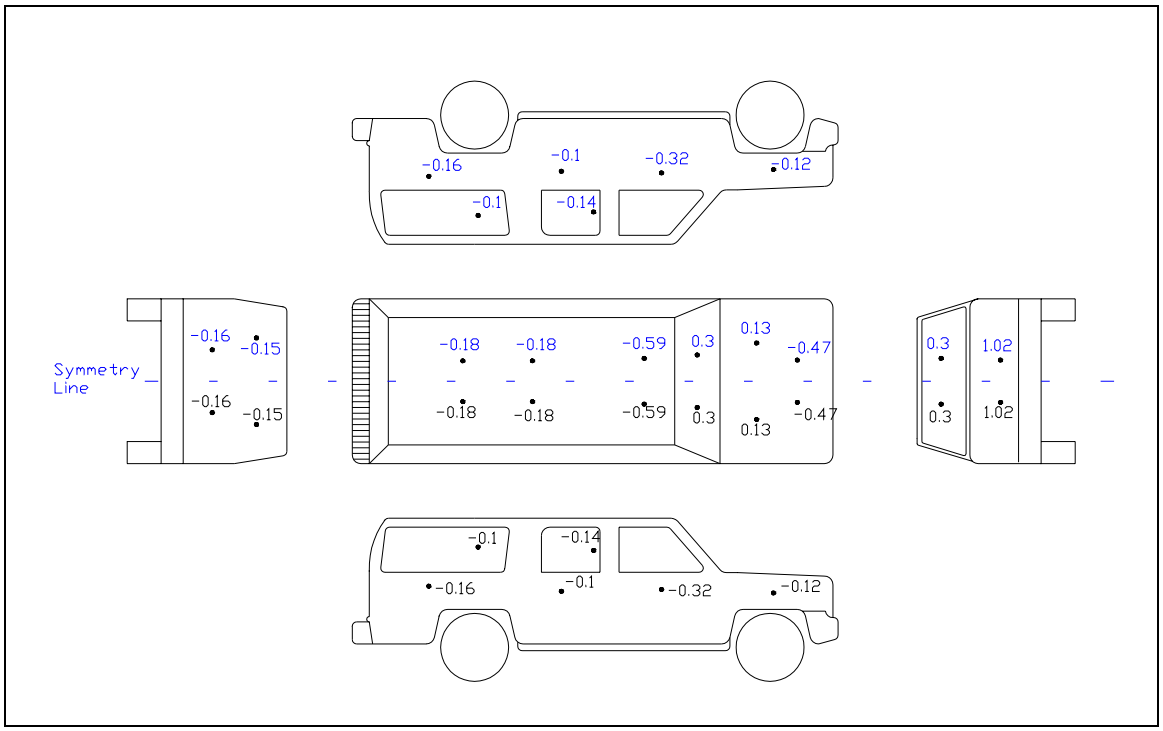

Figure 4-2: 0 Degree Coefficient of Pressure Test results

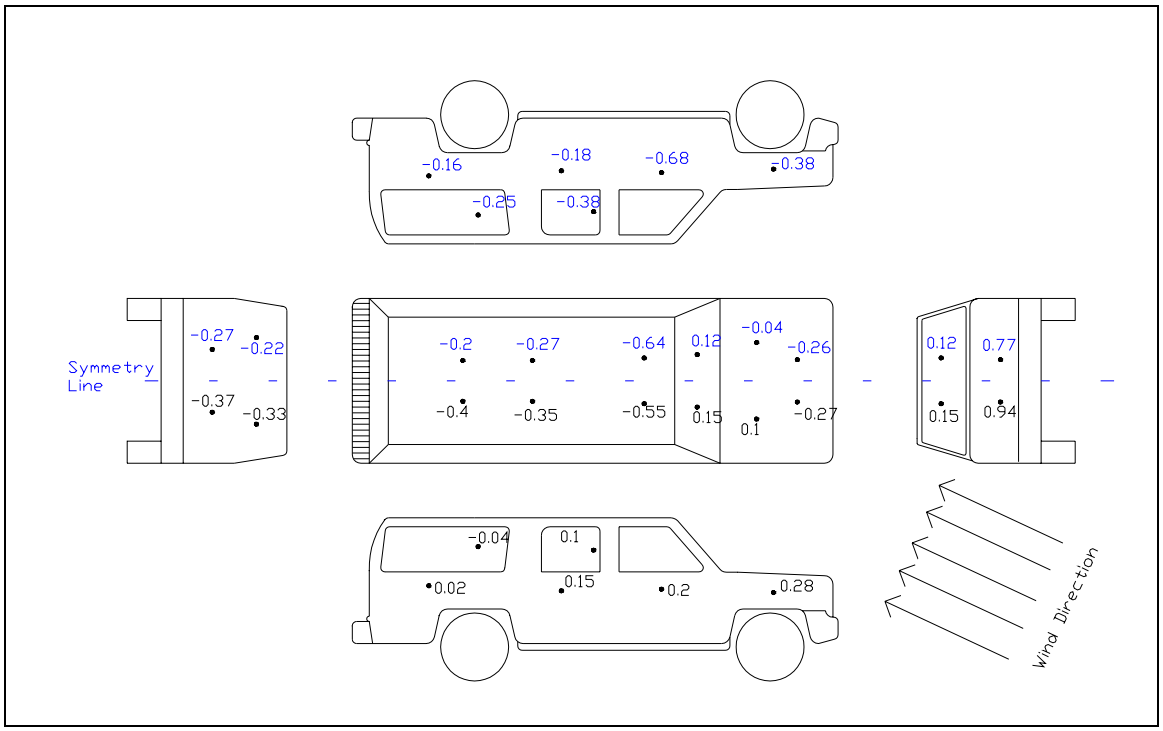

Figure 4-3: 25 Degree Coefficient of Pressure Test results

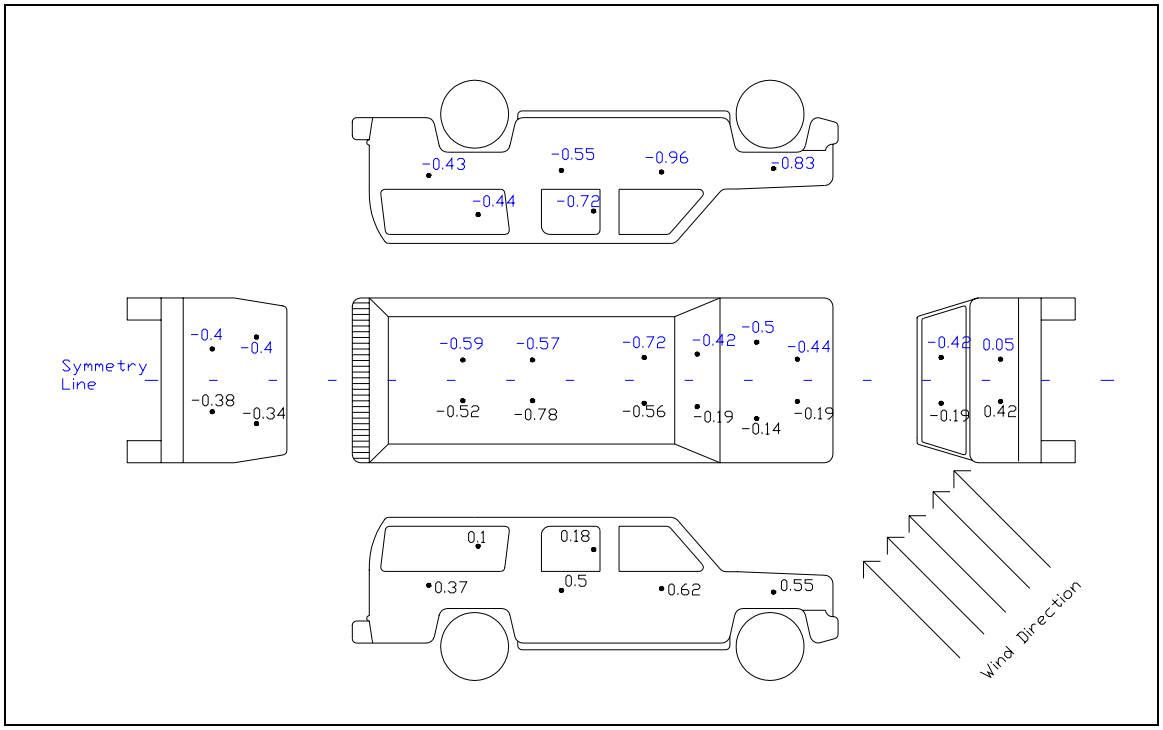

Figure 4-4: 45 Degree Coefficient of Pressure test results

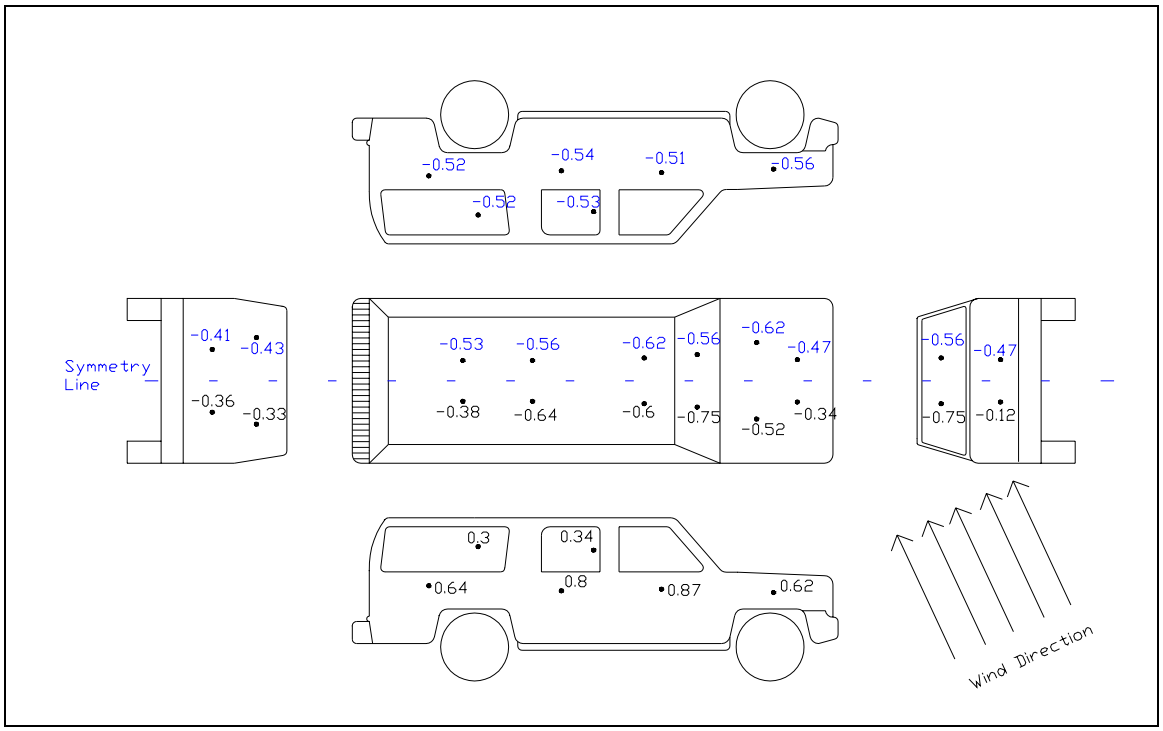

Figure 4-5: 65 Degree Coefficient of Pressure Test results

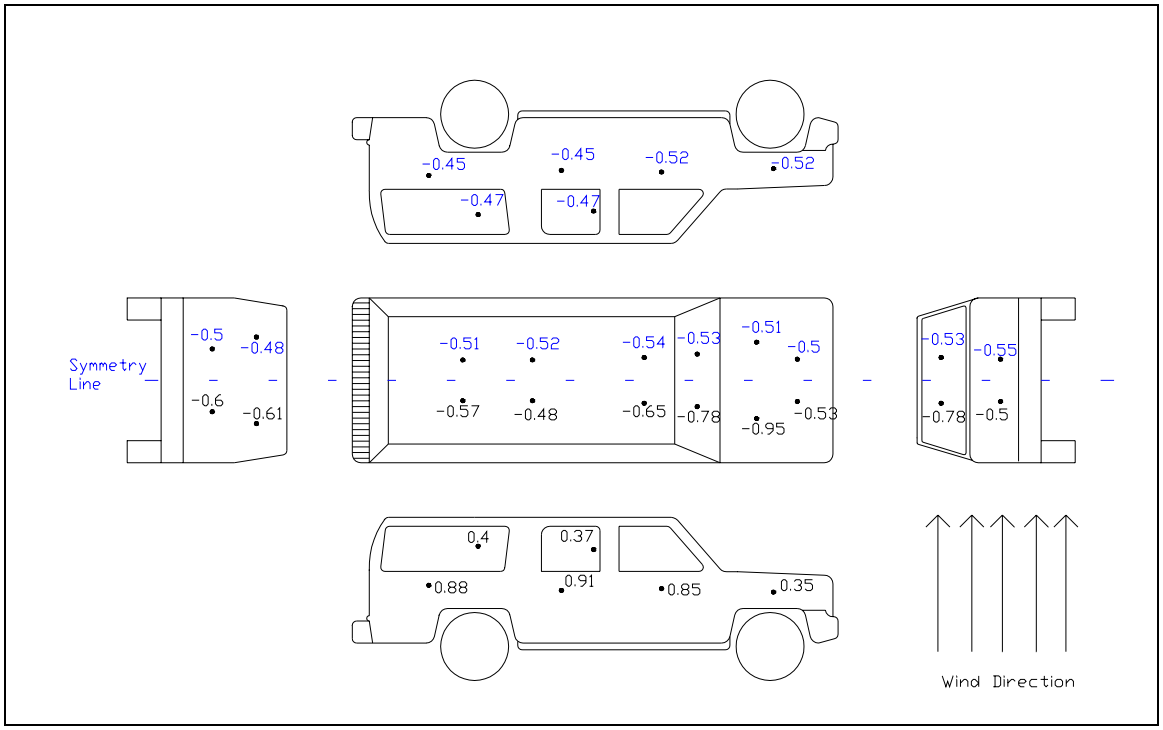

Figure 4-6: 90 Degree Coefficient of Pressure Test results

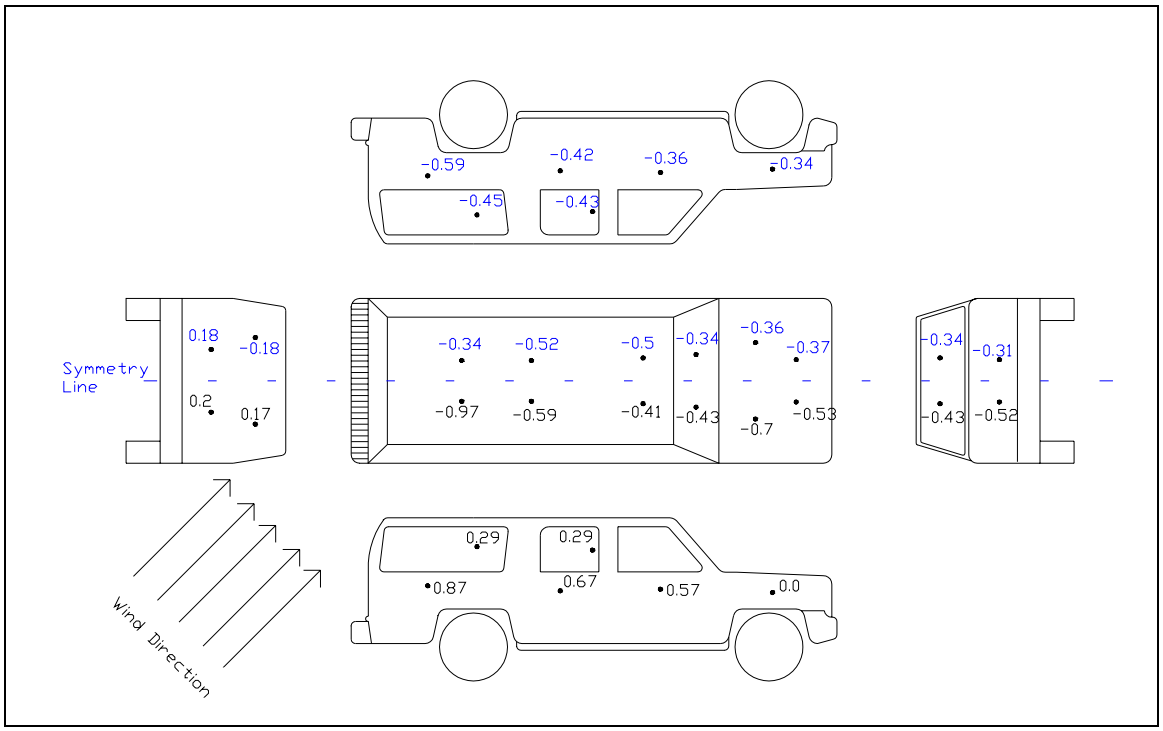

Figure 4-7: 135 Degree Coefficient of Pressure Test results

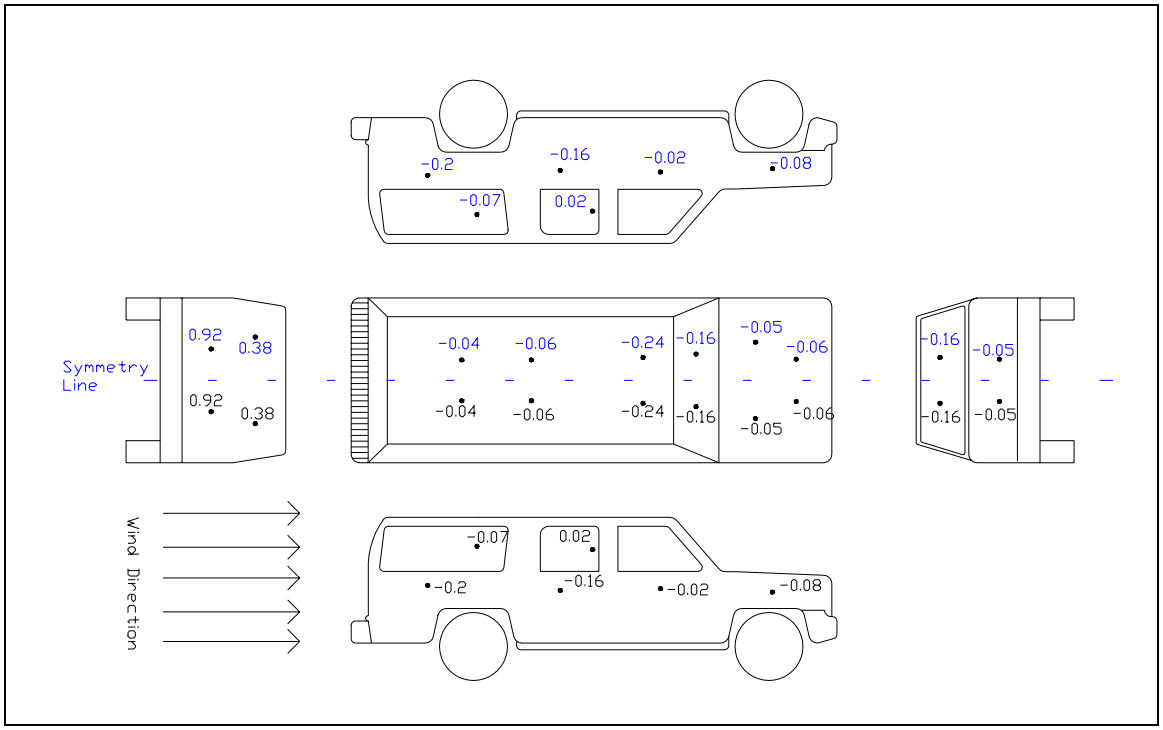

Figure 4-8: 180 Degree Coefficient of Pressure Test results

4.3 COMPARISON BETWEEN THE FORCE BALANCE AND PRESSURE DISTRIBUTION - VALIDATION OF THE RESULTS

4.3.1 Determination of Forces Acting on the Vehicle

(*Note this description for determining the forces acting on the vehicle was given in the fire truck section of the report but is repeated here as a reminder.)* From the wind tunnel tests, coefficients of pressure at various locations and various relative wind directions are known. This information is used to compute the forces acting on a vehicle as a function of wind speed. Coefficient of pressure is defined as local dynamic pressure divided by freestream dynamic pressure. As in the following equation:

$$Cp \equiv \frac{LocalDynamic\,\mathrm{Pr}essure}{TotalDynamic\,\mathrm{Pr}essure} \tag{4-3}$$

Pressure is defined as a force over an area. Wind speed is a function of freestream dynamic pressure through the following equation:

$$Vel = \sqrt{\frac{2(p_{Total} - p_{Static})}{\rho}} \tag{4-4}$$

Here ρ is the density of air (assumed to be 1.225 kg/m^3), and $(p_{Total} - p_{Static})$ was measured with the Pitot-static tube and is the freestream dynamic pressure. Rearranging equation 4-3 and combining with 4-4 gives

$$LocalDynamic\,\mathrm{Pr}essure = \frac{1}{2}V^2\rho \times Cp \tag{4-5}$$

Local force can therefore be computed using the local area, $Apanel$, and multiplying it by the local dynamic pressure. Dividing the model into sections or panels on which it is assumed that Cp is constant gives the following equation, which is a function of velocity:

$$Fpanel = V^2(\frac{1}{2} \times \rho \times Cp \times Apanel) \tag{4-6}$$

Summing the forces on all the panels over the vehicle for a certain wind angle and velocity gives the resulting force acting on the model. Some guesswork was used in deciding which area should be used for each panel. For the pressure taps where Cp is determined from symmetry of the vehicle, Cp values are labeled “prime” to indicate that they are a result of symmetry. For the parts of the vehicle where the surfaces were uniform the distance between the panels was chosen as half the distance between the taps. For surfaces with a lot of curvature, the panels were divided based upon the extent that a certain Cp would be likely to exist. The complete panel divisions are shown in the following figures.

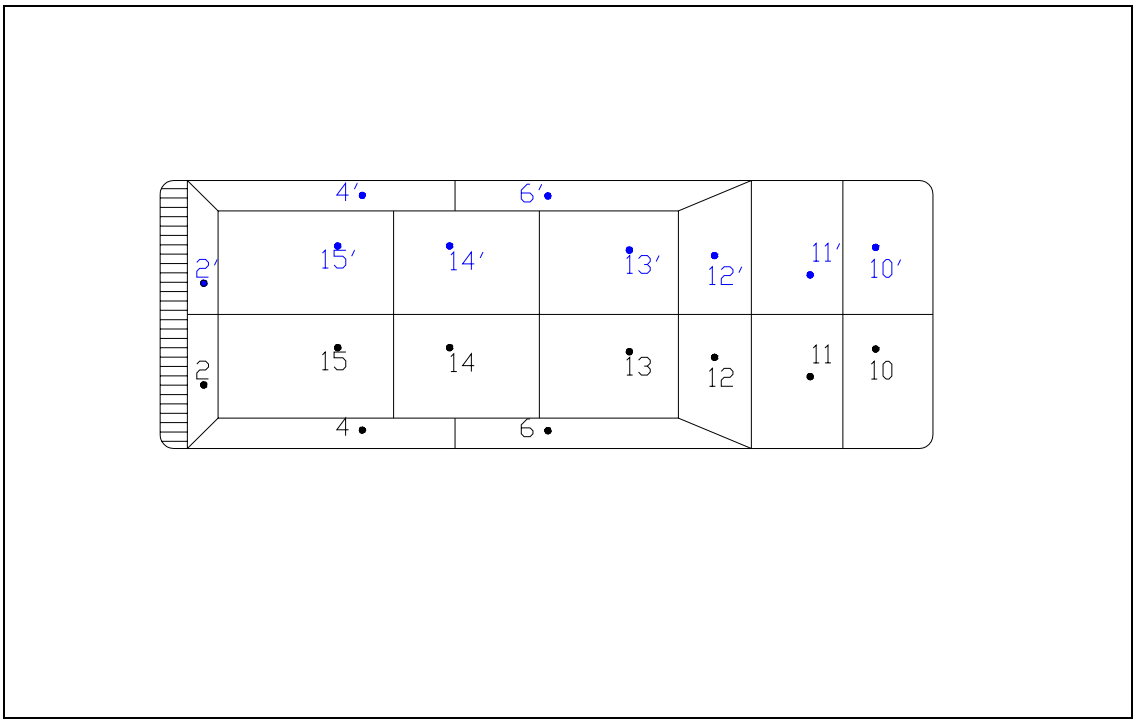

Figure 4-9: Panel division on the top of the Suburban

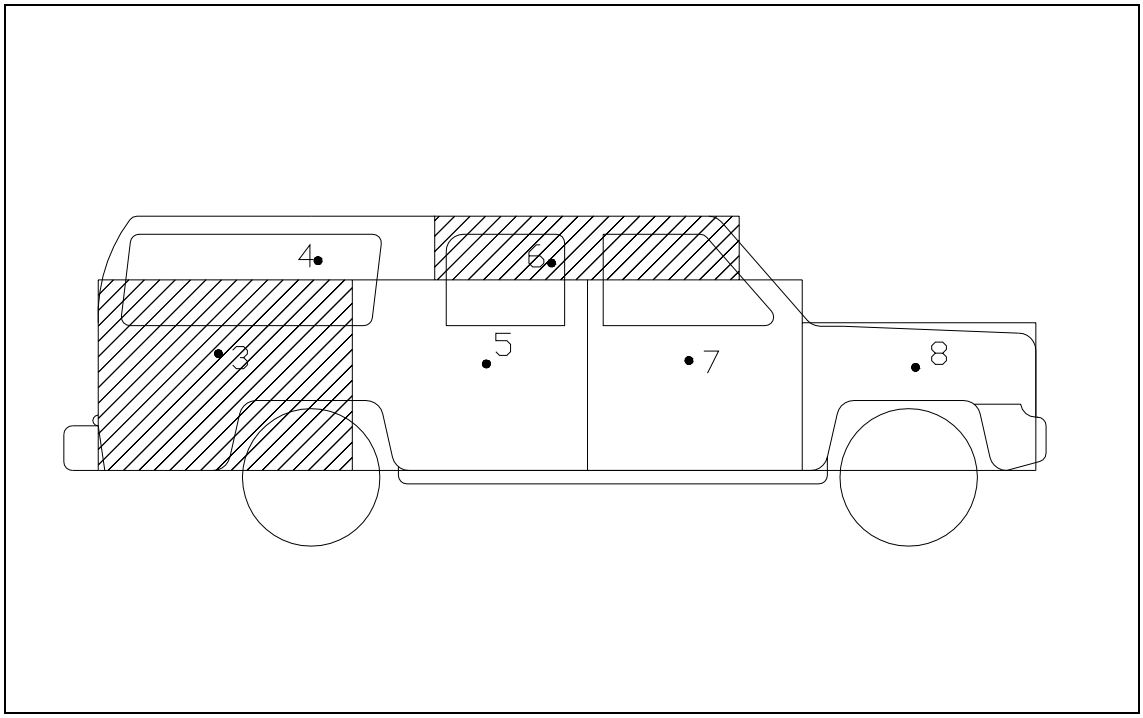

Figure 4-10: Panel division on the sides of the suburban

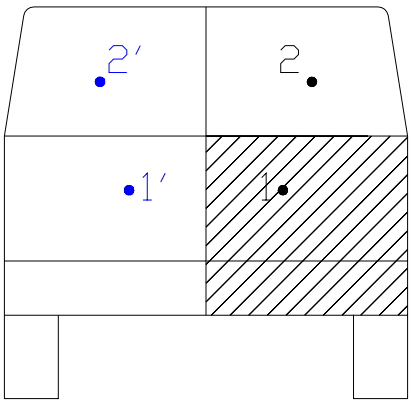

Figure 4-11: Panel division on the rear of the Suburban

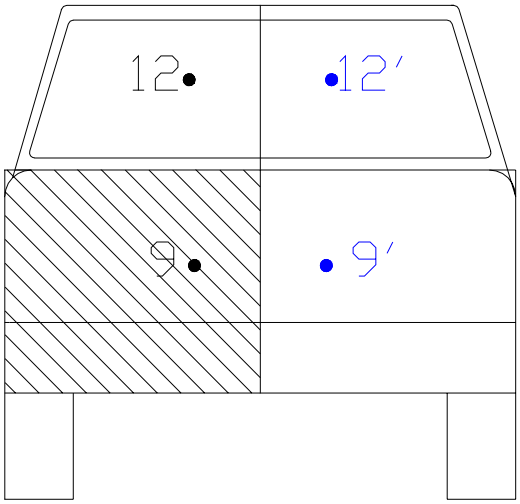

Figure 4-12: Panel Division on the front of the Suburban

4.3.1.1 Comparison between force balance results and measured pressure results

To help ensure the accuracy of the results a strain gage force balance to measure drag and side force on the model at different orientations and different velocities. The force balance was used to measure drag and sideways force at 0, ±45, and ± 90 degrees. Although the suburban model is a larger scale (1:19 over 1:21 for the ambulance and 1:25 for the fire truck) the model itself is smaller because a suburban is much smaller than a

fire truck or an ambulance. For this reason, when the model was tested in the wind tunnel the forces measured with the force balance and predicted by pressure distribution were much smaller and a small difference between the two became more noticeable. Initially there was a difference of almost 50% between the Force Balance measurements and the forces predicted by the pressure distribution. Because of this the sources of error were scrutinized more closely. As mentioned previously the force balance measures all forces on the model- pressure drag, skin friction drag, and stem drag (the drag on the aluminum rod that connects the model to the force balance). Whereas the pressure distribution only gives pressure drag. To improve the accuracy, a test was conducted in the wind tunnel at various speeds with only the aluminum rod inside the wind tunnel. The force balance was used to measure what drag the stem contributes at various wind speeds. This still ignores interference drag, which occurs between the stem and the model, but by correcting the force balance measurements to ignore stem drag the comparison between the force balance and the pressure distribution was very good. This is shown in the following figures.

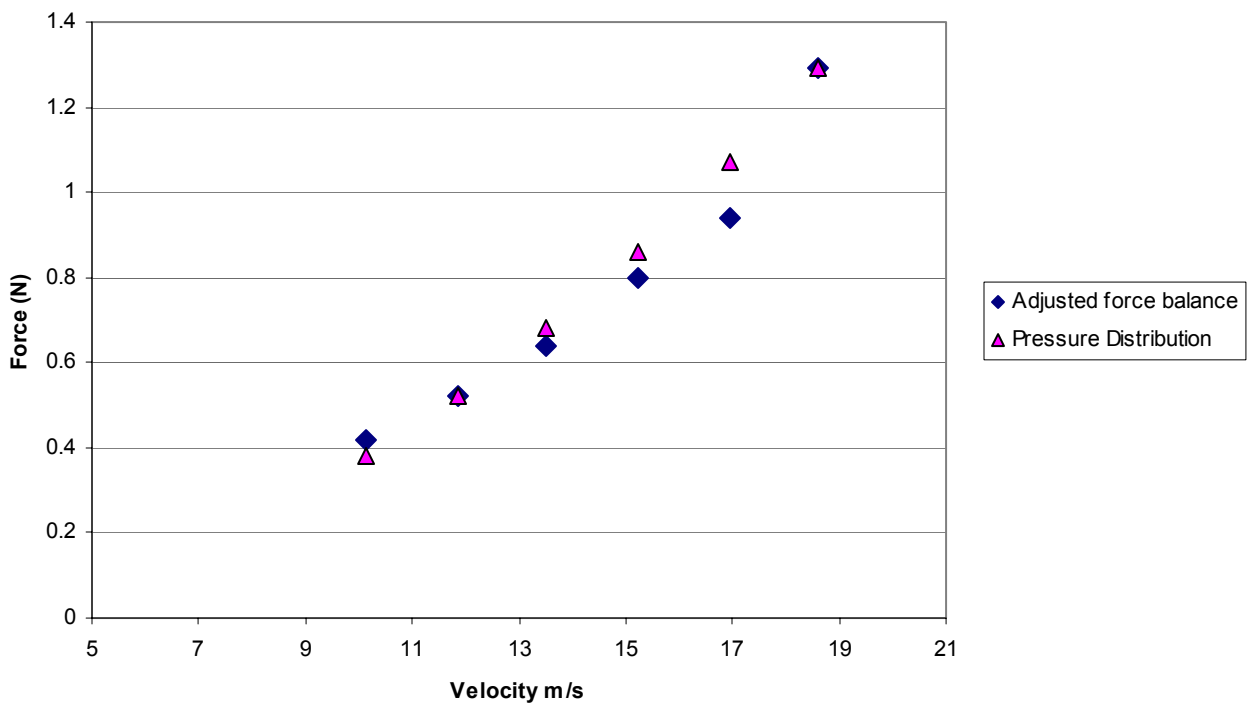

Figure 4-13: Force balance and pressure distribution comparison at 0 Degrees

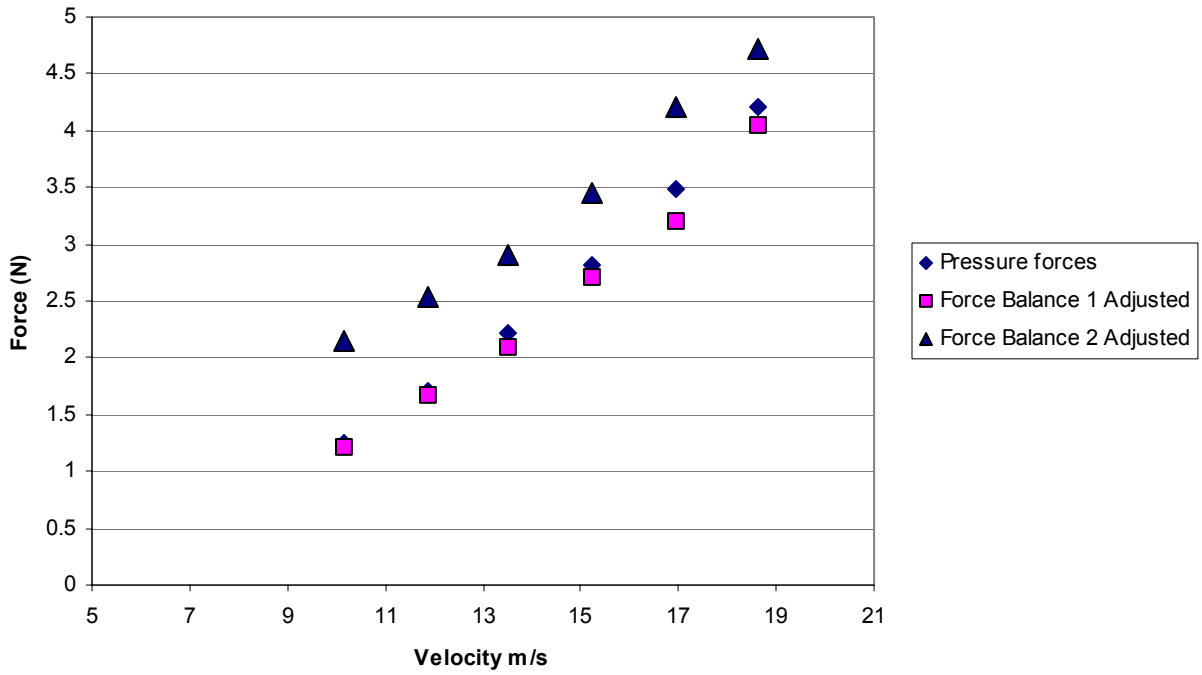

Figure 4-14: Force balance and pressure distribution comparison at 45 degrees

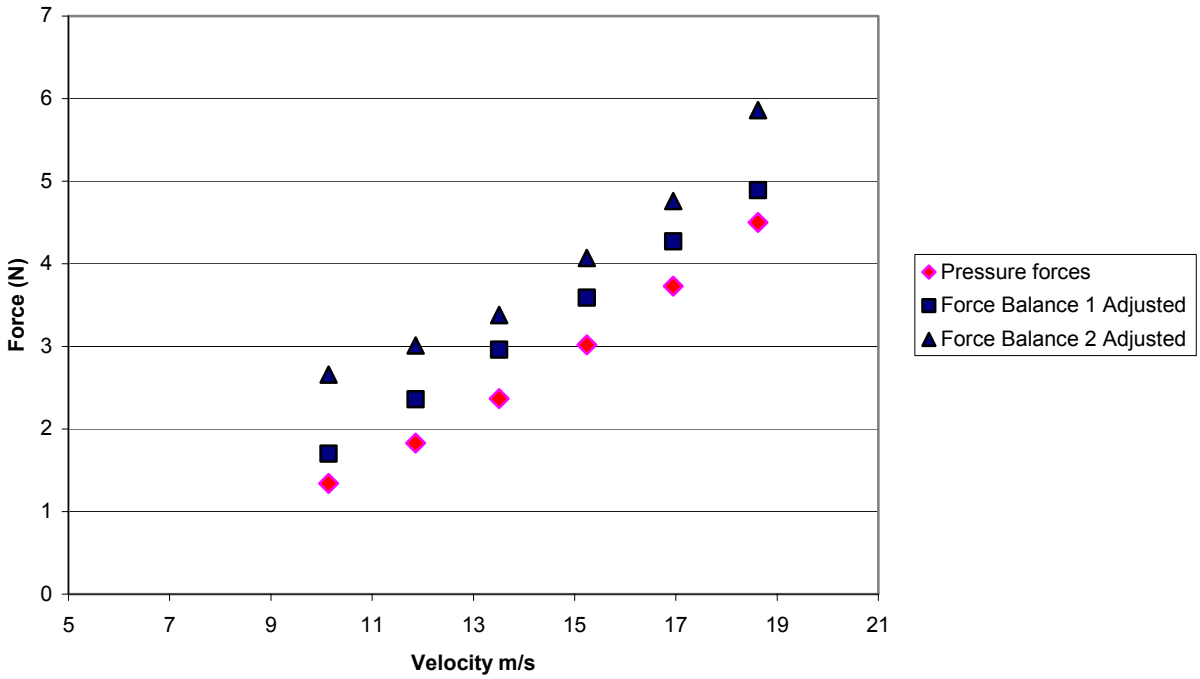

Figure 4-15: Force balance and pressure distribution comparison at 90 degrees

As before the symmetric argument was used about the vehicles lengthwise axis to assume that the forces acting on it for a wind angle of +45 degrees will be the same as if the wind were acting at –45 degrees. Therefore in the above plots force balance 1 represents the force balance measurements at +45 degrees, and force balance 2 represents the force balance measurements at –45 degrees. Even so, it can be seen that there is a linear difference between the two force balance measurements, at nearly all wind speeds. To try to correct this the model was checked to ensure that it was truly symmetric, and to balance the weight of the model at the stem by adding weights inside the front of the model. Even after these steps were taken, there was still a difference between the force balance readings.

4.3.1.2 Influence of Reynolds Number

For the model, testing was conducted for a Reynolds number range between 1.4×10^5 and 4×10^5. These values come from an equation in Anderson [2] below

$$R_e = \rho_\infty \frac{V_\infty x}{\mu_\infty} \tag{4-7}$$

In this equation:

R_e is Reynolds number
ρ is the density of air
V is the velocity
μ is the viscosity of air
x is the distance from the leading edge.

The subscript infinity defines far upstream from the model. The length of the model is 28 cm long (11 in), standard density and viscosity values for air were used at sea level. Velocity was the only parameter that changed giving the stated Reynolds number range.

Reynolds number is one of the simulation requirements Gawthorpe [3] mentions for effective wind tunnel modeling of a vehicle. The other two requirements are simulation of the ground plane, and the same onset of wind characteristics. These two were achieved in the setup. Testing is concerned with steady winds not gusting, and steady winds were modeled. The platform simulated the ground plane.

Reynolds number was not completely matched. For a full-scale vehicle Reynolds number would be above $\underline{4.5 \times 10^6}$. The largest Reynolds number tested with the model was only $\underline{4.9 \times 10^5}$. Both Gawthorpe & Anderson; however, suggest that if the boundary layer is turbulent then the same pressure forces can be generated on the surfaces at lower Reynolds numbers. From what was seen in the fire truck testing, it is assumed that there is a turbulent boundary layer for this model also. This is supported by the fact that scattering can be seen at each pressure tap at every velocity and orientation.

4.4 CRITICAL WIND SPEEDS

4.4.1 Introduction

(Note this description for determining the forces acting on the vehicle was given in the fire truck section of the report but is repeated here as a reminder.) In the book road vehicle Aerodynamic Design [7], Barnard indicates that vehicle accidents due to severe weather can result from overturning, course deviation, or hitting fallen trees and other debris. Course deviation and overturning will be considered in this analysis.

When a vehicle (assumed symmetric about it's centerline) is traveling down the expressway with no crosswind, normal forces acting on the vehicle will only include a Pitching Moment, a Lift force, and a Drag force. In a cross wind the vehicle will experience several additional actions. These actions can be a side force, a yawing moment, and a rolling moment. All the forces acting on a vehicle with a non-zero yaw angle (between vehicle axis and relative wind direction) are shown in Figure 4-16 below.

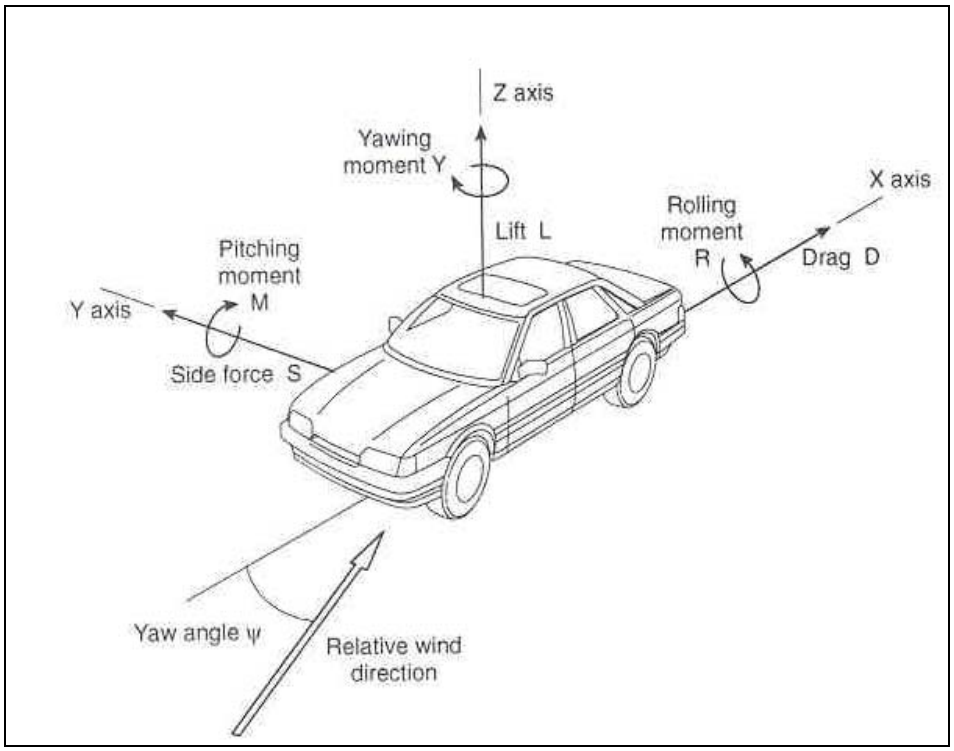

Figure 4-16: Definition of forces and moments acting on a vehicle [7].

4.4.2 Determination of Critical Wind Speeds Due to Course Deviation

4.4.2.1 Definition of Course Deviation

Course deviation occurs when a vehicle is blown off course. An accident as a result of course deviation can occur through a vehicle being blown off the road, into other vehicles, or other obstructions. It is likely that an experienced driver could correct for small course deviations; while violent course deviations will regardless result in an accident.

For this study the critical wind speed due to a course deviation will be defined as the speed at which due to combined forces and moments acting on a vehicle – a course deviation will begin to occur.

4.4.2.2 Calculating Forces and Moments on the SUV

A vehicle in a crosswind will have three forces and three moments acting upon it. From the wind tunnel testing the coefficients of pressure at different locations for different wind yaw angles are known. This information was used in conjunction with equation (2-4) to calculate the forces acting on the different panels of the model. The wind tunnel model, as stated earlier, is an exact replica of a G.M. 2001 Chevrolet Suburban. In terms of scaling factors between the two: it is a 1:19th scale along the wheelbase. This is the scale used for analysis.

4.4.2.3 Vehicle Weight and Center of Gravity

For a ¾ Ton 4x4 Suburban, Chevrolet [11] lists this vehicle as having a Gross Vehicle Weight Rating (G.V.W.R.) of 3900 kg (8,600lbm). Through a phone interview with a representative of General Motors it was discovered that the weight distribution is 53% on the front axle and 47% on the rear axle. Possible payload for this vehicle is 1290 kg (2840 lb). For analysis it will be assumed that the vehicle is full with 2067 kg (4547 lbm) on the front axle and 1833 kg (4032 lbm) on the rear axle.
In order to compute yawing and pitching moment acting on a vehicle it is necessary to reduce the forces acting on the vehicle to some arbitrary point. When this point coincides with the center of rotation, the resultant is a force. Otherwise, the resultant is a force and a moment. Some studies, [7] for example, use the midpoint between the front and rear axle as the point for the reduction of forces. In this part of the study, the forces are also reduced to the midpoint between the front and rear axle.

4.4.2.4 Lift, Drag and Side Forces

Lift, drag and side forces are defined as shown in Figure 4-16. The side force is computed by summing the forces acting on both sides of the vehicle. The drag force is computed by summing the forces on the front and rear of the vehicle. The lift force is computed by summing the forces acting on the roof of the vehicle. In reality there are forces acting underneath the vehicle and these should be accounted for in the lift force. But the pressure forces were not measured underneath the model, because the moving road condition could not be modeled. This will contribute an amount of uncertainty to the final results.

4.4.2.5 Pitching and Yawing Moments

The moments are computed by summing the wind forces acting about the midpoint between the vehicle axles. The yawing moment is computed from forces acting in the x-y plane, and the pitching moment is computed from the forces acting in the z-x plane. Knowing the forces on each panel, and the distance from the center of each panel to the origin of the x-y axis, the moment contribution from each force about the axis is known. Summing the total moments about the axis gives a single yawing moment about the

origin. The whole system of forces can therefore be reduced to a resultant force and resultant moment.

4.4.2.6 Combination of Moments and Forces to Determine Course Deviation

Using equation 2-4 and the summation of forces and moments method discussed in the previous two sections for any vehicle speed the forces on the vehicle can be predicted. In terms of course deviation analysis the side force and yawing moment can be balanced against the resistive force of the vehicle weight. This is shown in Figure 4-17 below.

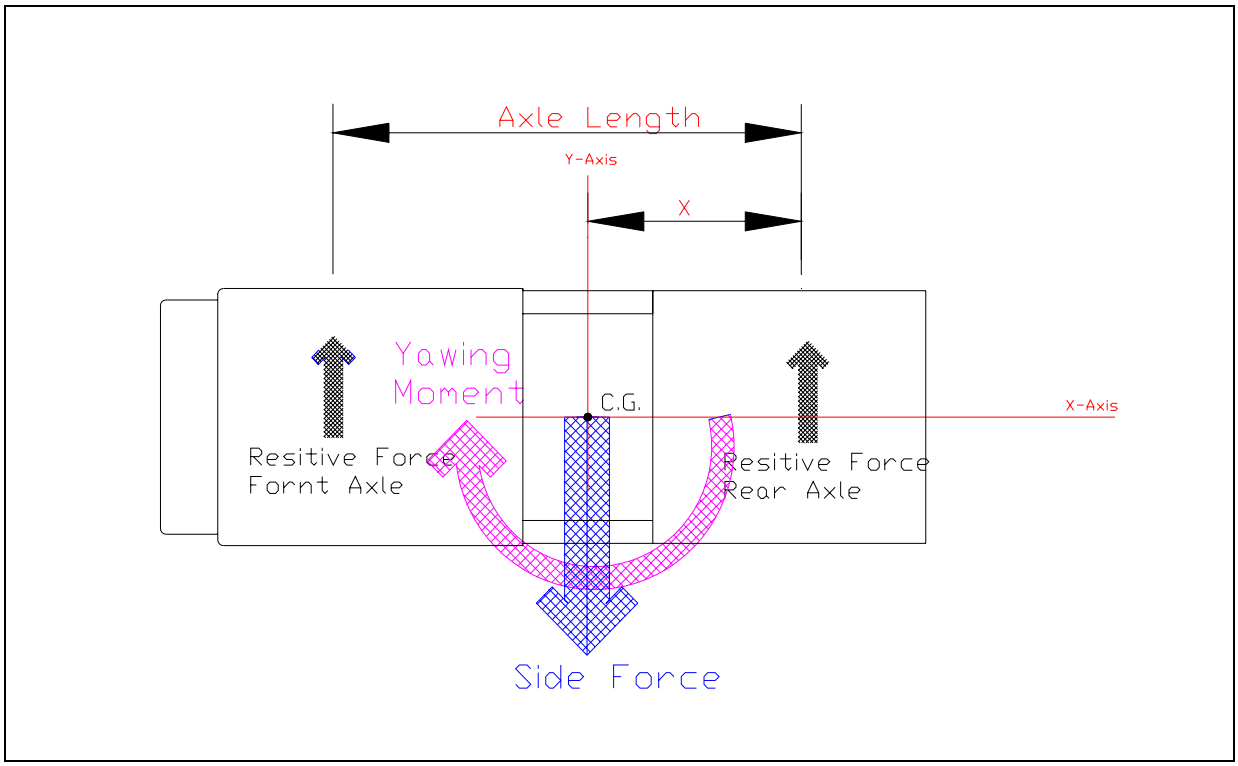

Figure 4-17: Balancing Yawing Moment & Side Force against the resistive force per axle.

In Figure 4-17 the yawing moment and side force are known as a function of velocity. The resistive force per axle depends upon vehicle weight per axle and the coefficient of friction between the tires and the roads. If two objects are being held together by some force (wheels on pavement, held together by gravity) the coefficient of friction tells what ratio of the force holding the objects together must be used to begin to slide one object over another.

In the above figure, the yawing moment, side force, and distance from each axle to the center of gravity are used to determine the side force acting on each axle. The equilibrium equations for each axle are shown below.

$$WindforceFrontAxle = \frac{YawingMoment + Sideforce * X}{AxleLength} \tag{4-8}$$

$$Windforce\,\mathrm{Re}\,arAxle = \frac{-YawingMoment + Sideforce * X}{AxleLength} \tag{4-9}$$

In these equations X is half the axle length (Recall that for the fire truck the forces and moments were reduced to the center of gravity, here they are reduced to the center between the two axles). The yawing moment and side force are calculated as a function of wind angle, and vehicle speed. The moment is positive counterclockwise, and negative clockwise. In order for a course deviation to be avoided the forces per axle must be less than the resistive force available on that axle.

The resistive force on each axle depends upon the coefficient of static friction between the tires and the road, and the weight acting on each axle. Due to the pitching moment and lift the weight per axle will differ with wind speed and yaw angle. The result is an effective weight per axle.

The following are the equations relating the effective weight per axle to the lift, pitching moment, and the G.V.W.R per axle.

$$E_f = G_f - \frac{Lift * X + PitchingMoment}{AxleLength} \tag{4-10}$$

In this equation E_f is the effective weight on the front axle, and G_f is the weight on the front axle based upon the gross vehicle weight rating, plus any adjustments due to an empty or full condition. X is half the distance between the axles. Similarly an equation can be defined for the rear axle:

$$E_R = G_R - \frac{Lift * (X) - PitchingMoment}{AxleLength} \tag{4-11}$$

In this equation E_R is the effective weight on the rear axle, and G_R is the weight on the rear axle based upon the gross vehicle weight rating, plus any adjustments due to an empty or full condition.

In terms of course deviation analysis the resistive force per axle can now be defined.

$$R_{force} = E\mu \tag{4-12}$$

In Equation 4-12 E is the effective weight for the front or rear axle from equation 4-11 or 4-10, μ is the coefficient of static friction, and R_{force} is the resistive force provided by that axle.

4.4.2.7 The Importance of the Coefficient of Static Friction

The coefficient of static friction (μ) is defined as the ratio of frictional force to the normal force pressing two surfaces together. It can also be known as the coefficient of adhesion. For some surfaces this value is known very well.

For galvanized rubber on different road surfaces this is a value that is not very well documented because it depends upon numerous variables. For example it is assumed that for racing slicks on dry pavement the coefficient of static friction (μ) will be approximately 0.9 or more, and for wet pavement about 0.1 or less (if hydroplaning occurs). This is why certain type of car races are not conducted in the rain.

For automobiles the coefficient of static friction (μ) will usually be somewhere between 0.1 and 0.9. These are unsubstantiated numbers, but in the National Highway Traffic Safety Administrations "Rating System for Rollover Resistance" [8] it states that "For a good dry paved surface, μ may be in the neighborhood of 0.9. But for wet, icy roads, μ is considerably less." There are several reasons for this broad uncertainty. The first is that this value depends upon the chemical composition of the tire and the road. Another factor is the tire pattern and the tire pressure. And finally, it depends upon the conditions of the road. For a hot, dry day μ will be highest. For a cold wet day μ will be considerably lower.

One of the worst-case scenarios for μ would be immediately after it begins to rain. Most roads are porous, and they absorb the oil and other products from the cars. When it rains, oil being less dense that water is displaced and a thin film of oil is produced on the surface road – this inevitably leads to slipperiest conditions. The only case where μ *might* be reduced more is when a road is covered in a sheet of ice.

4.4.3 Course Deviation

Gawthorpe [3] states that the shape of a vehicle largely fixes proneness of road vehicles to course deviation in a crosswind in addition to its weight distribution. Rear-engine cars with low tails are more prone than front-engine cars with high tails. For the wet road analysis a coefficient of static friction of 0.2 was used. For the dry road analysis a coefficient of static friction of 0.8 was used.

	Course Deviation Wind Speed	
Wind Angle	Dry Roads	Wet Roads
25*	166(370)	65(145)
45	206 (460)	67(150)
65*	102(228)	38 (85)
90*	100 (224)	37 (83)
135*	97(217)	38(85)

Table 4-1: Wind Speed to Cause a Static Course Deviation-Ambulance-The vehicle is not moving.
*Denotes instability in the rear axle.

Table 4-1 shows the static results. The first number has the units of meters per second and the number in parenthesis has the units of miles per hour. This information only indicates at which cross wind speed a parked vehicle will begin to move in its parking space. Note also that for all wind angles except 45 degrees the vehicle displays instability on its rear axle. The 45-degree case is unstable on the front axle with very little side-to-side resistance left on the rear axle. The reason for this is due to the unique shape of the vehicle itself. At low yaw angles such as 25 degrees there is positive pressure on the windshield and the hood just before the windshield. This contributes to a pitching moment downwards on the front axle. This dramatically increases the wind speed that

will cause a course deviation because now the rear axle is the one that deviates first. This is very different than what was seen for the fire truck and the ambulance.

Also note that course deviation analysis was not computed for 0 or 180 degree angles. This is because a course deviation will not occur for winds acting on these angles, but they will affect the vehicle in other ways. For example a strong tail wind will increase the stopping distance by an undocumented amount.

As with the other vehicles the static analysis cannot be considered by itself. When traveling down the highway, the vehicle speed in addition to the wind speed must be considered to determine the speed at which a course deviation will occur. This creates a resultant wind speed that for wind angles between 0 and 90 degrees will be higher than just the wind relative to the road.
The law of cosines must be used with vehicle speed, the resultant wind speed and the resultant wind angle to compute the crosswind speed; which will result in a course deviation. The law of cosines rearranged for this use is:

$$c = \sqrt{vs^2 + rs^2 - 2(vs)(rs)\cos 45} \tag{4-13}$$

In this equation c is defined as the crosswind speed, vs is defined as the vehicle speed, and rs is defined as the resultant wind speed. Taking vehicle speed into consideration the following tables demonstrates vehicle speed and necessary cross wind speed to create a resulting wind angle course deviation. This analysis was done for wet roads.

Vehicle Speed	Crosswind to cause a Course Deviation	Yaw Angle (Degrees)
12m/s (27mph)	54m/s (122mph)	30
16m/s (35mph)	51m/s (114mph)	33
20m/s (45mph)	48m/s (107mph)	35
25m/s (55mph)	44m/s (98mph)	39

Table 4-2: Suburban vehicle speed and necessary crosswind speed to cause a resultant wind speed of 65m/s at 25degrees.

Vehicle Speed	Crosswind to cause a Course Deviation	Yaw Angle (Degrees)
12m/s (27mph)	59m/s (132mph)	53
16m/s (35mph)	57m/s (127mph)	57
20m/s (45mph)	55m/s (122mph)	60
25m/s (55mph)	52m/s (117mph)	65

Table 4-3: Suburban vehicle speed and necessary crosswind speed to cause a resultant wind speed of 67m/s at 45degrees.

Vehicle Speed	Crosswind to cause a Course Deviation	Yaw Angle (Degrees)
12m/s (27mph)	35m/s (78mph)	83
16m/s (35mph)	34m/s (**77mph**)	90
20m/s (45mph)	35m/s (78mph)	97
25m/s(55mph)	36m/s (80mph)	105

Table 4-4: Suburban vehicle speed and necessary crosswind speed to cause a resultant wind speed of 38m/s at 65degrees.

As expected the above tables show that vehicle speed will decrease the necessary crosswind speed to cause a course deviation. What is surprising though is the worst-case scenario. For the ambulance and fire truck the worst case was seen to be for low resultant wind angles and somewhat lower wind speeds. Again this difference is explained by the shape of the vehicle. At low wind angles the windshield and low hood act as a "scoop" to help trap air and create a high pressure region, this results in a downward pitching moment on the front axle and because at small wind angles the greater forces are on the front of the vehicle the downward pitching moment allows the vehicle to resist greater wind forces.

4.4.4 Determination of Critical Wind Speeds Due to Overturning

As with the fire truck; overturning is defined as the case when the rolling moment exceeds the moment provided by the mass of the vehicle. Statically for different resulting wind angle the speeds to result in overturning are as follows.

Wind Angle	Wind Speed to result in overturning
25°	97m/s (217mph)
45°	107m/s (240mph)
65°	68.3m/s (153mph)
90°	67.8m/s (152mph)
135°	85.5m/s (191mph)

Table 4-5: Suburban wind speeds to cause static Overturning at different Yaw Angles

Vehicle Speed	Crosswind to cause Overturning	Yaw Angle (Degrees)
16m/s (35mph)	63m/s (141mph)	78
20m/s (45mph)	62m/s (139mph)	82
25m/s (55mph)	62m/s (138mph)	86

Table 4-6: Vehicle speed and necessary crosswind speed to cause a resultant wind speed of 68m/s at 65degrees.

The possibility of overturning due to wind speeds for the SUV fall into the wind speed region for a Category Four Hurricane (131-155mph). Based upon the Course Deviation analysis the vehicle would start sliding sideways before these wind speeds were ever reached. But as with any vehicle, overturning may still occur as a result of a violent course deviation at a lower crosswind speed.

5 CONCLUSIONS AND RECOMMENDATIONS

5.1 TYPES OF VEHICLE ACCIDENTS

Based upon the studies conducted here there are two possibilities of vehicle accidents as a result of strong winds. The first possibility is a course deviation, which can lead to accidents between vehicles or the vehicle being blown off the road. This event is very dependent upon the abilities of a driver to handle a vehicle in extreme driving conditions (abilities of multiple drivers if an accident involves more than one vehicle). Course deviation is also very dependent upon road conditions (i.e. how slippery the road is) and this is an uncontrollable variable.

The second possibility is overturning of a vehicle due to strong winds. If a vehicle is not permitted to slide sideways (parked against a curb, or a day when the roads are hot and dry- conditions leading to high coefficient of static friction.) then wind speeds which will cause overturning are very definite and they can not be corrected for by the driver or good driving conditions.

5.2 FIRE TRUCK CONCLUSIONS

For a range of vehicle speeds between 35 and 55 mph, the wind speed required to cause a course deviation for an empty Typhoon fire truck model decreases from 70 to 64 mph. For the Cyclone model, based upon an extrapolation, the allowable wind speeds are only slightly higher. Overturning, for the fire truck, is unlikely to happen based upon wind speeds alone, but it is possible that it could be blown off course and hit an obstacle in just the right way to cause overturning.

In conclusion for the fire truck, the critical wind speed falls in the range of 64-70mph. Yaw angles for this event range between 45 and 90 degrees. But this is not to say wind angles outside this range are not dangerous. Wind yaw angles between 90 and 180 degrees will contribute largely to a tailwind and not so much a crosswind and will make stopping difficult. For wind yaw angles less than 45 degrees they will contribute largely to a headwind, and will resist the vehicles' motion.

5.3 AMBULANCE CONCLUSIONS

For the ambulance model, for a range of vehicle speeds between 27 and 55 mph, the wind speed required to cause a course deviation decreases from 48 to 34 mph. The ambulance is at risk of overturning for wind speeds above 90 mph. The possibility can be delayed to about 100 mph if the vehicle is driven slowly. As with the fire truck it is possible that overturning can occur at lower wind speeds during a violent course deviation.

In conclusion for the ambulance, the critical wind speeds falls in the range of 35-50mph. The corresponding yaw angles are between 68 and 117 degrees. One explanation for why this range of wind speeds is so much lower than for the fire truck or the SUV is because it has a lower *density*- or mass per unit volume. The fire truck is a large vehicle but it does not have much empty space. The same holds for the SUV. Because of the

large patient module on the ambulance- this is mostly empty space- the vehicle is very susceptible to wind effects.

5.4 SUV CONCLUSIONS

From the analysis for the SUV model, for a range of vehicle speeds between 27 and 55 mph, the wind speed required to cause a course deviation is around 77 mph, for yaw angles between 83 and 100 degrees. The SUV is at risk of overturning for wind speeds above 138 mph. As with other vehicles, overturning can result at lower wind speeds during a violent course deviation.

In conclusion for the SUV, the critical wind speeds occur when wind speed is close to 77 mph. As with the other vehicles lower wind speeds will likely lead to dangerous driving depending upon various conditions.

5.5 RECOMMENDATIONS

Wind speed rather than wind direction should be used in determining safe driving conditions. Roads in a city go in every direction; a vehicle going to and from a location will encounter the critical yaw angle regardless of the yaw angle at the beginning of its trip. To define the critical wind speed, a factor of safety should be used with the numbers provided in this report, to reflect the fact that:

- There is a margin of error inherent in any experimental study. For example, turbulence could not be simulated in the wind tunnel and the forces that would contribute to lift and a pitching moment beneath a vehicle were not measured because the moving ground plane could not be simulated.

- The actual wind induced forces might change for different models of the same vehicle.

- The actual weight of the vehicle is a random variable that depends on the amount of people and type equipment on board. In the case of the SUV it was assumed that the vehicle was a 4x4 ¾ ton Suburban. If the vehicle were in fact a 2x4 ½ ton suburban then the vehicle would not be as heavy as the one studied here and thus more prone to course deviation or overturning at lower wind speeds. The same is true for the ambulance, the study here was for a F-450, but there exists a lighter F-350 which would also be more prone to course deviation or overturning at lower wind speeds. Finally, with the fire truck there exists the variable of how much cargo or water is carried.

- The coefficient of friction for the tires is highly dependent on a number of factors that make its actual value determination uncertain. Because heavy rains usually accompany strong winds this is the assumed worst-case scenario for this study and hence the coefficient of static friction of 0.2 was used. It cannot be stressed enough that this is not an exact value.

- Some conditions like centrifugal forces in a curve, or operation on open causeways were not taken into account.

- Finally, the actual wind speeds in the field can be different than the one announced by the weather service.

Therefore, it is recommended that a factor of safety of 1.25 be adopted when applying the results of this study. Any final decision concerning safe wind speeds should be made by the fire chief based on the results of this study, the urgency of the situation, and personal judgment.

Consequently, a classification of wind speeds is provided in the following table for each vehicle. The lower end of the Critical range is for wind speeds that will make driving the vehicle difficult. The upper end of the Critical range is for extremely dangerous driving conditions, and finally Seek Shelter indicates the wind speed for which this vehicle should not be driven, and parked indoors if possible.

The lower wind speed limit for Critical conditions for each vehicle was computed as the lowest critical wind speed from the tests that marks the onset of course deviation at a vehicle speed of 55 mph divided by 1.25, and rounded to the nearest multiple of 5.

	Critical	Seek Shelter
Fire Truck	**50**-70 mph	70+ mph
Ambulance	**30**-50 mph	50+ mph
Suburban (SUV)	**60**-70 mph	70+ mph

Table 5.1: Classification of wind speed driving conditions for each vehicle

It is the firefighter's job to routinely put the safety of others above their own. Regardless of the fact that it has been stated that it is unsafe to drive these vehicles in winds in the Critical zone, it is likely occur anyway. But there are some basic recommendations that can be done to ensure the safety of the personnel as much as possible. First ensure that the vehicles have good tires at all times. Secondly, send only experienced drivers into winds within the Critical zone. Finally; remember that the critical wind speed is a function of the speed of the vehicle.

Therefore, the information in Table 5-1 is repeated in Figures 5-1 to 5-3, where the Critical zone is divided into a Hazardous (yellow) and a Dangerous (orange) zone. If the vehicle must be operated in wind speeds in the Critical zone, slow down and make sure to drive slowly at vehicle speeds that will put you in the Hazardous zone. For example, at wind speeds of 60 mph, the graph of Figure 5-1 shows that a fire tuck should never be driven at speeds higher than 23 mph, and that extreme caution should be taken at speeds at or below 23 mph. It is recommended that under no circumstances should a vehicle be driven in wind speeds approaching the “Seek Shelter Category”.

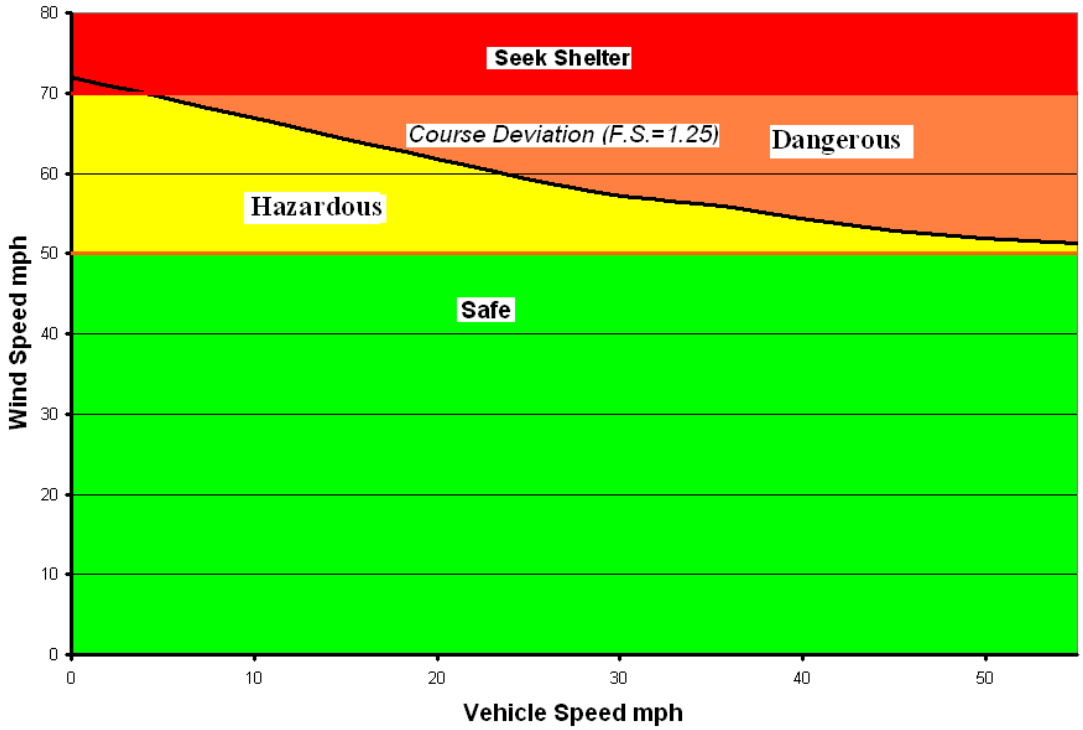

Figure 5-1: Wind speed- vehicle speed recommendations for the Typhoon fire truck

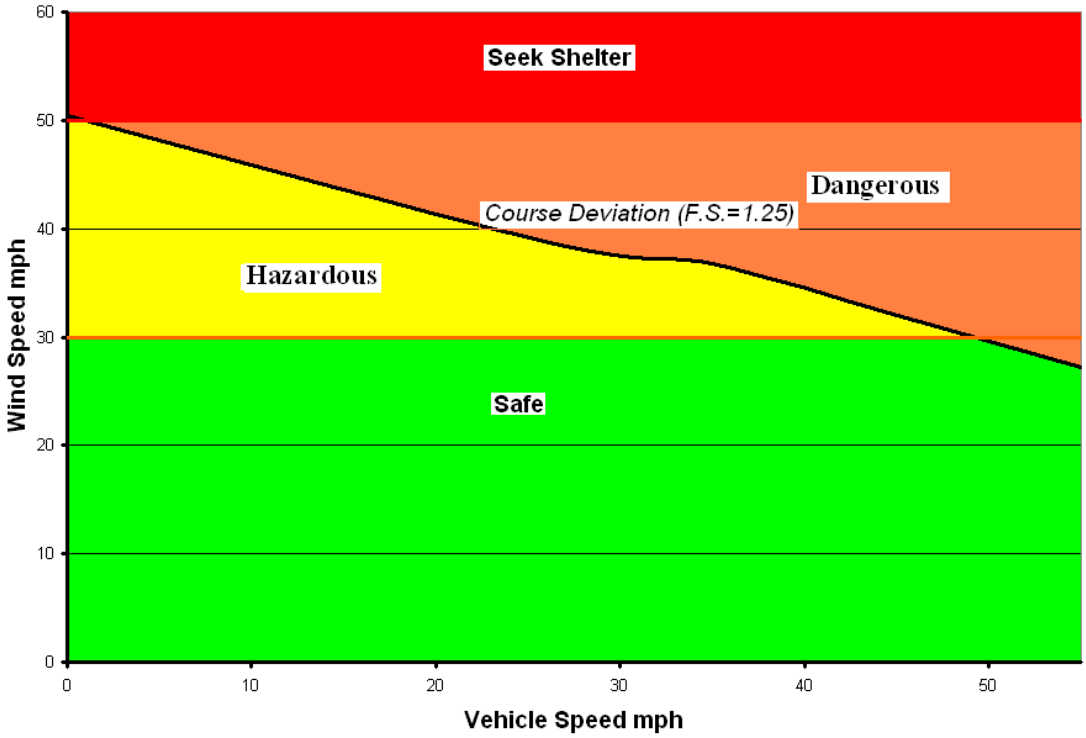

Figure 5-2: Wind speed – vehicle speed recommendations for a F-450 Type I ambulance

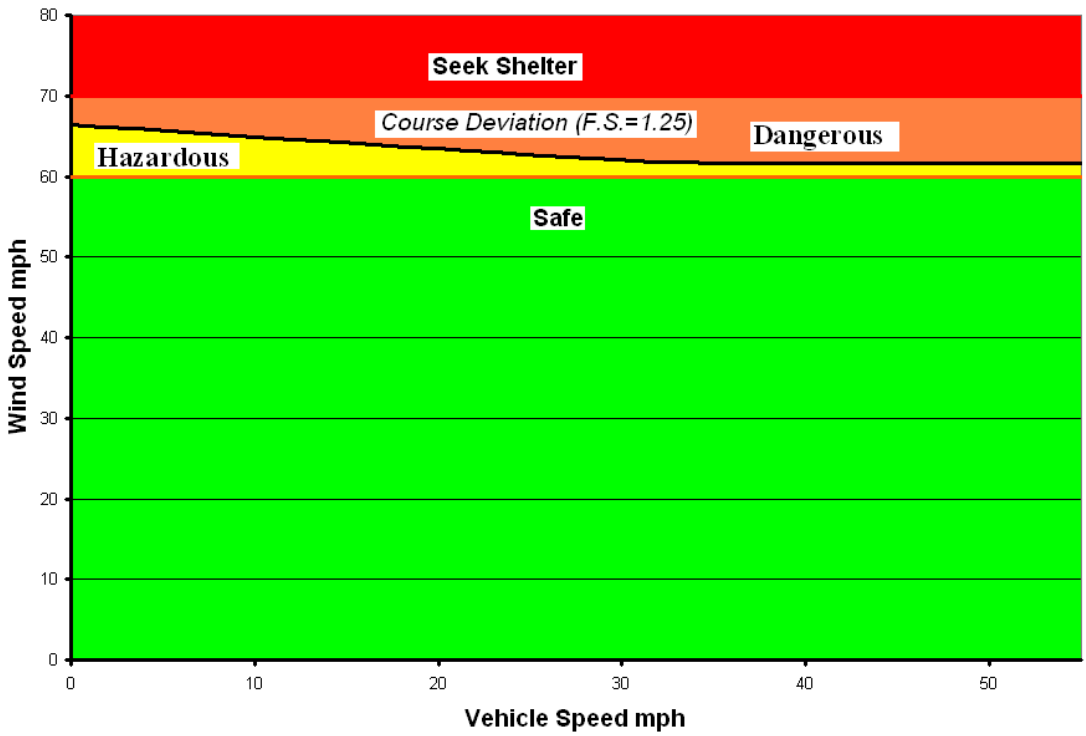

Figure 5-3: Wind speed – vehicle speed recommendations for a 4x4 ¾ ton Suburban (full of equipment)

5.6 RECOMMENDATIONS FOR FURTHER STUDIES

The project scope and objectives of this investigation was to define the upper limit wind speeds at which a fire truck, ambulance, and emergency SUV vehicle can operate safely. In a second phase, the investigative team could carry on similar studies on other types of vehicle such as:

- buses used to evacuate elderly residents or hospital patients,
- bucket trucks used by electric companies to fix line problems;
- types II and III ambulances;
- other law enforcement vehicles;
- trucks with aerial ladders.

Similarly, research could be carried out to define the upper limit wind speeds at which the overall safety of response personnel will not be compromised. Such a study could include impact tests of vehicles and related materials, and look at the issues of:

- flying debris, shattered windshields, and safety of personnel;
- protective clothing and equipment;
- effect of the rain;

- opening of building bay doors as well as vehicle doors;
- how road conditions affect the coefficient of static friction for different tires.

6 AKCKNOWLEDGMENTS

The authors wish to acknowledge the support and advice of Fire Chief Daniel H. Rocque, Satellite Beach Fire Department, and Mr. David Halstead, Senior Management Analyst, Division Of Emergency Management, Florida Department Of Community Affairs, who acted as project managers for this study. The authors also acknowledge Dr. John Luchini Chief research scientist of the Cooper Tire Company for his input on the coefficient of static friction for different tires on different road conditions. The encouragement of Mr. Robert Lay, Emergency Manager, Brevard County is also gratefully appreciated. Finally, many thanks to the whole team of the Satellite Beach Fire Department, and in particular to Operations Commander Donald Hughes, and Captain James Keating.

7 REFERENCES

[1] Picture on Cover: Typhoon Pumper, manufacturer Emergency One. Figures 15 & 16 also adapted from the E-One website, www.e-one.com, April 12, 2003

[2] Anderson, John D. "Introduction to Flight " McGraw-Hill, 3rd edition 1989

[3] Gawthorpe, R.G. "Wind effects on ground transportation" Journal of Wind Engineering and Industrial Aerodynamics 52 (1994) 73-92

[4] Subrata Roy and Pradeep Srinivasan: "External flow analysis of a truck for drag reduction"-2000 Society of Automotive Engineers

[5] Masan, W.T.; Sovarn, G. " Ground plane effects on the aerodynamics characteristics of automobile models-An experimentation of wind tunnel test technique"

[6] AIRFLOW Technical Products Inc- http://www.airflow.com/instr/stat-pit.htm, May 28, 2003

[7] Barnard, R. H. "Road Vehicle Aerodynamic Design" 2nd ed. MechAero Publishing 2001

[8] National Highway Traffic Safety Administrations *"Rating System for Rollover Resistance"* Special Report 265, National Academy Press; Washington, D.C 2002

[9] The National Weather Service – Tropical Prediction Center- National Hurricane Center website: http://www.nhc.noaa.gov/aboutsshs.shtml accessed May 28, 2003

[10] Wheeled Coach Industries – http://www.wheeledcoach.com, August 21, 2003

[11] Chevy Suburban Capacities
http://www.chevrolet.com/suburban/library/fs/index_capacities.htm, July 29, 2003

[12] Schlichting, Hermann "Boundary Layer Theory" 4th ed. McGraw-Hill, New York, 1951

[13] Baker, C.J. "The Problems of road vehicles in cross winds" Journal of Highways and Transportation, May 1991

[14] Jones, Childers "Contemporary College Physics" Chapter 4.8- Force and Motion McGraw-Hill College 2001

[15] Baker, C J; Coleman, S. A. "High sided Road Vehicles in Cross Winds" Journal of Wind Engineering and Industrial Aerodynamics v.36 (1990), pgs 1383-1392

[16] Baker, C J; Humphreys, N D "Forces on vehicles in cross winds from moving model tests" Journal of Wind Engineering and Industrial Aerodynamics v41-44 (1992), pgs 2673-2684

[17] Baker, C J "The quantification of accident risk for road vehicles in cross winds" Journal of Wind Engineering and Industrial Aerodynamics v.52 (1994) pgs 93-107

[18] Anon, "AUTOMOBILE AERODYNAMICS; WAKES, WIND EFFECT, VEHICLE DEVELOPMENT." SP-569. Publ by SAE, Warrendale, PA, USA 128p

[19] Baker, C. J., "SIMPLIFIED ANALYSIS OF VARIOUS TYPES OF WIND-INDUCED ROAD VEHICLE ACCIDENTS." Journal of Wind Engineering and Industrial Aerodynamics, v 22 n 1 Apr 1986 p 69-85

[20] Bruhn, Hauke, Schneider, Carl-Thomas, "Optical measurement of vehicle body-shapes in the wind-tunnel" Proceedings of SPIE - The International Society for Optical Engineering, v 1395 pt 2 1990 Publ by Int Soc for Optical Engineering Bellingham WA USA p 900-907

[21] Burgin, K.,Adey, P. C.,Beatham, J. P., "WIND TUNNEL TEST ON ROAD VEHICLE MODELS USING A MOVING BELT SIMULATION OF GROUND EFFECT." Journal of Wind Engineering and Industrial Aerodynamics v 22 n 2-3 Jun 1986, 6th Colloq on Ind Aerodyn: Veh Aerodyn, Aachen, West Ger, Jun 19-21 1985 p 227-236

[22] Hurst, D.W.; Allan, J.W.; Burgin, K. "Pressure measurements on a full-scale tractor-trailer combination and comparison with data from wind tunnel model tests" International Journal of Vehicle Design, Special Publication SP3, 1983. (U.K.) pgs 471-479

[23] Ericsson, L.E., "Effects of transition on wind tunnel simulation of vehicle dynamics"Progress in Aerospace Sciences, v 27 n 2 1990 p 121-144

[24] Garry, Kevin P., "Wind tunnel tests on the influence of fixed ground board length on the aerodynamic characteristics of simple commercial vehicle models" Journal of Wind Engineering and Industrial Aerodynamics, v 38 n 1 Jun 1991 p 1-10

[25] Goenka, Lakhi N., "Numerical model to determine vehicle pressure-simulation accuracy in a slotted-wall automotive wind tunnel JSAE Technical Paper Series 1990 Publ by SAE Warrendale PA USA 15p

[26] Lingzhe, Kong, Parkinson, G.V., "Road vehicle model testing in a blockage tolerant wind tunnel" NASA Technical Memorandum no. 10909825 May 1994 p 239

[27] Mitschke, Manfred, "Control loop 'driver-vehicle' under the influence of cross wind" American Society of Mechanical Engineers, Applied Mechanics Division, AMD.

Transportation Systems 1990 Am Soc Mech Eng Appl Mech Div, v 108 1990 Publ by ASME New York NY USA p 109-115

[28] Noguchi, H. "ANALYSIS OF VEHICLE BEHAVIOUR IN A CROSS WIND." Journal JN: International Journal of Vehicle Design v 7 n 5-6 Sep 1986 p 304-317

[29] Ryan, A., Dominy, R.G. "Aerodynamic forces induced on a passenger vehicle in response to a transient cross-wind gust at a relative incidence of 30 degrees" Developments in Vehicle Aerodynamics SAE Spec Publ v 1318 Feb 1998 SAE Warrendale PA USA p 181-189

[30] Schmidlin, Thomas W.,King, Paul S., Hammer, Barbara O., Ono, Yuichi, "Behavior of vehicles during tornado winds," Journal of Safety Research 29 3 1998 p 181-186

[31] Templin, J. T., Raimondo, S., "EXPERIMENTAL EVALUATION OF TEST SECTION BOUNDARY INTERFERENCE EFFECTS IN ROAD VEHICLE TESTS IN WIND TUNNELS." Journal JN: Journal of Wind Engineering and Industrial Aerodynamics v 22 n 2-3 Jun 1986, 6th Colloq on Ind Aerodyn: Veh Aerodyn, Aachen, West Ger, Jun 19-21 1985 p 129-148

[32] Tran, Van Tuan, "Calculation method for estimating the transient wind force and moment acting on a vehicle" SAE (Society of Automotive Engineers) Transactions v 100 n Sect 6 1991 p 477-488

[33] Watkins, Simon, Saunders, Jeff, "Review of the wind conditions experienced by a moving vehicle" Developments in Vehicle Aerodynamics SAE Spec Publ v 1318 Feb 1998 p 259-266

[34] Suzuki, Minoru; Tanemoto Katsuji; Maeda Tatsuo " Aerodynamic characteristics of train/vehicles under cross winds" Journal of Wind Engineering and Industrial Aerodynamics 91 (2003) pgs 209-218